ECC Report 260

Description of methodologies to estimate the technical impact of wind turbines on Fixed Radio Links

Approved 27 January 2017

0   EXECUTIVE SUMMARY

This report collects studies and information on the technical impact of wind turbines on various radio communication services. This report covers only fixed service point to point radio links.

Measurements performed on several link paths in Sweden have shown that interferences from wind turbines are usually small under normal atmospheric conditions. However, when the signal strength is reduced by significant fading events, the interference may be not necessarily small.

Various methodologies to estimate the impact of wind turbines are applied or planned to be applied in some CEPT administrations. However, it has not been possible within the scope of this study to evaluate the suitability and accuracy of each method, which would require much more significant work. Therefore, this report reflects only the state of the art on this issue for some administrations.

TABLE OF CONTENTS

LIST OF ABBREVIATIONS

Abbreviation	Explanation
BBER	Background Block Error Ratio
BER	Bit Error Ratio
CEPT	European Conference of Postal and Telecommunications Administrations
ECC	Electronic Communications Committee
EPO	Error Performance Objective
ES	Errored Second
ESR	Errored Second Ratio
FMV	Försvarets Materielverk (Swedish Defence Materiel)
FOI	Totalförsvarets forskningsinstitut (Swedish Defence Research Agency)
GTD	Geometric Theory of Diffraction
I/N	Interference to Noise ratio
LOS	Line Of Sight
PE	Parabolic Equation
RCS	Radar Cross Section
SD	Space Diversity
SES	Severely Errored Second
SESR	Severely Errored Second Ratio
SNR	Signal to Noise Ratio
TD	Threshold Degradation
UHF	Ultra High Frequency
VHF	Very High Frequency

1 INTRODUCTION

The growing number of wind turbines all over the world can be a critical performance problem for microwave radio links.

The scope of this report is limited to fixed service point to point radio links.

It has been noted that there are various methodologies to estimate the impact on wind turbines.

However, it has not been possible to evaluate the suitability and accuracy of each method, which would require much more significant work.

The calculation models, described in this report, originate from the University of the Basque Country (UPV/EHU) and from a project involving several Swedish organisations.

2   CONTRIBUTIONS RELATED TO FIXED RADIO LINKS

Several contributions have been received during the study period and can be found as Annexes to this report:

ANNEX 1: contains contributions provided by Sweden:
- Annex A1.1 - Measurements and Modelling Effects of wind turbines on Fixed Radio Links
- Annex A1.2 - System parameters for reference radio links
- Annex A1.3 - Model Explanation
- Annex A1.4 - Example of Wind turbine fade margin Reduction

ANNEX 2: contains a contribution by University of the Basque Country (Spain).

Annex A1.1 is a contributed study from Sweden providing a methodology used to define how scattering from wind turbines may impact the performance of fixed radio links, and describes a method to model the effects.

According to measurements, performed on several link paths in Sweden, interferences from wind turbines are usually small under normal atmospheric conditions. However, when the signal strength is reduced by naturally occurring tropospheric fading events, the interference may be not necessarily small. The strength of the direct signal component and the scattered components from the turbines are in the study, for multipath fading, considered by Sweden, not to be correlated. In the study the wind turbine field is modelled as pure forward scattering through a time/blade-rotation variable aperture.

To verify and explain the measurement results from real radio relay paths a research model, using the parabolic equation model was developed. This was used to calculate the combined effects of wind turbine scattering and natural fading. A way to build a "production model" has also been developed and tested.

The study presents a method how wind turbines effect on radio relays can be calculated.

One key aspect in the Swedish study is that the level of the wanted direct field under fading events is considered to be un-correlated to the level of the scattered field from the wind turbine. That is, when the wanted signal fades down, the level of the interfering signal may be more or less unaffected. Another aspect of the Swedish study is that the delay of the scattered field, compared to the direct field, needs to be taken into account in the analysis. These key aspects are necessary for explaining measurements results done on radio relays equipment with wind turbines close to the radio link's line of sight.

Furthermore, the aperture model allows detailed analysis of the propagation effects introduced by a wind turbine close to a radio link's line of sight. In other cases than close to line-of-sight, the aperture model needs to be used in combination with other models.

The Swedish study suggests that even if the degradation from wind turbines are small or negligible under normal propagation conditions, there may be a significant effect on the available fade-margin, reducing the performance and availability of the radio link.

Annex A1.2 gives the system parameters for the radio links included in the Annex A1.1 study.

Annex A1.3 gives an in depth technical explanation of a simple calculation model of the same type as used in Annex A1.1 for explanation purposes.

Annex A1.4 gives an example of a method of using the aperture model in assessing the impact of wind turbines on radio links. This method also discusses dependence of various radio parameters, transmission capacity, error performance requirements etc. as well as the size of the wind turbine.

ANNEX 2: describes a methodology developed by the University of the Basque Country (Spain), which is used to analyse the impact of a wind farm on the surrounding radio communication services. The calculations are based on the configuration of a specific wind farm and the different transmitters and receivers over a terrain database containing high resolution altimetry data.

Graphic and numerical results of the analysis are presented on a map, which allows an on-the-spot evaluation of the degradation mechanisms for each wind turbine.

The prediction of the potential impact of a wind farm on the existing radio communication services before its installation is used for the planning of alternative solutions to ensure the coexistence of wind energy and telecommunication facilities. Although some guidelines for safeguarding radio communication services have been recently published, the precise impact on a specific service can only be determined on a case-by-case basis, due to the multiple factors that must be considered in the analysis.

3   CONCLUSIONS

This report collects studies and information on the technical impact of wind turbines on various radio communication services. This report covers only fixed service point to point radio links.

Measurements performed on several link paths in Sweden have shown that interferences from wind turbines are usually small under normal atmospheric conditions. However, when the signal strength is reduced by significant fading events, the interference may be not necessarily small.

Various methodologies to estimate the impact of wind turbines are applied or planned to be applied in some CEPT administrations. However, it has not been possible within the scope of this study to evaluate the suitability and accuracy of each method, which would require much more significant work. Therefore, this report reflects only the state of the art on this issue for some administrations.

ANNEX 1: CONTRIBUTIONS PROVIDED BY SWEDEN

A1.1 MODELLING THE EFFECTS OF WIND TURBINES ON FIXED RADIO LINKS

A1.1.1   Introduction

The growing number of wind turbines all over the world could be a critical performance problem for microwave radio links. Many of these radio links serve as a fixed backbone network for the military defence as well as for other community-critical services. Fixed radio links are also a vital part of radio and television distribution systems. In general, the users of those networks have very high demands on link availability.

Interference from wind turbines on various radio services has been investigated over the years. In particular, the effects on television broadcast services in the VHF and UHF bands have been studied quite extensively and models to predict the effects on both analogue and digital television reception have been suggested. For example, in [1], Spera and Sengupta propose a simple model for prediction of the scattered television signal from wind turbines. Their model is based on a large empirical material from measurements in USA during the late 1970s and early 1980s, see references in [1]. Other works dealing with effects from wind turbines on the reception of broadcast services can be found in several ITU reports, for example, analogue and digital television and radio services [2],[3],[4].

Wind turbine effects on radar is also rather well covered in the literature, see for example [5],[6],[7],[8].

Interference effects from wind turbines on fixed radio links seem not to have reached the same attention as the effects on broadcast services and radar systems. However, the effects of wind turbines on fixed radio links are investigated in [9],[10],[11],[12] and these works shall be discussed in more detail in A1.1.1.1.

In this report we study how scattering from wind turbines may impact the performance of fixed radio links and suggest a way to model the effects. The turbines are assumed to be located between the link terminals and relatively close to the direct path between the antennas. That means that the contributions from the turbines can be described by forward scattering only. Because most fixed radio links use highly directive antennas, interference from turbines outside the validity region of the forward-scatter approximation is expected to be sufficiently attenuated by the antennas. This approximation is not possible for many other services (e.g., broadcast and radar).

A1.1.1.1 Previous Work

In the work by Bacon [9], a method for establishing an exclusion zone around a fixed radio link is proposed. The exclusion zone is based on three criteria: near-field distance, Fresnel zone, and excessive reflection/scattering zone. The first criterion excludes wind turbines within an area where the antenna far-field pattern is not valid –- that is, where the antenna gain for scattered components cannot be determined easily. The second criterion excludes wind turbines within the second Fresnel zone (to reduce shadowing). The third criterion excludes positions where the scattered power may exceed a certain threshold. The scattered power in criterion three is assumed to be computed based on the bistatic radar cross section (RCS) of the wind turbine. However, as acknowledged in [9], this property is often not readily available. Furthermore, RCS is a measure that is valid only when both transmitter and receiver are located in the far-field region of the scattering object. For large objects, such as wind turbines, one, or both, of the link terminals may easily be located in the near-field region of the object.

A case study of interference from wind turbines on a non-line of sight UHF radio telemetry link is presented in [10]. The reported predicted path loss for this link exceeds the free space path loss with about 34 dB and the closest wind turbines have a line of sight path to both link ends. The findings in this case were that the wind turbines were causing a variation in signal strength at the receiver of more than 40 dB.

In [11], a method to calculate clearance zones for UHF telemetry systems is outlined. The method is based on the method described in [9] but allows for propagation paths that do not have the first Fresnel zone clear.

Measurements of effects from wind farms at different frequency bands between 0.4 and 38 GHz are reported in [12]. The interference levels were characterized by the fading amplitude in several angles from a single wind turbine as well as from a wind farm with 17 turbines. Power delay profile measurements were also performed at two frequency bands for a more limited number of positions. Furthermore, under the assumption that the scattering can be described by the standard bistatic radar equation [9], RCSs are inferred from the estimated interference levels. The complications from that the measurements were performed within the near-field regions of the turbines are, however, not discussed. Nevertheless, the RCSs obtained were, in general, 5-20 dB larger for forward scattering than for backscattering.

A1.1.1.2 Swedish Study Contributions

The Swedish study show that the scattered power from a wind turbine, located within the forward scattering region, can be predicted accurately with an aperture model. The field at the receiver is obtained by numerical integration over the silhouette of the turbine. That eliminates the reliance upon uncertain RCS values and is valid also in the near field region of the wind turbine.

Analysis of measurements from several fixed links, with wind turbines in close proximity, indicates that the strength of the signals scattered from the turbines are more or less unaffected by atmospheric fading events that affect the wanted signal. Computer simulations of scattering from wind turbines under anomalous atmospheric conditions support those observations. The low correlation observed between the wanted and unwanted signals has important implications on estimates of link availability.

Finally, we also present a simple software tool for evaluating the impact of wind turbines on radio links. The tool is based on an aperture model for forward scattering and can compute the effects from multiple wind turbines. Terrain obstructions can be accounted for by a diffraction model.

A1.1.2   Measurements

In this section we present results from measurements on three different radio links that have wind turbines in close proximity to the link path. Two of the links are civilian and operates at 8.2 GHz and have a path length of approximately 21 km. The third link is military and operates at 2 GHz and has a path length of 60 km. One of the 8.2 GHz links and the 2 GHz link are frequently affected by natural fading events and the effects from the wind turbines have been measured under both normal and faded conditions.

A1.1.2.1 Falkenberg − Varberg

This is a 21.5 km link that operates at 8.2 GHz between Varberg and Falkenberg in Sweden. The link path, which is located near several wind turbines, can be seen in Figure 1. The path is relatively steep, which makes this link quite insensitive to fading caused by atmospheric effects (i.e., refraction index variations). However, the most interesting part with this radio link is that two of the wind turbines are located very close to the direct path of the link and that the effects of these turbines are clearly visible in measurements of the received signal level when the turbines are turning.

In Figure 2, which shows the view from the antenna in Falkenberg towards Varberg, the two wind turbines to the right in the picture are close to the direct path of the link. These turbines are located about 45–50 metres and 70–75 metres from the direct path, respectively, and are of the Vestas V80 model with a rotor diameter of 80 metres and a hub height of 80 metres above the ground. The turbines are located approximately 7 km from the Falkenberg end of the link and the radius of the first Fresnel zone at the turbines is about 13 metres. As a result, the influence of these turbines is more or less always visible in measurements. Figure 3 shows a typical registration of received signal level, where the level varies in the order of ± 2.5 dB. The variations are periodical and the only reasonable explanation is that those are caused by interference between the direct field component and components scattered by the turbines. As far as we know, the atmospheric conditions were normal during the measurements. Moreover, the link geometry appears to be rather insensitive to variations in atmospheric conditions as no severe fading events have been observed during long term measurements. In addition, when computing the propagation for this link with a Parabolic Equation (PE) model, it was difficult to construct a realistic refraction index profile that would produce any deep fading of the signal level at the receiver.

Although, the interference does not affect the performance of this link, it raises some questions of the performance of other links that may be affected by atmospheric fading more easily than this one. Another question is how much worse the effects from larger wind turbines would be.
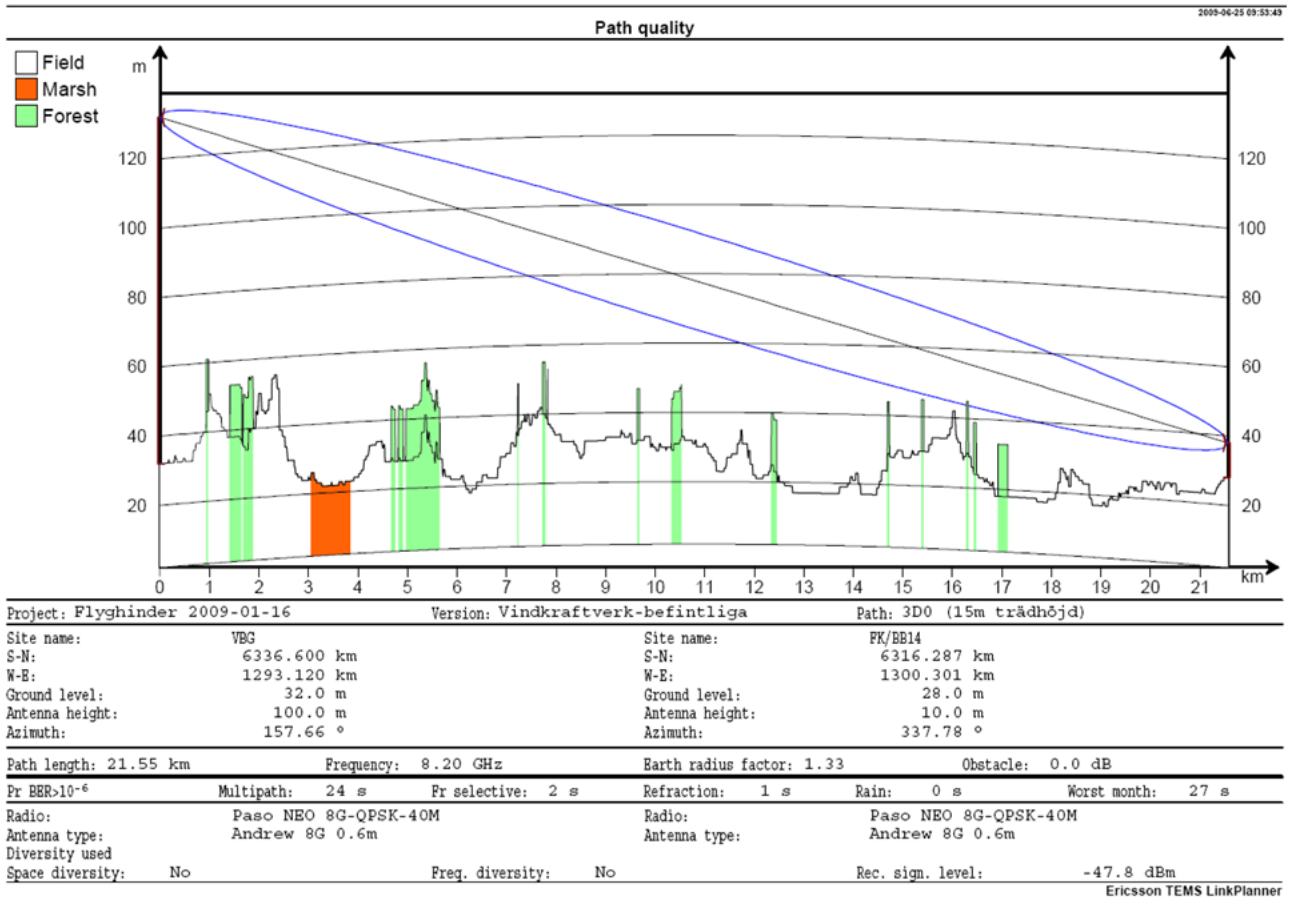

Figure 1: Propagation path of the Falkenberg-Varberg radio link

**Figure 2: View from the antenna at Falkenberg towards Varberg.
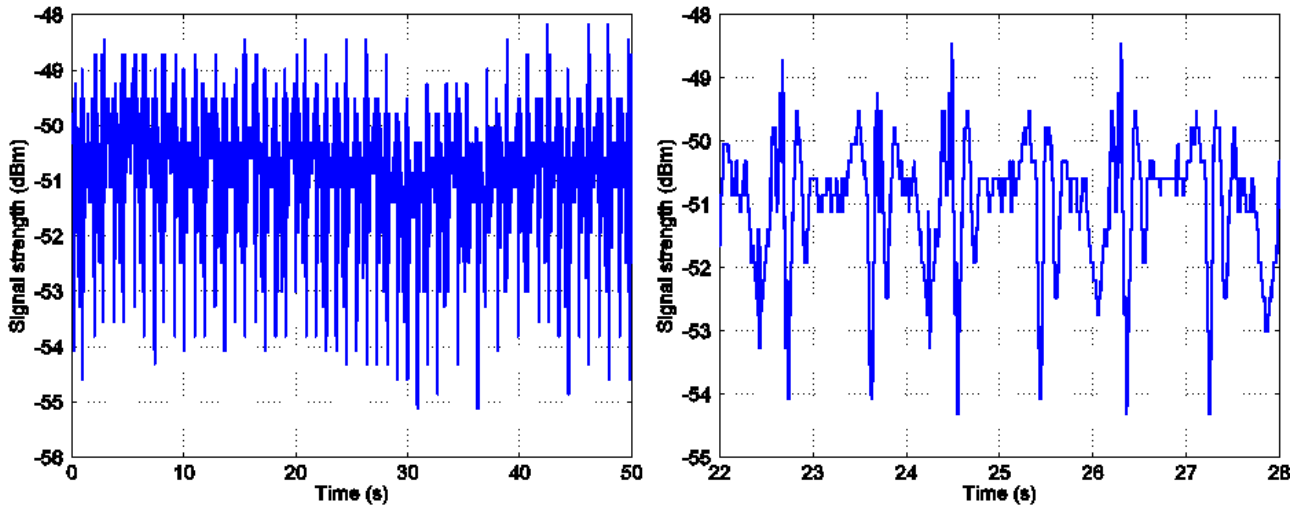The Varberg antenna position is marked by a red circle**

Figure 3: A typical measurement result for the Falkenberg-Varberg radio link

A1.1.2.2 Malmö − Barsebäck

The second link to show results from is a 21 km link between Malmö and Barsebäck in southern Sweden. The link operates on 8.2 GHz and a significant part of the path is over water. Because of the latter fact, water reflections may, under certain atmospheric conditions, result in significant fading. To mitigate fading, the link has a diversity arrangement consisting of a dual polarised antenna at Barsebäck and one antenna for each polarization, located at two different heights, at Malmö. A wind turbine is located at about 120 metres perpendicular to the direct path, at a distance of about 7 km from the link end in Malmö, which results in that the turbine blades sweep Fresnel zones in the range from about 42 to 139. The rotor diameter is 70 metres and the hub is located about 75 metres above ground. In Figure 4, which shows the view from the antenna in Malmö towards Barsebäck, the wind turbine can be seen to the right of the marked antenna position. The water at the Barsebäck side of the path is also visible in the distance in the same photo.

Figure 5 shows a fading event for the horizontal polarization in four different timescales. In Figure 5(a), which shows both polarizations, we see that the vertical polarization is only slightly affected throughout the whole event, whereas the horizontal polarization is highly affected. Moreover, superimposed on a rather slow fading component we can see a component that varies very rapidly. The latter component is probably caused by interference from the field scattered by the wind turbine.

In Figure 5(b), the blue curve shows the instantaneous received signal level, whereas the red curve shows a moving average of the signal level. Interestingly, the amplitude (in decibels) of the rapidly varying component seems to increase as the averaged values (red curve) decreases. That is, the relative contribution from the interfering component increases. The black curve is formed by subtracting the moving average (red curve) from the instantaneous values (blue curve) and adding an offset of -20 dB. From Figure 5(c) and Figure 5(d), which show the instantaneous signal level in shorter time frames, it is clear that the rapidly varying level is periodic and consistent with interference from a rotating wind turbine.

**Figure 4: View from the antenna at Malmö towards Barsebäck.
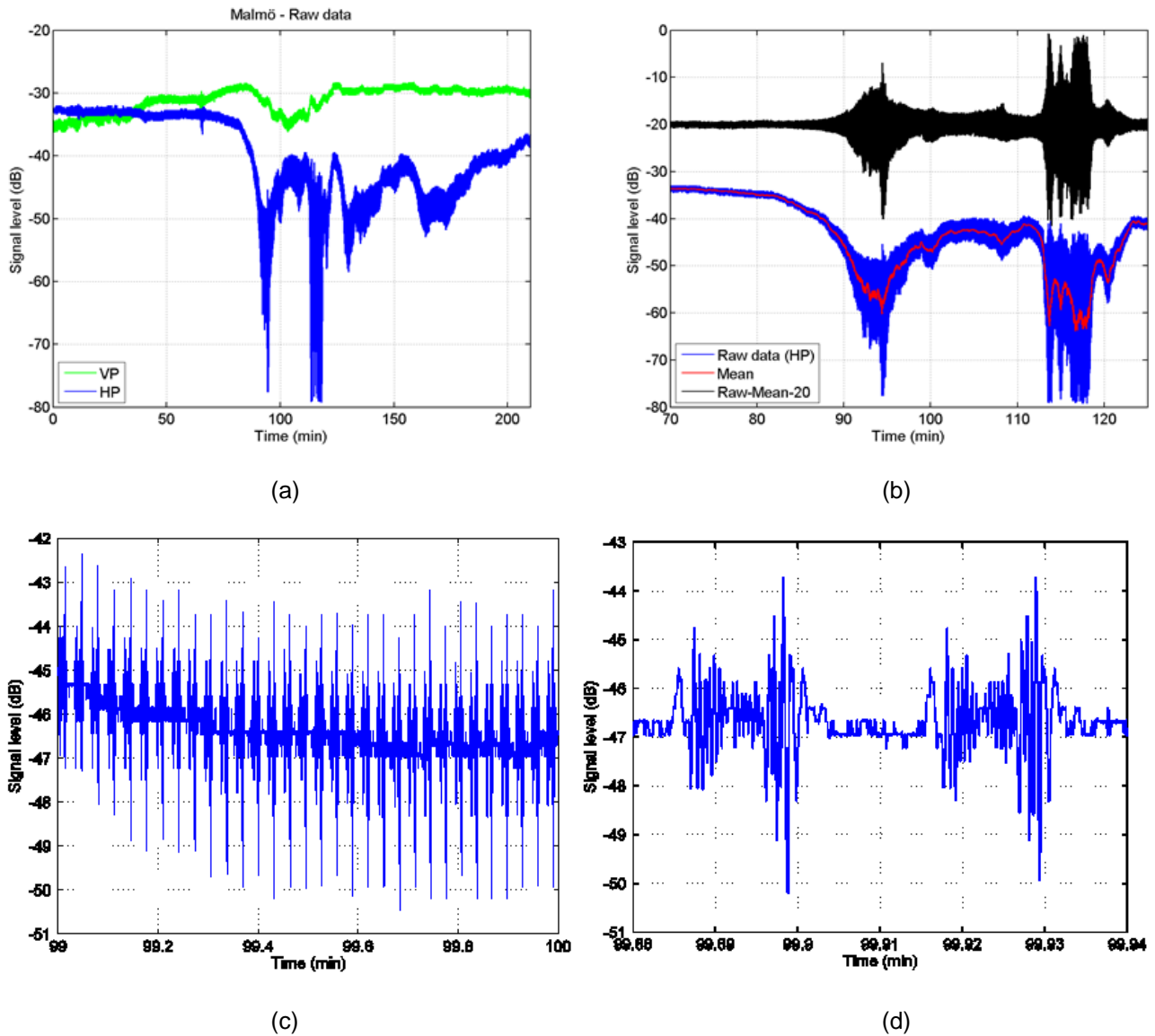The Barsebäck antenna position is marked by a red circle.**

(a)

(b)

(c)

(d)

Figure 5: Fading events for a 8 GHz 21 km path over water in different time scales: (a) 210 minutes, (b) 55 minutes, (c) 60 s, and (d) 3.6 s

A1.1.2.3 Military 2 GHz link

The third measured link is military and operates at 2 GHz. The path length is 60 km and no significant water reflections can occur along the path. The link is, however, frequently affected by fading events of various degrees. In Figure 6 a fading event for the link is shown. Here, the signal strength is reduced by a naturally occurring tropospheric fading event of about 15–30 dB. The turbines located near the direct path are quite small and have a rotor diameter of 52 m (Vestas V52). The two turbines closest to the radio link are located about 50 m perpendicular to the direct path. Even though the turbines are small, the interference from the scattered field becomes significant when the signal strength fades down. Clearly, the strength of the direct signal component and the scattered components from the turbines are not correlated in this measurement. The interference from the wind turbines worsens when the direct signal component of the radio link fades down. In this report, we investigate how significant the effect of wind turbines can be on the available fading margin for a link.
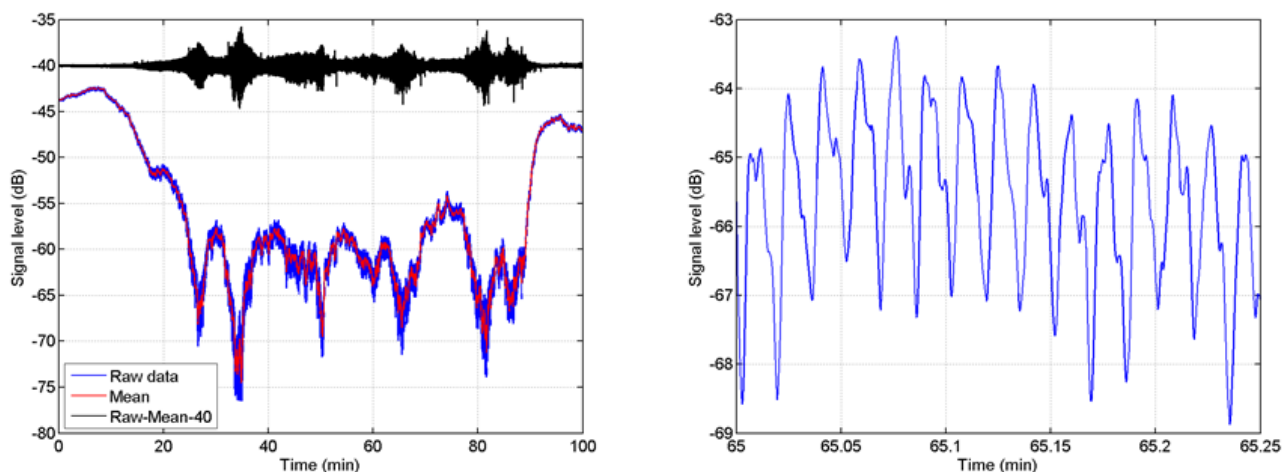
Figure 6: Fading events for a 2 GHz 60 km path in different time scales: (a) 100 minutes and (b) 15 s

A1.1.2.4 Observations from the measurements

The most important observation from the measurements is that the signal level of the scattered (interfering) components from wind turbines in our measurements seems to be more or less unaffected by the fading event. The hypothesis that the level of the scattered field from a wind turbine has a low correlation with the level of the direct component is investigated further in the following sections.

A1.1.2.5 Conclusions from the measurements

The following items are the main conclusions from the measurements:

1   The scattering from wind turbines can have severe effects on fixed radio links, even when the turbines are located at distances well beyond the first Fresnel zone of the link.

2   The level of the scattered signal is much less affected by natural fading than the wanted signal and the correlation between the signal levels seems to be low. The largest risk for degradation is thus when the wanted signal is affected by natural tropospheric fading. However, under normal propagation conditions, it can often be difficult to detect any significant effects from wind turbines.

3   The rapidly varying phase and magnitude of the scattered signal, as the turbine turns, can easily give rise to destructive interference between the direct and scattered signals, even when viewed in timespans of only a few seconds.

4   The depth of the fades caused by destructive interference between the direct and scattered signal depends on the relative levels of the direct and scattered signal.

A1.1.3   Modelling

Fixed radio links that operate at microwave frequencies are generally equipped with antennas providing fairly narrow beams. As a consequence, scattering from outside the combined beam patterns will be suppressed rather effectively. Given this fact, the important region to consider for potential interference from wind turbines is located within an area between the two link terminals that is limited by the beam widths of the antennas. That is, the interference field from wind turbines would be well described by forward scattering if the beam widths are sufficiently narrow. Forward scattering can be viewed as a form of diffraction effect, in which an object located somewhere between the transmitter and receiver disturbs the propagating field. It is not necessary that the object is blocking the direct path − an optical analogy to this would be a diffuse shadow.

A1.1.3.1 Modelling assumptions

Based on geometrical considerations (mentioned in the introduction above) and conclusions drawn from our measurements we make the following assumptions:

1   The scattered field from a wind turbine is dominated by forward scattering.

2   The forward scattering can be computed by an aperture model.

3   The variations of the scattered field from the turbine rotor is at least one magnitude faster than the natural fades caused by tropospheric multipath propagation. This implies that there is a high probability that the scattered turbine field will cause destructive fades during a natural fading even.

4   For geometries where the scattered signal level is significant, the excess delay of the scattered signal is typically shorter than the modulation symbol time. Hence, in many cases, any fading caused by interference between the direct and scattered signal can be considered flat over the bandwidth of the radio link. However, as the fading can be very fast, it is quite reasonable to believe that the effects on link performance may be equipment dependent; for example, control loops for automatic gain control and carrier phase recovery, as well as equalising, may have primary been designed with slow tropospheric fading in mind.

A1.1.3.2 Aperture model

In a case where the angle from the transmitter to the object and the angle from the object to the receiver both are small, we can compute the forward scattering by using a combination of Kirchhoff-Fresnel theory [10] and Babinet's principle [10]. First the undisturbed field is computed, i.e. the field without wind turbines. Then the part of the field that is screened by the turbines is computed. This so called aperture field is computed by applying Kirchhoff-Fresnel theory to the apertures (in planes perpendicular to the direct path) that the turbines form. In this work, the turbine blade is divided in to a number of apertures with the size 50×50 cm or 25×25 cm and the fields of all apertures are then summed up to give the total aperture field. The resulting field is the part of the undisturbed field that is screened by the turbines. According to Babinet's principle, the total field is then the undisturbed field subtracted by the aperture field of the turbines.

A1.1.3.3 Link margin degradation

The simplest (and most optimistic) model for link margin degradation is based on the assumption that the only detrimental effect caused by the scattered field is a reduction in the received signal level by destructive interference. If we assume that the phase of the scattered signal varies rapidly, as the turbine turns, the probability for cancellation between the direct and scattered signal is high. If A_d denotes the direct signal amplitude and A_s the scattered signal amplitude, the resulting signal amplitude becomes

$$A_r = A_d - A_s. \tag{A1-1}$$

The radio between the resulting signal amplitude and the direct signal amplitude can be expressed in decibel as

$$\left[\frac{A_r}{A_d}\right]_{\text{dB}} = 20\log_{10}\left(1 - \frac{A_s}{A_d}\right) \tag{A1-2}$$

Whether the simple model for link margin degradation is adequate for assessment of interference effects may depend on the radio equipment and on how much excess delay the scattered signal from a wind turbine has. For example, if the scattered signal is delayed one symbol time, or more, the interfering signal will contain symbols that are independent of the current symbol and the interference must be considered as an additive random signal. Hence, the simple model is not valid in that case. On the other hand, if the scattered signal is delayed much less than one symbol time, the interfering signal can be viewed as a phase shifted version of the direct signal. The validity of the simple model in this case depends on whether the time constant of the phase and amplitude recovery circuits in the receiver is fast enough with respect to the

variation of the scattered signal. Similarly, the performance of equalisers in the presence of multipath signals from wind turbines is expected to be equipment dependent.

Laboratory measurements on a number of different radio link equipment, both with and without equalizers, suggest that performance differs widely, both between types and between manufacturers of similar types of equipment. Particularly, large differences were observed for channels with fading frequencies of 100 Hertz, and above, at delays shorter than one symbol time. In general, the equalizers could handle delays up to about ten times the symbol time, but their performance degenerated rather rapidly for fading frequencies over a few Hertz.

A1.1.3.4 Model validity regarding forward scattering

As the aperture model considers forward scattering only, the overall model validity depends on that the antennas attenuate any interference outside the validity region of the aperture model.

To accurately characterize the validity region of the aperture model, comparisons have to be made with a full scattering model that uses a detailed three-dimensional description of the turbine blades. This have not, however, been feasible within the study. Attempts to estimate the validity region from a more simplified description of the turbine blades, based on a rectangular single-curved plate, oriented for a worst case that allows specular reflection, were shown to provide results that were not fully conclusive because of the crude geometrical approximations involved.

However, analysis of data from our measurements on several radio links has not revealed any signal variations that could not be satisfactory explained by the aperture model. This supports our assumption that an aperture model would be adequate for microwave links with directional antennas.

A1.1.4 Simulations

A1.1.4.1 Parabolic Equation Modelling

Parabolic equation (PE) models are efficient means to solve a parabolic approximation of the elliptical wave equation over a variable terrain profile [11]. One important advantage of these models, compared to other models, is that the refractive index profile of the atmosphere can be considered easily. The latter is important in our investigation of what influence the atmospheric effects have on the level of the scattered field from wind turbines. Furthermore, the PE model used is based on the finite difference method in [12]. This method is computer intensive but gives very accurate result for hilly terrain.

Thus, one part in the investigation is to use a PE model when computing the field. This field is then used as the input field to the aperture model above. The field will be calculated for normal and non-normal atmospheric conditions, which should give some information of what influence atmospheric effects have.

A1.1.4.2 Atmospheric Effects

Here, some PE-results are shown for a military radio link with centre frequency of about 2 GHz; see Figure 7. The location of the link is restricted, which means that the terrain profile has been masked to some extent. One reason for using this link for our simulations is the large set of measurements available for this link. (An example of the measurements was given in Figure 6).

In Figure 7 simulation results for normal atmospheric conditions and two ducts are shown. The results are presented as propagation factors, i.e. fields above the free space field. The three atmospheric conditions give different results in the area of interest. The differences should be significant enough for our investigation of what influence atmospheric effects might have on the level of the scattered field from wind turbines. Results for the different atmospheric conditions are presented in the next section. The chosen ducts are from a set of ducts used in an earlier work, from which duct 1 and 3 were the interesting ones. The reason for this choice is that duct 1 is a ground based duct and duct 3 an elevated one, i.e. two different types of ducts, see Figure 7 (b) and (c).
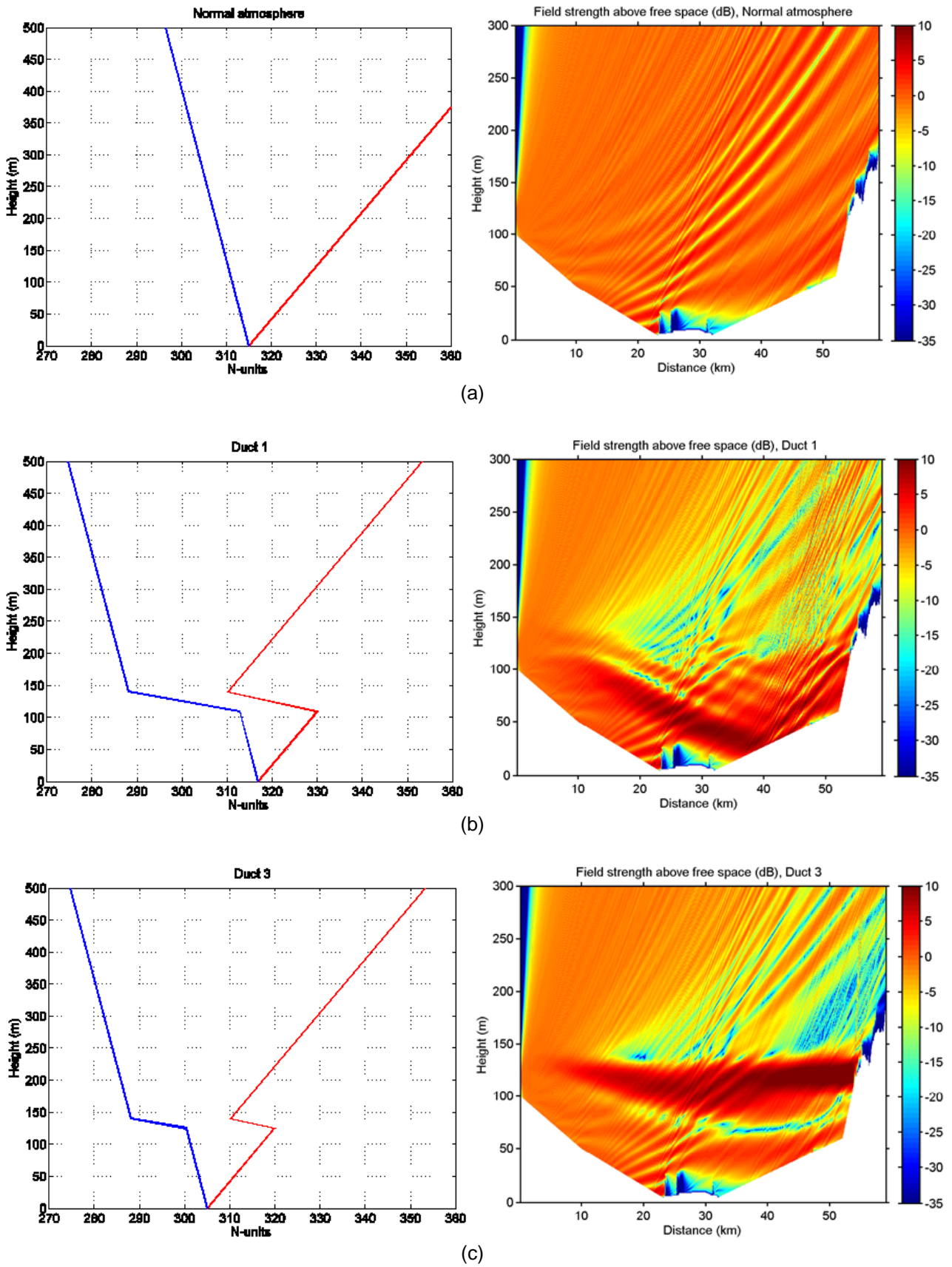
Figure 7: Refractivity (blue) and modified refractivity (red) for different atmospheric conditions (left) and the corresponding field computed with the PE-model (right): (a) normal atmosphere; (b) duct 1; (c) duct 3

A1.1.4.3 wind turbine Simulations

In this section, simulation results for a radio link with wind turbines near its direct path are shown. The results are for the 2 GHz link in A1.1.2. The first result is for a Vestas V52 turbine (or a corresponding one) and is shown in Figure 8. The second is for a Vestas V100 turbine and is shown in Figure 10. The turbines are placed at a distance of 38.8 km from the transmitter and 50 m perpendicular out from the direct path (with a total path length of about 60 km). The rotation plane of the blades is perpendicular to the direct path, which should represent a worst case as far as interference from the turbine is considered.

Considering the result in Figure 8, the maximum turbine field is quite stable in all three of the left figures, where the maximum field is the maximum value during one revolution (with a period of 5 s). The variation in each figure is within a few dB regardless of the antenna height. Also, the variation between the figures with different atmospheric conditions is within a few dB. Both these observations are important. One consequence is that there is no reason for using a complex propagation model such as a PE model, as the atmospheric conditions seem to be of little importance. In other words, a simple propagation model for normal atmospheric conditions should give a turbine field of correct order within a few dB. For instance, considering the left hand plot in Figure 8(a), the difference in dB between the field with no turbine (the undisturbed field) and the maximum turbine field is about 30 dB, which would mean that the undisturbed field has to fade down about 30 dB before the interference from the turbine gets severe. In the right hand plot in Figure 8(b), the undisturbed field is down faded about 25 dB, which results in a visible ripple of about ±2.5 dB. This variation is probably not big enough for the radio link to go down. In the right hand plot in Figure 8(c), the ripple is of the same order. Furthermore, considering the measurement result in Figure 6(b), the signal is here down faded about 25 dB, which also is the case in the right hand plot in Figure 8(b). The turbine closest to the direct path in the measurement is located about 50 m out from the direct path and the turbine corresponds to a Vestas V52. The ripple in Figure 6 (b) and the ripple in right hand plot in Figure 8(b) is of the same order, i.e. about ±2.5 dB, which at least in this case means that the aperture model works.

The interference seen in Figure 8 is not that severe. However, it depends a little on the chosen height. Considering the right hand plot in Figure 9, where the chosen height is 211 m above sea level, the undisturbed field is here down faded about 32 dB and the interference from the turbine is severe. It can be seen that the momentary fade depth increases by the turbine induced ripple, and that outage on the radio can occur during shallower natural fades than otherwise. For example, a relay with 35 dB margin would not be affected without turbines, but would get transmission errors with turbines present.

Figure 8: Result for the PE model and a Vestas V52 turbine, with the rotation plane perpendicular to the direct path and a rotation frequency of 0.2 Hz. Left figures: result for heights between 206-222 m. Right figures: result for a single height of 219 m. (a) Normal atmosphere, (b) duct 1, and (c) duct 3

Figure 9: Result for the PE model, duct 1, and a for Vestas V52 turbine, with rotation planes perpendicular to the direct path and a rotation frequency of 0.2 Hz. Left figure: result for heights between 206-222 m. Right figure: result for the height 211 m

The next example is for a Vestas V100 turbine, with a blade diameter of 100 m. The result for this turbine is shown in Figure 10. Again, the maximum turbine field is quite stable in all three of the left figures. The variation in each figure is within a few dB regardless of the antenna height. Also, the variation between the figures (the different atmospheric conditions) is within a few dB, i.e. -21 ±4 dB. According to the left plot in Figure 10(a), if the undisturbed signal is down faded about 20–24 dB, the interference from the turbine can be severe. In the right plot in Figure 10(b), the undisturbed signal is down faded 26 dB and the interference is severe. In Figure 10(c), the undisturbed signal is down faded 18 dB and the interference is even more severe here. Although the resulting field probably is large enough, its variations are too large and rapid, i.e. the radio link would probably go down.

Clearly, considering the left hand plot in Figure 10(a), it is possible to estimate the fading margin of a link by analysing the field from turbines in normal atmospheric conditions. The Left hand plot in Figure 10(a) gives a margin of about 20–24 dB. The Left hand figures in Figure 10(b) and (c) give margins of about 20–25 dB and 18–21 dB, respectively. How bad the interference from a turbine can be depends how destructive it can be. For instance, if the undisturbed signal is completely cancelled, the received signal will be zero (i.e. −∞ dB). In the right figures in Figure 10(b) and (c), the interferences are both destructive and constructive, which result in very rapid variations. Thus, considering Figure 10(a), if the undisturbed field fades down 20 dB in this case, one can conclude that the risk for severe interference from the turbines is imminent. Note that we in this example have assumed that the detection threshold of the link is lower than the level of the turbine field. If that is not the case, the link will be affected by the natural fading before the interference from the turbine has any significant effect on the link margin.
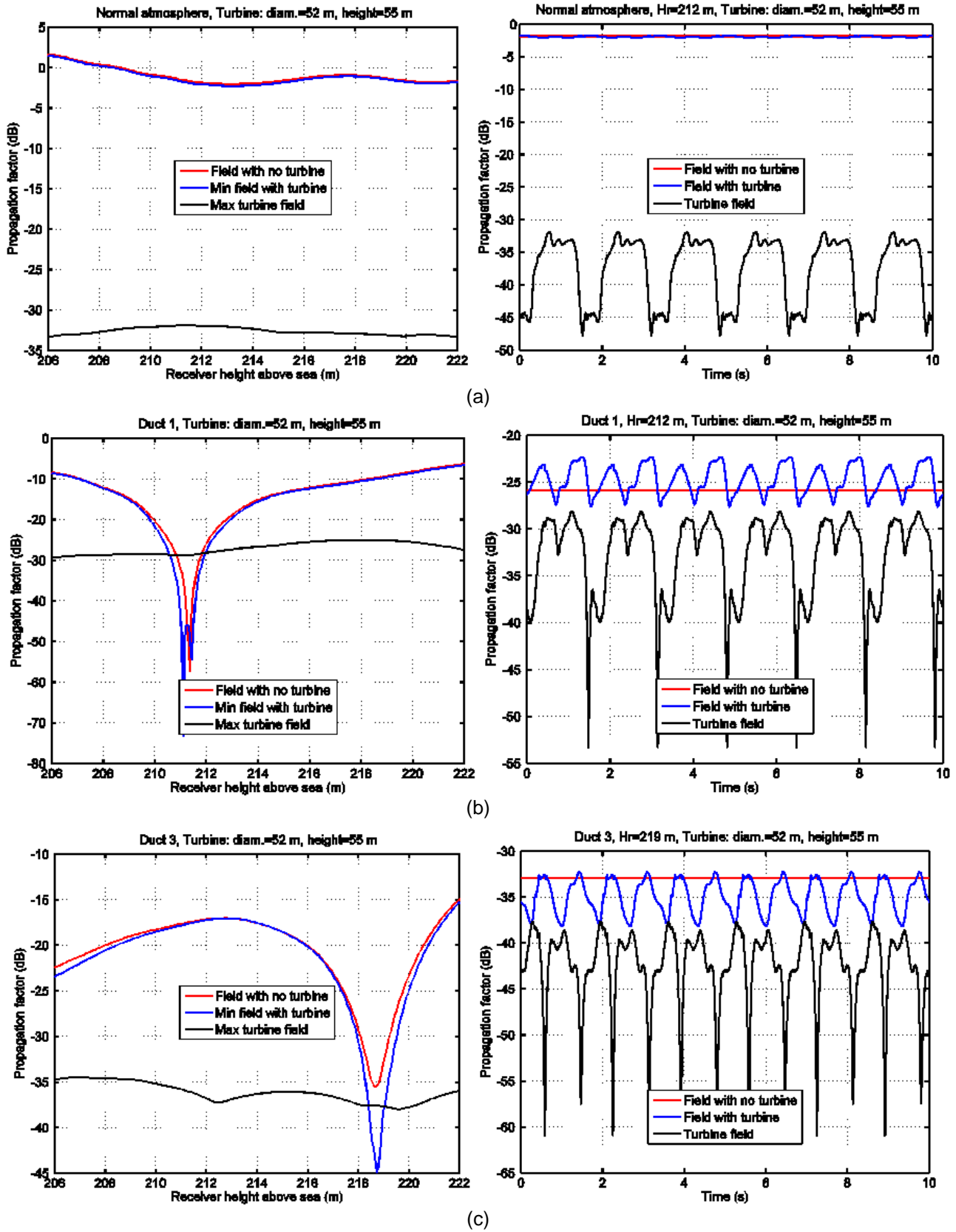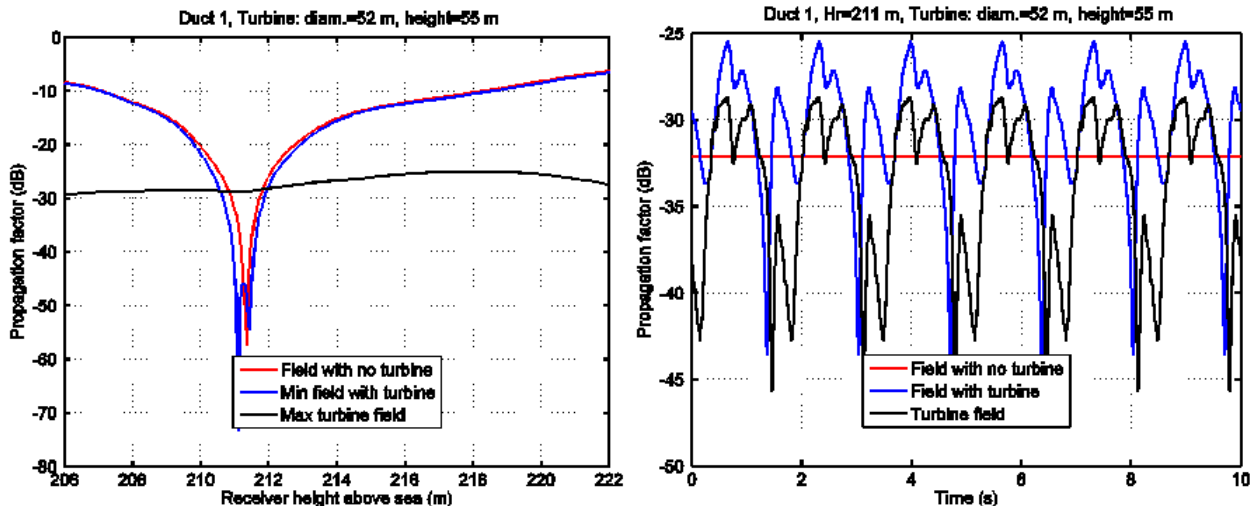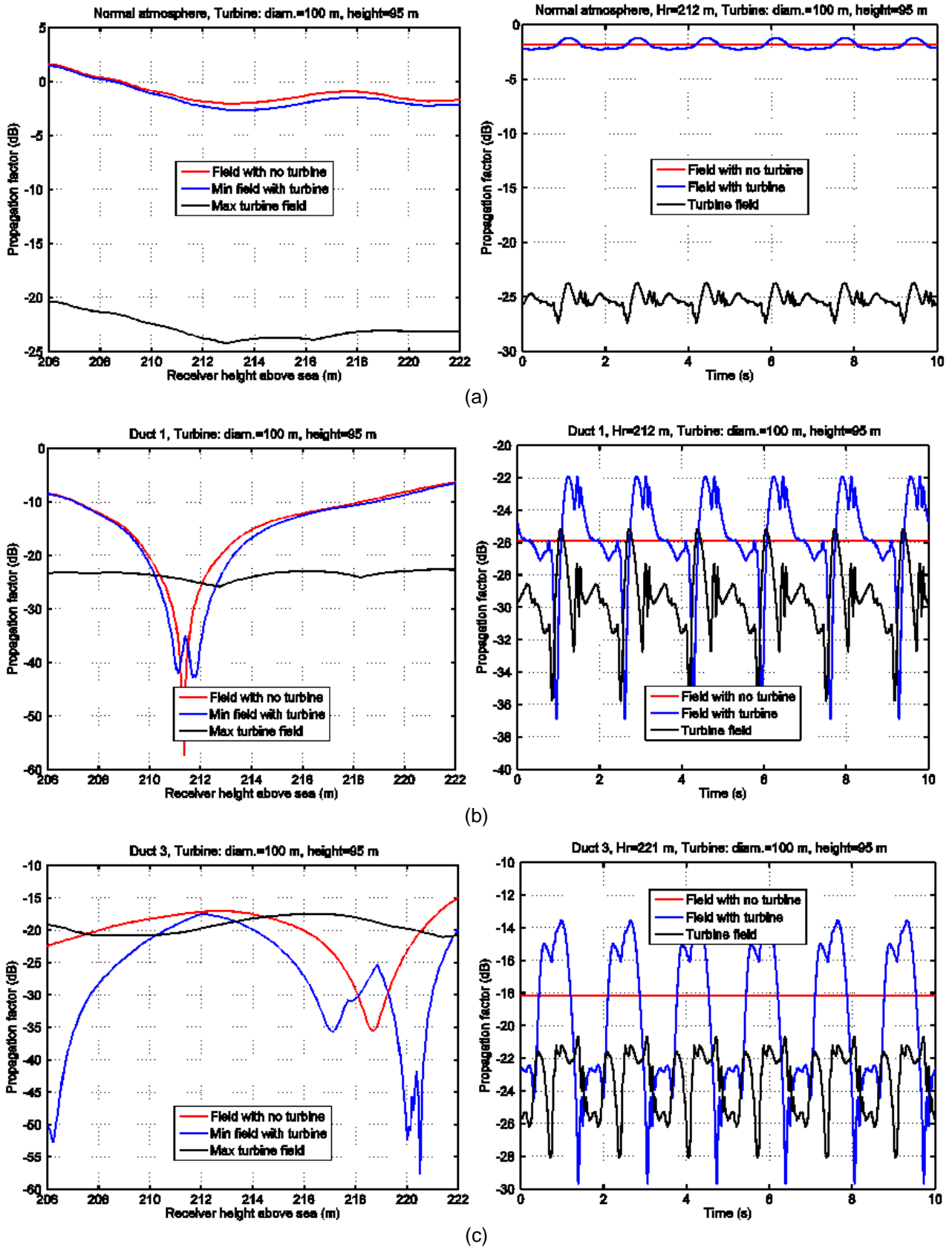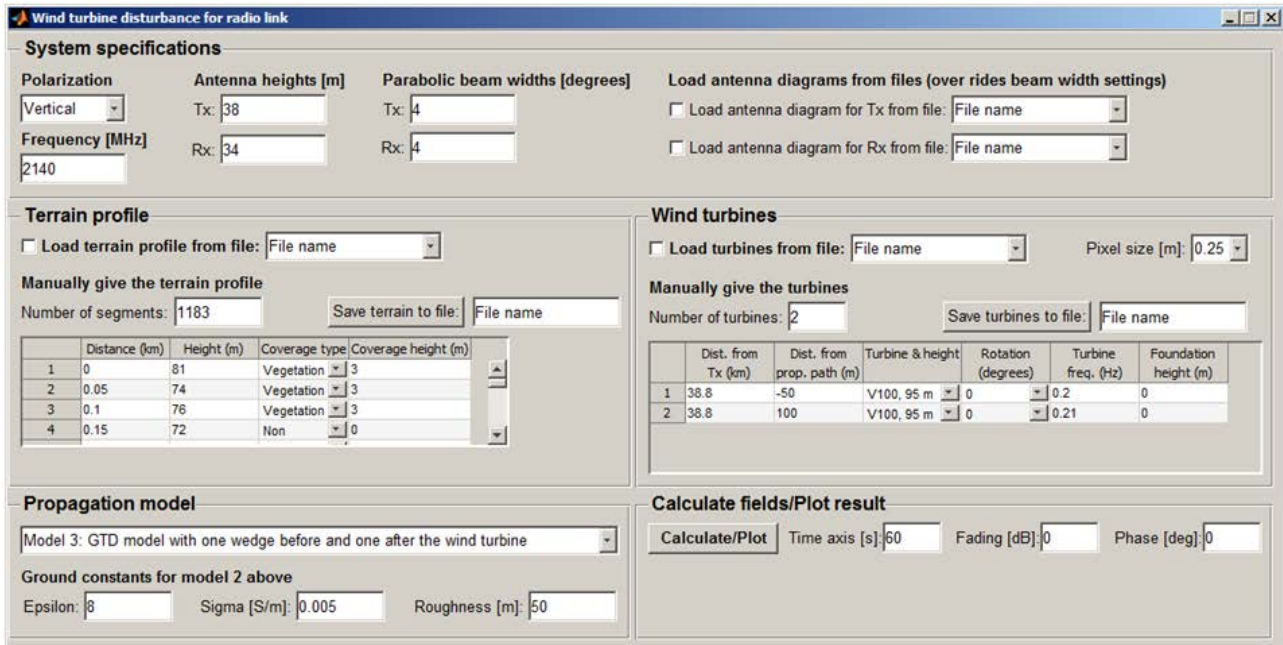
Figure 10: Result for the PE model and a Vestas V100 turbine, with the rotation plane perpendicular to the direct path and a rotation frequency of 0.2 Hz. Left figure: result for heights between 206-222 m. Right figure: result for a single height. (a) Normal atmosphere, (b) duct 1, and (c) duct 3

A1.1.4.4 Simulation tool

A simulation tool using a graphical user interface has been developed in MATLAB. With this tool the influence of different wind farm scenarios can be simulated using different propagation models, which all are simple and valid for normal atmospheric conditions only. Furthermore, each turbine is defined by its type, height, distance from the transmitter, distance perpendicular out from the direct path, rotation relative the direct path, turbine frequency, and foundation height. The implementation can calculate the scattering from the tower itself, the blades as well as the total field using user defined antenna patterns. Currently the tool only support one single terrain profile but that limitation will be omitted in future releases and it will also be possible to read the profiles from a terrain data base (manual input as an option). In Figure 11 a snapshot of the guide window of the tool is shown.

Figure 11: User interface of the developed wind turbine tool

A1.1.4.5 Comparison between PE and GTD calculations using the Simulation tool

In the following figures some results for two Vestas V100 turbines are shown. The two turbines are placed at a distance of 38.8 km from the transmitter (total path length approx. 60 km). Furthermore, they are placed 50 and 100 m out from and on opposite side of the direct path. The parameters chosen for this simulation are shown in Figure 11.

In Figure 12, obtained with the PE model, the difference between the undisturbed field (red solid line) and the turbine field (black solid line) is at least 19 dB for the height 219 m above sea level.

In Figure 13, the output from the wind turbine tool is shown. This result corresponds to the one in Figure 12.

The difference between the undisturbed field (red solid line) and the turbine field (black solid line) is in Figure 13 at least 16 dB for the height 219 m above sea level, which is 3 dB less than in Figure 12. On the other hand, 3 dB is not a big difference when it comes to this type of comparison. In addition, the signal patterns are very similar in the both cases.

The propagation model used in the wind turbine tool is a simple GTD model, where one wedge before and one after the turbines are considered. The tool also includes models for free space and flat earth.
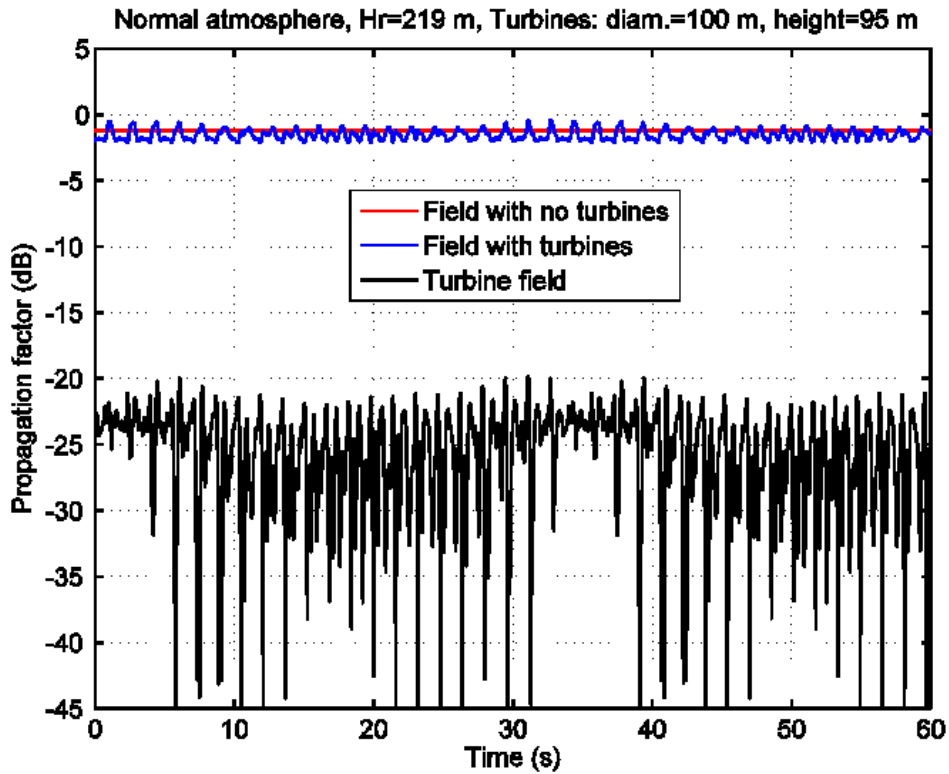
Figure 12: Propagation factor for the PE model and the height 219 m.
The result is for normal atmosphere and two Vestas V100 turbines, with rotation planes perpendicular to the direct path and rotation frequencies of 0.2 and 0.21 Hz
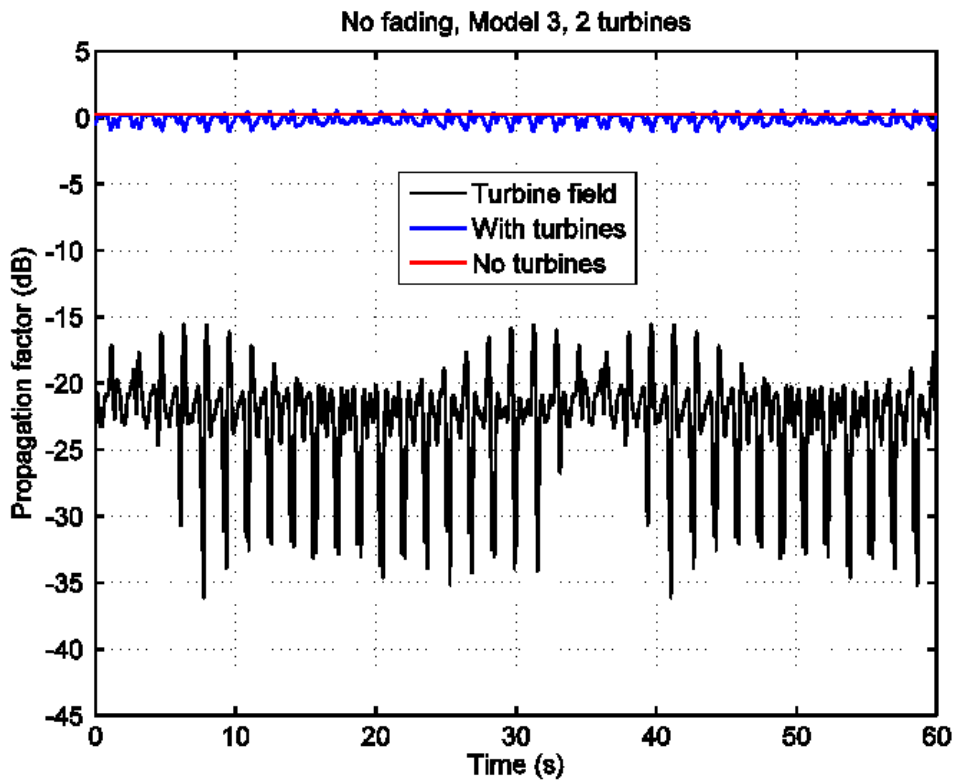
Figure 13: Propagation factor for the wind turbine tool and the height 219 m.
The result is for two Vestas V100 turbines, with rotation planes perpendicular to the direct path and rotation frequencies of 0.2 and 0.21 Hz

A1.1.4.6 Conclusions from simulations

From the simulation results, we make the following conclusions:

1   The observed phenomena in the measurements can be satisfactorily reproduced by a time-varying aperture model. The aperture is defined by the projection of the wind turbine on a plane through the turbine, perpendicular to the link path. The time variation is obtained by computing new apertures as the rotor of the turbine turns.

2   The level of the scattered field can be quite well approximated as independent of the natural tropospheric fading.

3   For assessment of the effects on fixed radio links, the scattered field may be computed with an aperture model under standard atmospheric conditions. In cases where either the link path or the wind turbine, is obstructed by terrain, the results can be improved by using a simple diffraction model, such as GTD, instead of a free space model when computing the fields on either side of the aperture.

A1.1.5   Conclusions

We have shown that the scattered power from a wind turbine, located within the forward scattering region, can be predicted accurately with an aperture model. The field at the receiver is obtained by numerical integration over the silhouette of the turbine. That eliminates the reliance upon uncertain RCS values and is valid also in the near field region of the wind turbine.

Furthermore, we have analysed measured signal levels from several fixed radio links and this analysis suggests that the interference level from wind turbines, in general, are not affected by the same fading as the wanted signal during atmospheric fading events. That observation was investigated further by computer simulations with a parabolic equation (PE) model under different atmospheric conditions. Simulations show that the atmospheric conditions have little effect on the magnitude of the interference from a wind turbine on the investigated link paths, whereas the wanted signal, at a particular antenna position, can easily fade down by tens of decibels under ducting propagation conditions. This result implies that the fading margin of a link always will be upper bounded by the signal to interference ratio in normal atmospheric conditions. That is, to be acceptable, the interference level from wind turbines (in normal atmosphere) must be well below the level of the wanted signal reduced by the fading margin needed to account for multipath fading at the designed link availability.

A1.2 SYSTEM PARAMETERS

Table 1: 8 GHz Falkenberg-Varberg

Parameter	Value
Frequency (GHz)	8.2
Link distance (km)	21.55
Site 1	Falkenberg
Site 2	Varberg
Turbine 1 location from direct path (m)	50
Turbine 1 distance from site 1 (km)	7.0
Turbine 1 type	Vestas V80 model with a rotor diameter = 80 m, hub height = 80 m
Turbine 2 location from direct path (m)	70
Turbine 2 distance from site 1 (km)	7.0
Turbine 2 type	Vestas V80 model with a rotor diameter = 80 m, hub height = 80 m
Antenna height above ground site 1 (m)	100
Height above sea level site 1 (m)	32
Antenna height above round site 2 (m))	10
Height above sea level site 2 (m)	28
Antenna type site1	Andrew VHLP2-7W
Antenna gain site 1 (dBi)	30.5
Wave guide loss site 1 (dBi	0
Antenna type site 2	Andrew VHLP-7W
Antenna gain site 2 (dBi)	30.5
Wave guide loss site 2 (dB)	0
Transmitter output power (dBm)	29
Modulation type	QPSK
Carrier-to-interference Ratio BER 10-E6 (dB)	15
Bandwidth (MHz)	28
Receiver threshold level BER 10E-6 (dBm)	-84
Free space loss received signal level (dBm)	-47.8

Table 2: 8 GHz Malmö – Barsebäck

Parameter	Value
Frequency (GHz)	8.2
Link distance (km)	20.83
Site 1	Malmö
Site 2	Barsebäck
Turbine 1 location from direct path (m)	120
Turbine 1 distance from site 1 (km)	7.2
Turbine 1 type	model with a rotor diameter = 70 m, hub height = 75 m
Turbine 2 location from direct path (m)	-
Turbine 2 distance from site 1 (km)	-
Turbine 2 type	-
Antenna height above ground site 1 (m)	62.6 (MAN), 42.6 (SD)
Height above sea level site 1 (m)	23
Antenna height above round site 2 (m))	15
Height above sea level site 2 (m)	0
Antenna type site1	Andrew VHLPX4-7W-4WH (MAN, V-pol), RFS SU4-W7 1WB (SD H-pol)
Antenna gain site 1 (dBi)	37 dB for both Main and SD
Wave guide loss site 1 (dBi	0.5 dB for MAN, 0 dB for SD
Antenna type site 2	Andrew VHLPX4-7W-4WH
Antenna gain site 2 (dBi)	37
Wave guide loss site 2 (dB)	0.5
Transmitter output power (dBm)	25
Modulation type	32 QAM
Carrier-to-interference Ratio BER 10-E6 (dB)	27
Bandwidth (MHz)	28
Receiver threshold level BER 10E-6 (dBm)	-75
Free space loss received signal level (dBm)	-39.3

Table 3: 2 GHz Military Link

Parameter	Value
Frequency (GHz)	2.1
Link distance (km)	60
Site 1	Restricted info
Site 2	Restricted info
Turbine 1 location from direct path (m)	40
Turbine 1 distance from site 1 (km)	21 km, ground height 10 m
Turbine 1 type	Vestas V52 model with a rotor diameter = 52 m, hub height unknown
Turbine 2 location from direct path (m)	100 m
Turbine 2 distance from site 1 (km)	100 m
Turbine 2 type	21 km, ground height 10 m
Antenna height above ground site 1 (m)	Vestas V52 model with a rotor diameter = 52 m, hub height approximately 50 m.
Height above sea level site 1 (m)	-
Antenna height above round site 2 (m))	120 m (antenna)
Height above sea level site 2 (m)	-
Antenna type site1	Restricted info
Antenna gain site 1 (dBi)	Restricted info
Wave guide loss site 1 (dBi	Restricted info
Antenna type site 2	Restricted info
Antenna gain site 2 (dBi)	Restricted info
Wave guide loss site 2 (dB)	Restricted info
Transmitter output power (dBm)	Restricted info
Modulation type	Restricted info
Carrier-to-interference Ratio BER 10-E6 (dB)	Restricted info
Bandwidth (MHz)	Restricted info
Receiver threshold level BER 10E-6 (dBm)	Restricted info
Free space loss received signal level (dBm)	135 dB

A1.3 MODEL EXPLANATION

A1.3.1 General

This annex exemplifies a basic method for estimating wind turbine interference on radio relay links. The selection of propagation method and assumptions is discussed in A1.1.To calculate the impact on a radio relay from a wind turbine, the scattered field first has to be calculated for a full blade revolution. This is done by calculating Fresnel diffraction through an aperture, which represents the wind turbine.

In the radio-relay geometry addressed here, the scattered field from the turbine will manifest itself as a ripple on the receive signal level and not as a noise level increase. As the scattered signal level is assumed to be independent of the natural fading, the ripple increases during natural fading events. This causes a reduction of the fading margin on the link and may give bit errors if the receiver's signal threshold momentarily is reached. In other words, shallower natural fading can cause transmission errors if wind power turbine interference is present.

The margin reduction can be viewed as equivalent to a threshold degradation, which is a common input in most radio relay performance calculation tools for final performance assessment. Alternatively, the reduction can be expressed as an interference-to-noise ratio, although less general, as the ratio will depend on the modulation formats required SNR.

The models field calculation, as shown here, is still of the simulation type giving receive signal ripple curve forms as intermediate results if needed.

At the end of this annex Fortran code is provided which shows a simple (although inefficient) implementation of the method. Antenna discrimination is for clarity not implemented in the code, but it is indicated were it should be put. The antenna discrimination is very important and it must be used in real calculations.

A1.3.1.1 Field calculations

It can be argued that the suggested method is too complex, as there are available expressions for geometries which should be possible to use to predict the signal level from blades, towers, etc. On the other hand, the described model has the advantage of being able to handling arbitrary shapes in a phase-correct way, at least for a single turbine.

As shown in A1.1of this Report, for the majority of radio-relay wind turbine geometries, it is enough to calculate the forward scatter field from the wind turbines. This can be done by calculating the field through an aperture, equivalent to the wind turbines projection on a plane orthogonal to the radio relay line of sight.

The method shown here uses expressions based on Fresnel diffraction integrals. The coordinate system used in the calculations is shown below.

All example calculations in this document are done for a 20 km radio-relay link at 8 GHz with a wind turbine located at the middle of the path and 100 m perpendicular out from line-of-sight.
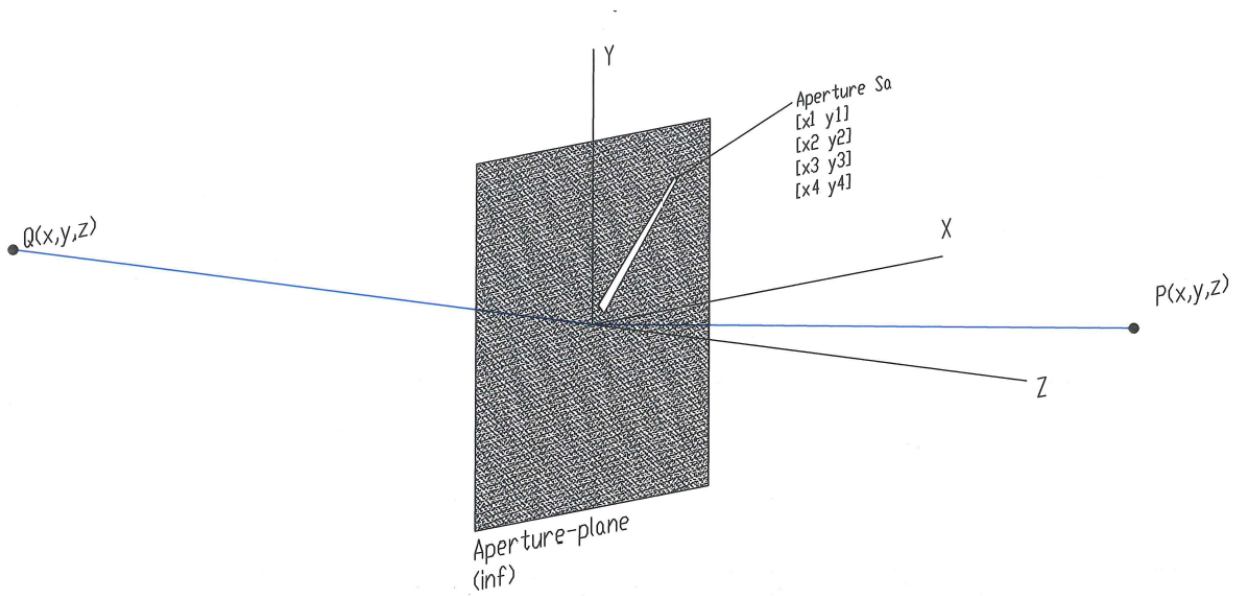
Figure 14: Aperture field calculations coordinate system

All amplitudes are presented as transmission factors. The modelled blade is 45 m long with a ½ root chord of 3 m and ½ tip chord of 1 m. Geometrical angel of attack is 45 degrees at the root and 10 at the tip. The blade is assumed to sit on a spinner with 1 m radius.

The expressions used assume the aperture to be described in a coordinate system with its origin in the vicinity or in the aperture. The coordinates of the source and the field point, P and Q, respectively, in Figure 14, is used to place the aperture related to the line-of-sight of the radio relay. The aperture is the area S_a in Figure 14.

The Fresnel diffraction can be expressed as ([16], Eq. 10.28):

$$E = \frac{jk}{2\pi R_0 r_0} e^{-jk(R_0 + r_0)} \iint e^{jkF(\acute{x},\acute{y})} d\acute{x}\acute{y} \tag{A1-3}$$

The integral is a surface integral over the aperture. The function F is ([16], Eq. 10.29):

$$F(\acute{x}, \acute{y}) = \left(\frac{x}{r_0} + \frac{x_0}{R_0}\right)\acute{x} + \left(\frac{y}{r_0} + \frac{y_0}{R_0}\right)\acute{y} - \frac{1}{2}\left(\frac{1}{r_0} + \frac{1}{R_0}\right)(\acute{x}^2 + \acute{y}^2) \tag{A1-4}$$

The integral in the example code is solved by Monte-Carlo integration having the advantage of simplicity and easy handling of arbitrary aperture shapes, but at the cost of calculation speed. The Monte-Carlo integration is straightforward and can be written as

$$\iint F_1(\acute{x}, \acute{y}) d\acute{x} d\acute{y} \approx \frac{A}{N} \sum_{i=1}^{N} F_1(\acute{x}, \acute{y}) \tag{A1-5}$$

where the function $F_1(\acute{x}, \acute{y}) = e^{jkF(\acute{x},\acute{y})} = e^{jk\left(\frac{x}{r_0}+\frac{x_0}{R_0}\right)\acute{x}+\left(\frac{y}{r_0}+\frac{y_0}{R_0}\right)\acute{y}-\frac{1}{2}\left(\frac{1}{r_0}+\frac{1}{R_0}\right)(\acute{x}^2+\acute{y}^2)}$ inside the aperture and zero otherwise. The quantity A is the area over which the samples are scattered and N is the number of samples.
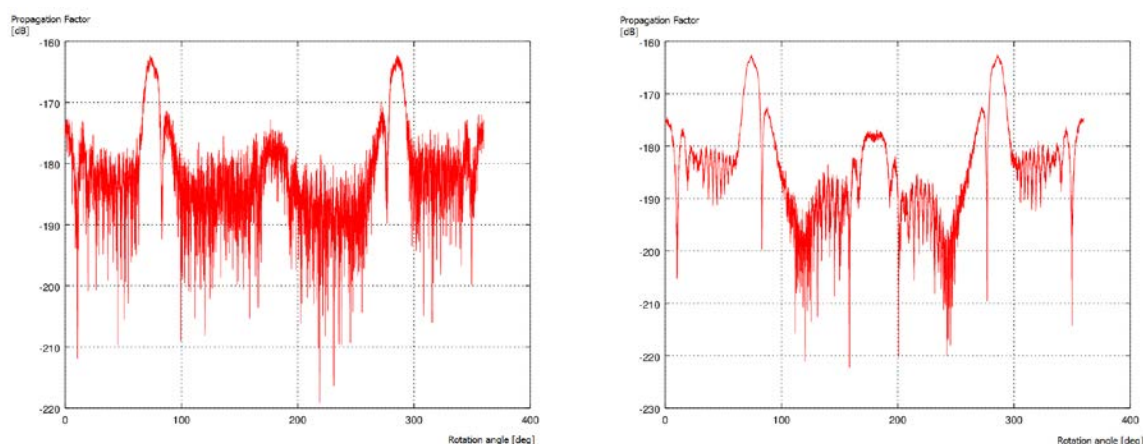
Figure 15: Example of the scatter-field, dependence on N. Left N=1E6, right N=3.7E7

Regarding the accuracy of the example model, the calculation gets more and more difficult to perform as the turbine/aperture gets farther and farther away from line-of-sight, which is due to the fact that the radial length for each phase revolution decreases further out. In the example code, one has to manually select a value in N that gives an accuracy good enough for the problem at hand. Also, the number of calculated angles affects the capability of describing the received field in details, i.e. good max/min values of the field.

A1.3.1.2 Aperture

A perquisite for the field calculation is a description of the aperture to integrate over. For static obstacles, it is easy to do by hand, but as the calculation in question analyses the turbine during revolution, it is more or less necessary to make a computer model for calculation of the apertures/projections.

Turbines with three blades seem to be most common ones and are the turbine types analysed so far. During the work with the model, the turbines have been modelled relatively simple by proper polygons with four corners, where a polygon is an aperture of a tower, a blade, or a machine house. When the scattered field from the turbine is calculated, the field is integrated over the polygons using Monte-Carlo integration.

The choice of modelling the blades as simple truncated cones is to get reasonable realistic wing profiles in 3D with variable angle of attack and chord along the blade. The 2D projection of the blade will in any case be similar to a truncated wedge (i.e. a polygon with four corners), which will be the aperture opening in the example code. Furthermore, in this aperture model, only the moving blades are considered. The static part of the turbine, i.e. the tower and the housing (the machine house), will also cause scattering and thus contribute to the resulting field. However, the moving parts of the turbine (i.e. the blades) give a scattered field that varying in time both in level and phase. The varying is faster than the natural fading, which means that there is a larger possibility for destructive interference due to the moving parts.

There are two angles to consider when making the aperture of the blades. One for the rotation of the blades (see Figure 16) and one for the rotation of the tower (i.e. the machine house; see Figure 17) The former angle is for the turbine rotor position, which gives rise to a fast varying field as the blades rotate. This fast varying field has the potential to be harmful for a radio link. In order to find harmful rotor positions, several aperture realisations of the blade position have to be used. In the simulations, the used resolution for the blade rotation is 0.1 degree.
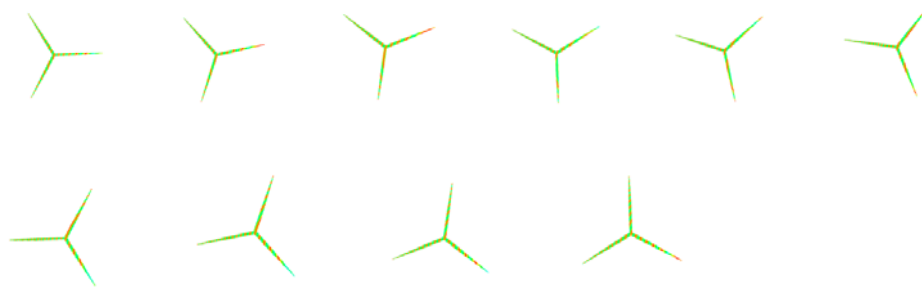
Figure 16: Example a turbine projection, shown in 10 degree steps through ¼ turn

**Figure 17: Example a turbine projection, shown for different rotor axis direction,
and the same rotor position**

The next angle is for the machine house position, i.e. the direction of the turbine rotation axis. Only one value in this angle will be considered, namely, the worst case position of the machine house, which is when the rotation axis is parallel with the radio relay LOS (leftmost picture in Figure 17). Also, a realistic direction for the rotation axis would require knowledge of prevailing winds.
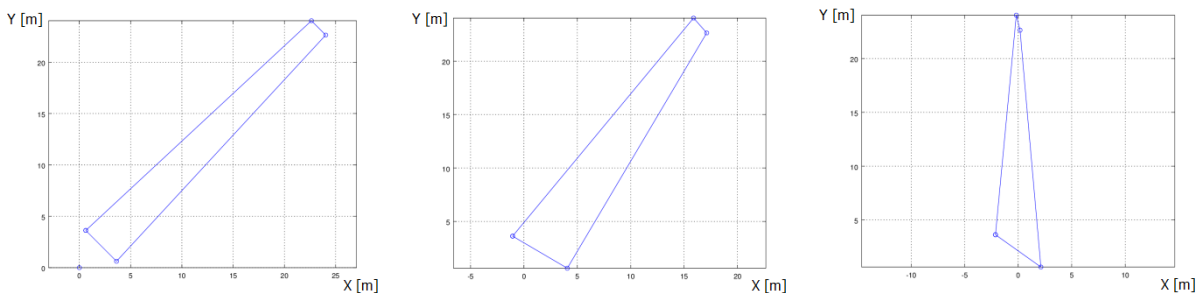
**Figure 18: Test program blade polygon examples, for rotation-axis angle 45 degrees,
and 0, 45 & 90 degrees axis direction. Corresponding to the axis directions equal to leftmost,
middle and rightmost picture in figure 17**

In the test code, the blade is simply modelled by a polygon with four corners determined by length, root chord, tip chord, inner end distance from the rotational axis, and angle of attack at root and at tip. The blade corners are first laid out along the x-axis, then rotated along the z-axis (rotor revolution), and finally rotated around the y-axis (rotor axis direction). For the result, see Figure 18.

To calculate the field from a complete turbine, an aperture plane is created with the projection of (normally) three blades. This simple model works as long as the blades projections do not overlap. Other more efficient approaches is also possible, but omitted for clarity. Note: The slight up-tilt of the rotor axis used on many turbines is not modelled at the moment.

Most other methods used during the work presented in A1.1 approximate the aperture as a large number of small square apertures, where the square apertures are taken from a two level black and white picture of the turbine. This approach is easier to performance optimize.

A1.3.1.3 Calculation sequence

The aperture field is thus calculated for a full rotation of a turbine, where calculated fields are stored for each position, or alternatively, only the highest scatter level is stored, which depends on if signal ripple curve form prediction or only performance prediction is intended.

If one wants to predict the approximate curve form of the receive signal, the direct field has to be calculated also. The normal field should be calculated including terrain effects and the static parts of the turbines. The receive power is then calculated as:

$$P_{rx}(t) = 10 \log_{10} \frac{[E_b - E_s(t)]^2}{377} \tag{A1-6}$$

where E_b is normal field and $E_s(t)$ the time variable scattered field (where both are complex quantities). It should be noted that even a small error in the phase relationship between the scattered and the direct wave will alter the curve-form, as destructive interference is very sensible with regard to the phase relationship. The overall number and general size of the oscillation will however not be affected much. The phase of the direct field during fading is not assumed to be known.
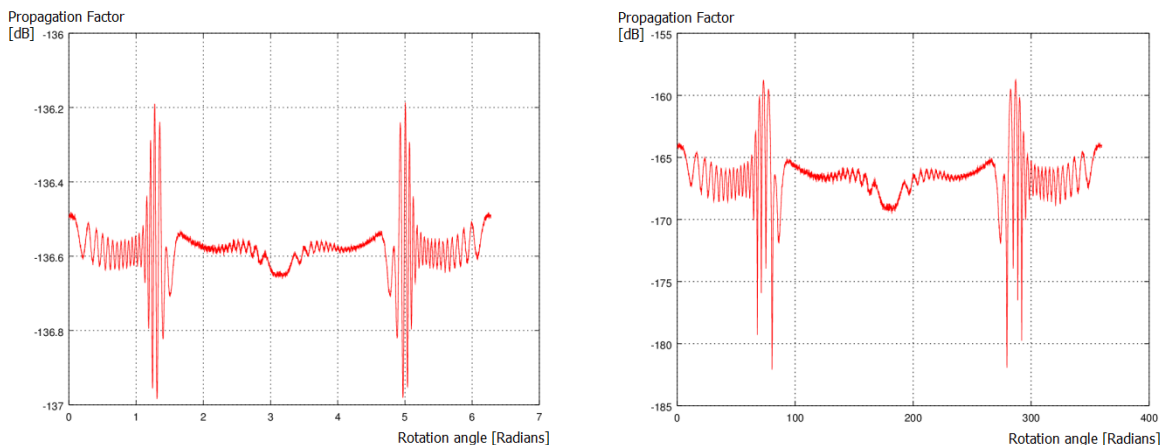
Figure 19: One realisation. Predicted receive signal ripple for nominal and 30 dB faded direct field

If a whole wind farm is present, a simulation has to be made for each turbine and then added together to give the total scattered field. Also, the turbines should rotate with slightly different frequency in order to catch as many different rotational positions as possible over a given time period.

A1.3.1.4 Results evaluation

The predicted curve form of the receive signal is interesting from an understanding point of view, but the curve form only is difficult to use in a performance degradation analysis. An alternative method has to be used in this case.

The prediction of the low level parts of the resulting receive signal are extremely prone to cancellation errors, and as the dips in the receive signal is interesting this makes the method unfeasible.
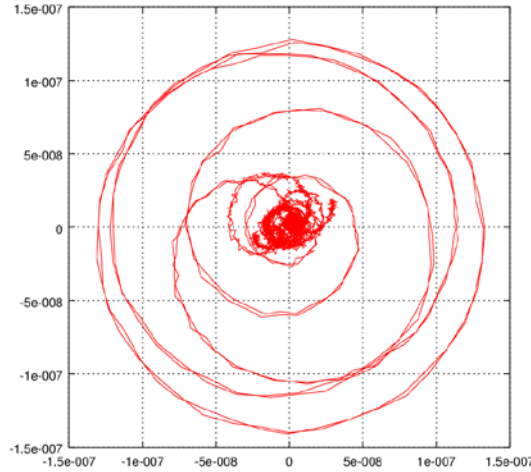
Figure 20: Complex scattered field, vector plot. Showing the highest signal peak trajectory emerging from the low level "noise" and falling back again, while running through all phase angles at relative high level

Under the assumption the scatter field rapidly run through most phases under a few ripple burst whereas the normal field under the same time period can be assumed semi static, the maximum possible destructive fade depth in the field is interesting; see Figure 19 and Figure 20.

Let us define the notch depth in the ripple as the difference between the wanted signal and a multipath propagated signal component, and write the notch depth as

$$N(SNR) = 20 \log_{10}\left(1 - 10^{-SNR/20}\right). \tag{A1-7}$$

This can be used to calculate how much margin the radio relay will lose by solving the equation

$$P_{tr} = P_{nominal} - F_{natural} - N(SNR) \tag{A1-8}$$

where the fading from the nominal received signal level down to the threshold is separated in a natural and a ripple-notch related part. As shown in reference 1, the scatter field is uncorrelated from the normal field during clear-air fading. This makes the SNR of the notch depth in (6) related to the level of the naturally down-faded signal and the interference signal, that is:

$$P_{tr} = P_{nominal} - F_{natrual} - N(P_{nominal} - F_{natural} - P_{scatter}). \tag{A1-9}$$

By solving equation (7) for a given value in $F_{natural}$, one gets the maximum fade which naturally can occur without the threshold being undershot by the turbine ripple notches.

This method of analysis does not take into account eventual receive problems due to rapid signal level variation and/or channel distortion. However, the present simplified evaluation is believed to be acceptable for analysing of moderate degradations of low capacity radio-relay systems and high capacity systems with good equalisers. The modelling of radio equipment's robustness against fast variations in signal level and distortion needs to be studied further.

A1.3.1.5 Sample code, main

Main program, for test of the wind-turbine degradation calculation.

```fortran
! Simple program to show aperture calculation for wind-turbine/vkv analysis.
!
program VKV
 use Auxilliary
 implicit none
 real, dimension(:,:), allocatable   :: bladePol ! Holds a polygon with the obstacle(blade) corners.
 integer, parameter :: AS = 360 ! Number angles to calculate in one rotor revolution.
 real, external :: rad ! Declaration of the external function rad.
 real   :: Qx,Qy,Qz,Px,Py,Pz,k ! Source and field point coordinates.
 real   :: nominal ! A parameter to hold the receive signal level during normal unfaded conditions.
 complex  :: En ! Field-strength, during normal unfaded conditions.
 complex  :: Ea ! Field-strength, aperture field.
 integer  :: ang ! Turbine rotor-position parameter. Integer.
 real     :: angr ! Turbine rotor-position parameter. Real.
 real     :: maxapfield ! Maximum field-strength of aperture field, during one turbine revolution.
 character(LEN=80)  ::  FD, file1 ! Character strings for format description and file name.
 ! Path characteristics, see geometry picture in model description. k = wavenumber
 data Qx,Qy,Qz,Px,Py,Pz,k/100.0,0.0,10000.0,100.0,0.0,10000.0,167.67/
 data nominal/-136.58/
 ! Output file name
 data file1/"dump.txt"/
! Start value of largest aperture field.
data maxapfield/-200.0/
 !
 open(12,FILE=trim(file1), STATUS='REPLACE')
 !
 En = cmplx(sqrt(377.0*10.0**(nominal/10.0)),0.0)
 !
 FD = "(F7.2,A1,F8.3,A1,E10.3,A1,E10.3,A1,F8.3,A1,E10.3,A1,E10.3)"
 do ang = 1,AS ! Loop over blade positions during a turbine revolution
   angr = (360.0/real(AS))*real(ang)
   call bladeProjection(rad(angr), rad(0.0), 1.0, 3.0, 1.0, 45.0, rad(45.0), rad(10.0), bladePol)
   call apertureField(Qx,Qy,Qz,Px,Py,Pz,k, bladePol, Ea)
   maxapfield = max(10.0*log10(abs(Ea*Ea/377.0)),maxapfield) ! Check and update of worst level.
   write(*,*)'Ang: ',angr,' Field: ', 10.0*log10(abs(Ea*Ea/377.0)),' dB' ! Write to console
   write(12,FD)angr,' ', 10.0*log10(abs(Ea*Ea/377.0)),' ',real(Ea),' ',aimag(Ea),' ', & ! Write to file
         10.0*log10(abs((Ea+En)*(Ea+En)/377.0)),' ',real(Ea+En),' ',aimag(Ea+En)
 end do
 !
 ! Calculate degradation
 write(*,*)'Max aperture field level: ',maxapfield,' dB'
 write(*,*)'Degradation: ',remainingMargin(nominal,38.3,maxapfield),' dB'
 !
 close(12)
 !
end program
```

Simple blade aperture generator

```
! Calculates the corner points of the projection of one simplified turbine-blade.
! The blade is modeled as infinite thin surface. Can be extended to abitrarily complexity,
! depending on purpose and need.
! Indata:
! beta: Turbine rotational axis direction in the horizontal plane in Radians, reference
!       direction is paralell to radio relay line of sigth.
! alfa: Turbine blade angle of rotation in Radians, to be swept 0 - 2pi.
! spin: Spinner diameter, as blades distance from rotational centre, in metres.
! b1:   Blade half root chord in metres.
! b2:   Blade half tip chord in metres.
! l:    Blade length in metres
! rc:   Blade root twist in radians.
! tc:   Blade tio twist in radians.
! Subroutine returns: blade corner polygon in pol variable.
subroutine bladeProjection(beta, alfa, spin, b1, b2, l, rc, tc ,pol)
      real, intent(in)   ::  beta, alfa, spin
      real, intent(in)   ::  b1, b2, l, rc, tc
      real, dimension(:,:), intent(out), allocatable ::  pol
      real, dimension(4,3)   ::  p
      if(allocated(pol) .eqv. .false.)then
         allocate(pol(4,2))
      end if
      ! Blade along X-axis
      p(1,:) = [0.0+spin,  cos(rc)*b1, -sin(rc)*b1]
      p(2,:) = [l+spin  ,  cos(tc)*b2, -sin(tc)*b2]
      p(3,:) = [l+spin  , -cos(tc)*b2,  sin(tc)*b2]
      p(4,:) = [0.0+spin, -cos(rc)*b1,  sin(rc)*b1]
      ! Blade rotation, rotation around z-axis
      p(1,1:3) = [p(1,1)*cos(beta)-p(1,2)*sin(beta), p(1,1)*sin(beta)+p(1,2)*cos(beta), p(1,3)]
      p(2,1:3) = [p(2,1)*cos(beta)-p(2,2)*sin(beta), p(2,1)*sin(beta)+p(2,2)*cos(beta), p(2,3)]
      p(3,1:3) = [p(3,1)*cos(beta)-p(3,2)*sin(beta), p(3,1)*sin(beta)+p(3,2)*cos(beta), p(3,3)]
      p(4,1:3) = [p(4,1)*cos(beta)-p(4,2)*sin(beta), p(4,1)*sin(beta)+p(4,2)*cos(beta), p(4,3)]
      ! Rotation axis direction, rotation around y-axis
      p(1,1:3) = [p(1,1)*cos(alfa)+p(1,3)*sin(alfa),p(1,2),-p(1,1)*sin(alfa)+p(1,3)*cos(alfa)]
      p(2,1:3) = [p(2,1)*cos(alfa)+p(2,3)*sin(alfa),p(2,2),-p(2,1)*sin(alfa)+p(2,3)*cos(alfa)]
      p(3,1:3) = [p(3,1)*cos(alfa)+p(3,3)*sin(alfa),p(3,2),-p(3,1)*sin(alfa)+p(3,3)*cos(alfa)]
      p(4,1:3) = [p(4,1)*cos(alfa)+p(4,3)*sin(alfa),p(4,2),-p(4,1)*sin(alfa)+p(4,3)*cos(alfa)]
      ! projection on the xy-plane
      pol(1,1:2) = p(1,1:2)
      pol(2,1:2) = p(2,1:2)
      pol(3,1:2) = p(3,1:2)
      pol(4,1:2) = p(4,1:2)
      !
end subroutine bladeProjection
```

Aperture field calculation

```
! Calculates the field thorugh a abitrary polygon, using the fresnel assumptions.
! The aperture-plane is located in the xy-plane (z=0), with the aperture described
! by the coordinates in the polygon-variable.
! Indata:
! Qx:  Source point x-coordinate [m]
! Qy:  Source point y-coordinate [m]
! Px:  Field point x-coordinate [m]
! Py:  Field point x-coordinate [m]
! k:   Wavenumber [radians/m]
! pol: Polygon coordinates
! Subroutine returns: Complex field [V/m] in Ea - parameter.
subroutine apertureField(Qx,Qy,Qz,Px,Py,Pz,k,pol,Ea)
   use auxilliary2
   implicit none
   real, intent(in)   :: Qx,Qy,Qz,Px,Py,Pz,k
   real   :: L1,L2,L3,L4
   real, dimension(:,:), intent(in), allocatable  :: pol
   complex, intent(out)   :: Ea
   complex :: sum
   real   :: r, t, R1, R2
   integer :: i, N, test
   integer,parameter :: seed = 86456
   complex, external  :: F
   real, parameter ::  pi = 3.14159265359
   !
   call random_seed
   sum = cmplx(0.0,0.0)
   ! Random number limits
   L1 = maxval(maxval(pol,DIM=1)) ! Montecarlo limits in x-direction
   L2 = minval(minval(pol,DIM=1))
   L3 = maxval(maxval(pol,DIM=2)) ! Montecarlo limits in y-direction
   L4 = minval(minval(pol,DIM=2))
   !
   N = 1E6 ! <== To change by user, depending on low signal level performance needed.
   !          Numerical noise in the lower level blade positions drenches true values
   !          If the value is set to low.
   !
   do i = 1,N
      call random_number(r)
      call random_number(t)
      r = L1 + (L2-L1)*r
      t = L3 + (L4-L3)*t
      test = windingTest(pol,[r,t]) ! Check if point within polygon
      if(abs(test) .gt. 0)then    ! If within, calculate an add
         R1 = sqrt(Px*Px+Py*Py+Pz*Pz)
         R2 = sqrt(Qx*Qx+Qy*Qy+Qz*Qz)
         ! Antenna discrimination should be used here, diagram for both
         ! Az & El is required. Left out for clarity of the model.
         sum = sum + F(r,t,Qx,Qy,Px,Py,R1,R2,k)
      end if
   end do
   ! Final calculations of field. ! Eq 10.28 of [16]
   sum = sum*cmplx(0.0,k/(2.0*pi*R2*R1))*exp(cmplx(0.0,-k*(R2+R1)))
   ! Scaling because of the Monte-carlo integration, and to give normalized field.
   sum = sum*cmplx((L4-L3)*(L2-L1),0.0)/cmplx(real(N)*k/(1.0*(pi**2.0)),0.0)
   Ea = sum;
   !
   end subroutine
```

```
! Integration-function
! Eq 10.29 of [16]
complex function F(xp, yp, Qx, Qy, Px, Py, R1, R2, k)
     implicit none
     real, intent(in)    :: xp, yp, Qx, Qy, Px, Py, R1, R2, k
     complex ans
     real :: IF
     IF = (Px/R1+Qx/R2)*xp + (Py/R1+Qy/R2)*yp - 0.5*(1/R1 + 1/R2)*(xp*xp+yp*yp)
     ans = cmplx(0, k*IF)
     ans = exp(ans)
     F =  ans
end function F
```

Winding test, to see if a point falls within a polygon

```
! Method similar to algorithm described at http://geomalgorithms.com/a03-_inclusion.html
! Tests if a point is located inside a polygon, by the winding-number method.
! Indata:
! pol:  Abritrarily sized polygon, stored in 2D array "dimension(number of points, 2)".
!       The polygon edges is between point 1 to 2, 2 to 3 etc, finallly closed
!       by a edge from the last to the first polygon point.
! point: Point to test
! Function returns: integer 0 if point not in polygon, 1 if point inside polygon
integer function windingTest(pol,point)
   implicit none
   real, dimension(2), intent(in)   :: point
   real, dimension(:,:), intent(in) :: pol
   real, dimension(:,:), allocatable  ::  pol2
   integer ::  i, sides, wn
   real, external  :: isLeft
   sides = size(pol,1)
   ! Make a extended array to allow easy loop through all sides
   allocate(pol2(sides+1,2))
   pol2(1:sides,:) = pol(:,:)
   pol2(sides+1,:) = pol(1,:)
   !
   wn = 0 ! the  winding number counter
   !
   ! loop through all edges of the polygon
   do i=1,sides   ! edge from V[i] to  V[i+1]
     if (pol2(i,2) .le. point(2))then        ! start y <= P.y
       if (pol2(i+1,2) .gt. point(2))then     ! an upward crossing
         if (isLeft( pol2(i,:), pol2(i+1,:), point) .gt. 0.0)then ! P left of  edge
            wn = wn +1          ! have  a valid up intersect
         end if
       end if
     else
       if (pol2(i+1,2) .le. point(2))then    ! a downward crossing
         if (isLeft( pol2(i,:), pol2(i+1,:), point) .lt. 0.0)then ! P right of  edge
            wn = wn -1           ! have  a valid down intersect
         end if
       end if
     end if
   end do
   !
   windingTest =  wn
   !
end function

! Support function, to winding algorithm
real function isLeft(P0, P1, P2 )
   real, dimension(2), intent(in)    ::  P0, P1, P2
   isLeft = ( (P1(1) - P0(1)) * (P2(2) - P0(2)) - (P2(1) -  P0(1)) * (P1(2) - P0(2) ) )
end function isLeft
```

Calculation of margin degradation

```
! Function to calculate margin degradation.
! Indata:
! nominal:   Nominal receive signal level [dBm]
! margin:    Original fade margin [dBm]
! maxapfield:  Maximum aperture field level [dBm]
! Function returns: degradation [dB].
real function remainingMargin(nominal,margin,maxapfield)
   real, intent(in)    :: nominal,margin
   real, intent(in)    :: maxapfield
   real    :: Ptrh, SNR, newFade, Fade
   !
   Fade = -10.0
   newFade = 0.0
   Ptrh = nominal - margin
   do while (Ptrh .lt. newFade )
      SNR = nominal - Fade - maxapfield;
      newFade = nominal - Fade + 20.0*log10(1.0-10.0**(-SNR/20.0));
      Fade = Fade + 0.01;
   end do
   !
   remainingMargin = nominal - Ptrh - Fade
   !
end function
```

Other
```
! Interface descriptions, needed for the assumed shape arrays.
!
module Auxilliary

 interface
    subroutine bladeProjection(beta, alfa, spin, b1, b2, l, rc, tc, pol)
       real, intent(in)    ::  beta, alfa, spin
       real, intent(in)    ::  b1, b2, l, rc, tc
       real, dimension(:,:), allocatable  ::  pol
    end subroutine bladeProjection
 end interface

interface
    subroutine apertureField(Qx,Qy,Qz,Px,Py,Pz,k, poly, Ea)
       real, intent(in)        ::  Qx,Qy,Qz,Px,Py,Pz,k
       complex, intent(out)    ::  Ea
       real, dimension(:,:), allocatable    ::  poly
    end subroutine apertureField
end interface

interface
    real function remainingMargin(nominal,margin,maxapfield)
       real, intent(in)   ::  nominal,margin
       real, intent(in)   ::  maxapfield
    end function
end interface

end module Auxilliary

real function rad(deg)
    real, intent(in)    ::  deg
    real, parameter ::  pi = 3.14159265359
    rad = 2*pi*deg/360.0
end function rad

! Interface descriptions, needed for the assumed shape arrays.
!
module Auxilliary2
!
 interface
    integer function windingTest(poly,point)
       real, dimension(:,:), allocatable   ::  poly
       real, dimension(2) ::  point
    end function windingTest
 end interface
!
end module Auxilliary2
```

A1.4 EXAMPLE OF WIND TURBINE FADE MARGIN REDUCTION

A1.4.1   Summary

This document exemplifies a method of assessing the impact of wind turbines on the error performance and availability of radio links.

The study show that the impact of Wind turbine on the error performance and availability of radio links depends on various radio parameters, transmission capacity, error performance requirements etc. as well as the size and location of the Wind turbines.

The following table give an example of distance, between a wind turbine and a radio link's line-of-sight, for about 1 dB reduction of the radio link's fade margin. The fade margin reductions have been calculated by using the Swedish FMV/FOI aperture model.

Table 4: Example of distance for about 1 dB fade margin reduction

Configuration	Distance from end point	Large WT, r(m)	Medium WT, r(m)	Small WT, r(m)
6 GHz/50 km/3.0 m antenna	25 km	450 m	425 m	400 m
	3 km	200 m	175 m	150 m
8 GHz/20 km/1.2 m antenna	10 km	325 m	300 m	300 m
	3 km	250 m	250 m	225 m
8 GHz/20 km/0.6 m antenna	10 km	400 m	325 m	300 m
	3 km	225 m	225 m	200 m
13 GHz/10 km/0.6 m antenna	5 km	225 m	225 m	225 m
	1 km	125 m	125 m	125 m
18 GHz/10 km/0.6 m antenna	5 km	150 m	150 m	175 m
	1km	75 m	75 m	50 m

Note: WT: Wind turbine

r(m): distance from the Line of sight (LOS) path between the radio link's transmitter and receiver

In general, the distance will be shorter for higher frequency bands compared to lower frequency bands. The distance can be found to be larger at the middle of the path and will be shorter closer to the end points.

Please note that the accuracy of the wind turbine's location as well as the accuracy of the radio links site coordinates are very important and may need revision

A1.4.2   Error Performance Objective (EPO)

The error performance objectives for real digital Fixed Service radio links are given in Recommendation ITU-R F.1668 [17], the parameters to be considered are:

- Errored Second Ratio (ESR): The ratio of ES to total seconds in available time during a fixed measurement interval.
- Severely Errored Second Ratio (SESR): The ratio of SES to total seconds in available time during a fixed measurement interval.

▪ Background Block Error Ratio (BBER): The ratio of Background Block Errors (BBE) to total blocks in available time during a fixed measurement interval. The count of total blocks excludes all blocks during SESs.

A1.4.2.1 Availability

Each direction of a path, which can consist of a single radio link or multiple radio links in a chain, can be in one of two states, available or unavailable. The criteria determining the transition between the two states are as follows; a period of unavailable time begins at the onset of 10 consecutive Severely Errored Second (SES) events. These 10 seconds are considered to be part of unavailable time. A new period of available time begins at the onset of 10 consecutive non-SES events. These 10 seconds are considered to be part of available time. Figure 21 illustrates the transitions between the availability states.
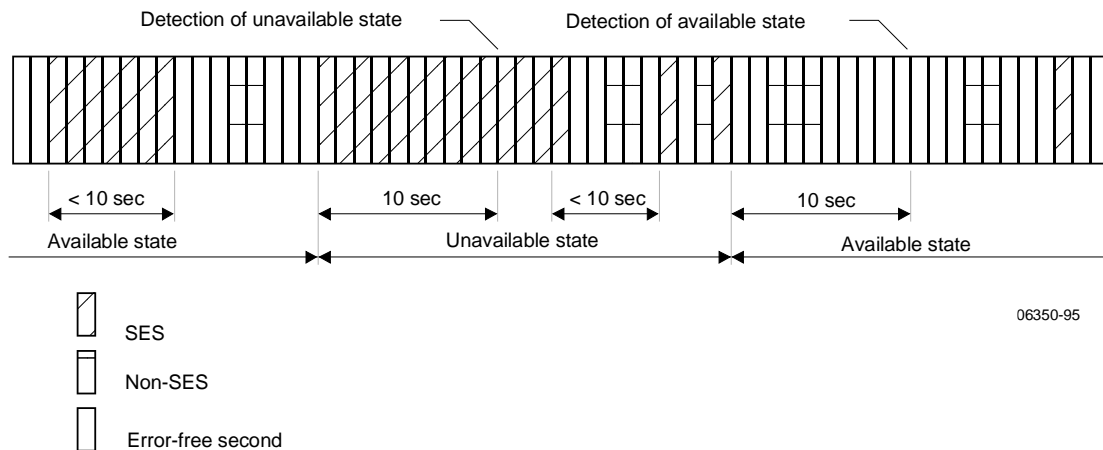
Figure 21: Availability states

A path is available if both directions are available. ITU-T Rec. G.827 [18] specifies the availability objectives for path elements of international digital paths. It should be noted that error performance should only be evaluated whilst the path is in the available state.

It is generally accepted that for a high performance radio link clear air fading is largely produced by multipath propagation which tends to produce fades lasting less than 10 seconds, hence are the SES criteria the dimensioning objective. Precipitation (rain, snow etc.) tends to produce fades lasting longer than 10 seconds contributing to unavailable time.

An example of a real fading event can be found in A1.1.2.2.

A1.4.2.2 EPO long haul

Long distance links in the 6 GHz frequency band are normally deployed within the long haul section of the national part of a network. Given the following assumptions;

Link distance = 50 km

Bit rate = 155 Mbit/s

A1 = 1 %

The EPO for a 50 km Long Haul link is given in Table 5.

Table 5: EPO for a 50 km long haul link

Parameter	ITU-T rec.G.828	ITU-T rec.G.826
ESR	0.00024	0.00096
ES/month	622	2488
SESR	0.000012	0.000012
SES/month	31	31

With reference to the SES criteria, the percentage of time without SES should be higher than 99.9988%

A1.4.2.3 EPO short haul

Short Haul radio links are normally deployed within the short haul section of the national part of a network. Given the following assumptions;

Link distance = 10 km

Bit rate = 155 Mbit/s

B = 7.5 %

The EPO for a short haul link is given in Table 6**.**

Table 6: EPO for a 10 km short haul link

Parameter	ITU-T rec.G.828	ITU-T rec.G.826
ESR	0.003	0.012
ES/month	7776	31104
SESR	0.00015	0.00015
SES/month	389	389

With reference to the SES criteria, the percentage of time without SES should be higher than 99.985%. Please also note that in a real scenario the short haul EPOs should be divided into smaller portions depending on the number of link comprising the short Haul portion of the national network.

The error performance objectives for the 8 and 13 GHz example links used in this report is the same as for the 18 GHz short haul.

A1.4.2.4 Design of a radio link

During the design of a radio link, the error performance can be predicted by using the prediction methods given in Recommendation ITU-R P.530 [19]. The prediction methods calculate the outage probability, i.e. percentage of time, during which time the received signal is predicted to have a Bit Error Rate (BER) level above a given value.

It is generally accepted that BER of 10^{-6} is a useful, slightly conservative, value in order to meet the SES criteria.

A1.4.2.5 Error Performance Degradation

Considerations regarding error performance degradations are given in the ITU-R Rec. F.758 [20]. For long-term interference it is recommended to use an I/N value of -6 dB or -10 dB, corresponding to a threshold degradation (TD) of 1 dB or 0.5 dB.

Even though a wind turbine could not be regarded as a radiating source of interference, the radio signals obstructed by or scattered from wind turbines should be taken into account. The receivers of a radio system will experience the impact of wind turbines as a reduction of fade margin, or equivalently as a threshold degradation.

The aggregated effect from multiple wind turbines needs to be further studied.

The actual reduction of fade margin that can be allowed for real scenarios should be determined in connection with consideration of the actual radio links EPOs, predicted error performance as well as the radio links overall interference received from other fixed radio links.

A1.4.3 Predicted Error Performance

The error performance has been calculated for some typical radio link configurations used in fixed service applications:

- Long Haul 6 GHz, 50 km, with 3.0m antennas;
- Short Haul 8 GHz, 20 km, with 1.2m antennas respectively with 0.6 m antennas;
- Short Haul 13 GHz, 10 km, with 0.6 m antennas;
- Short Haul 18 GHz, 10 km, with 0.6 m antennas.

The examples of EPO, frequency band, link distance and antenna size combinations have been selected in order to illustrate the impact of wind turbine on a radio link receiver performance due to antenna size and used frequency band. Other combinations of system parameters could also be valid.

Regarding radio links in the higher frequency bands where precipitation fading often is the dimensioning factor, it is assumed that both the wanted signal between the radio links transmitter and receiver and the signal scattered from the wind turbine will experience mainly correlated rain fade events. The expected correlation improves the situation compared to the clear air fading case, but the situation is not fully investigated yet. Thus have the unavailability contribution due to rain fading been excluded from the calculations and analysis in this document.

The radio link error performance predictions in this report assume similar effective antenna height above sea level at both transmitter site and receiver site, thus giving no path inclination. The ITU-R rec. P.530 models favours, from an error performance point of view, the use of a high magnitude of path inclination, $|\varepsilon_p|$ (mrad). The calculated availability values given in this report should thus be regarded as conservative values. Real radio links with a significant path inclination will normally have a better error performance prediction.

Typical radio data, link budget and predicted availability for various configurations can be found in A1.4.5, A1.4.6 and A1.4.7.The radio links availability has been calculated in an interference free environment as well as for TD between 1, 3, 6 and 10 dB. The Interference over noise ratio (I/N) values is given in the table below.

Table 7: I/N values

TD (dB)	I/N (dB
1	-6
3	0
6	5
10	10

A1.4.3.1 6 GHz, 50 km

Long paths, such as a 6 GHz radio link over a 50 km distance, are normally equipped with Space Diversity (SD), dual antennas and dual receivers, from which the received signals are combined in order to improve transmission quality. The calculations do take the diversity systems improvement on required fade margin in account, but not the effect that wind turbine ripple pattern differ slightly in time in the diversity receivers. Use of the latter is equipment dependant, and need to be studied further. The predicted uni-directional availability at BER 10-6 for the different capacity/modulation rates can be found in Figure 22.

Figure 22: 6 GHz availability with SD

If it is required that the probability of having an error performance better than BER 10-6, corresponding to SES, during more than 99,9988% of the time, the maximum capacity is 160 Mbit/s using 128 QAM. In an interference environment (moving from TD=0 dB to TD=10 dB) there will only be two options, if not changing the radio equipment, either to preserve the high availability at a lower capacity, or to preserve the same capacity but with a lower availability.

A1.4.3.2 8 GHz, 20 km

The availability for a 8 GHz 20 km radio link has been calculated given different configurations, without and with SD, and with 1.2 m antennas respectively with 0.6 m antennas. In case of diversity an antenna separation of 5 m was used. The predicted uni-directional availability at BER of 10^{-6}, under clear sky conditions for various capacity/modulation rates can be found in Figure 23 when using 1.2 m antennas.
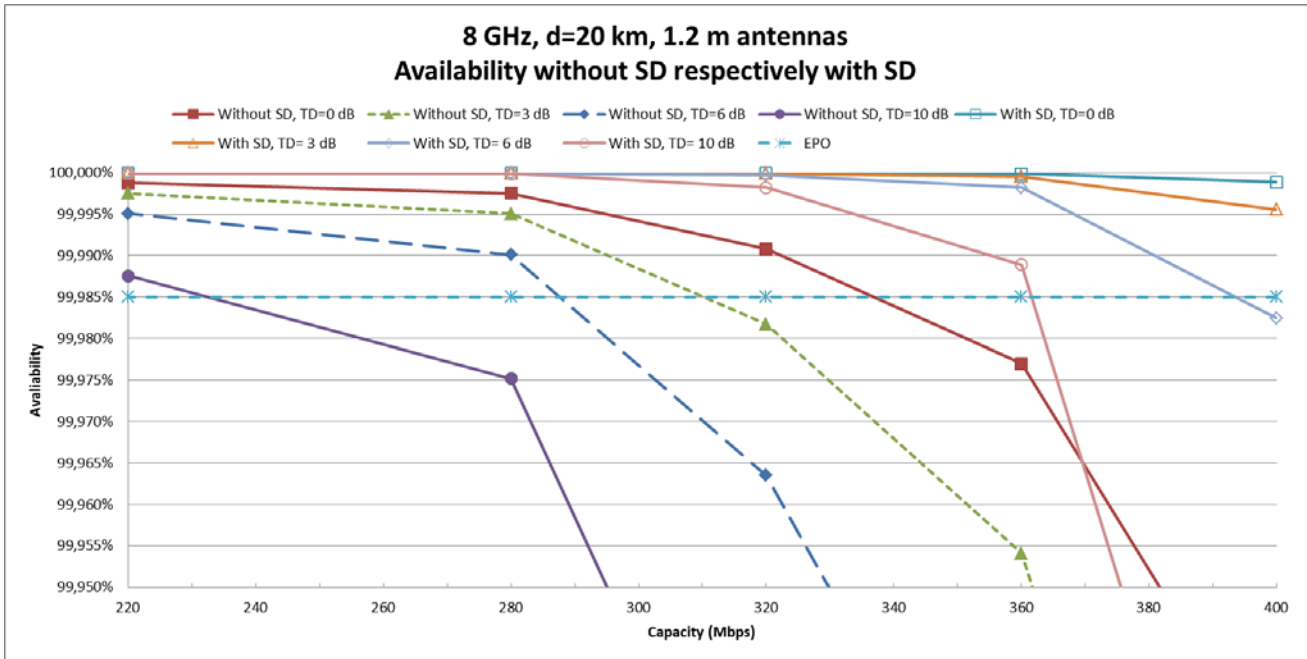
Figure 23: 8 GHz/20 km/1.2 m antennas availability without SD respectively with SD

If it is required that the probability of having an error performance better than BER of 10^{-6}, corresponding to SES, during more than 99.985% of the time, the maximum capacity is 320 Mbit/s using 128 QAM without SD.

The fade margin when using 0.6 m antennas is 26 dB compared to 38 dB when using 1.2 m antennas, the difference is due to the lower antenna gain for the smaller antennas, and consequently the predicted error performance will be significantly worse in case of 0.6 m antennas compared with 1.2 m antennas. The predicted uni-directional availability at BER of 10^{-6}, under clear sky conditions for various capacity/modulation rates can be found in Figure 24 when using 0.6 m antennas.
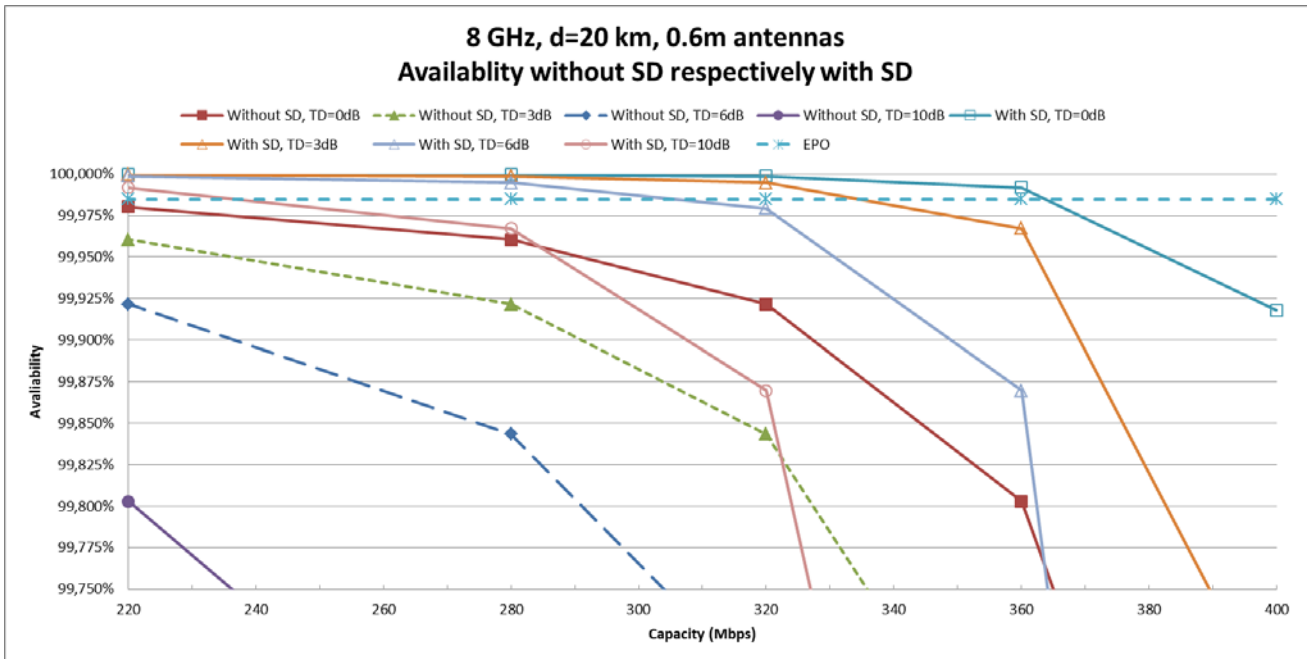
Figure 24: 8 GHz/20 km/0.6 m antennas availability without SD respectively with SD

The requirement of having an BER of 10^{-6} probability better than 99.985% of the time cannot be met with 0.6 m antennas in this scenario without using SD. In case of SD the maximum capacity is 360 Mbit/s.

Introduction of dual antennas in a SD configuration will increase the radio link's availability for a given modulation. The SD functionality is normally used to meet high quality objectives for long distance links by increasing the radio link's effective fade margin. The SD increase of effective fade margin could also be used on shorter distance links in order to mitigate the effect of surface reflections.

A1.4.3.3 13 GHz, 10 km

The predicted uni-directional availability at BER of 10^{-6}, under clear sky conditions for various modulation rates can be found in Figure 25.
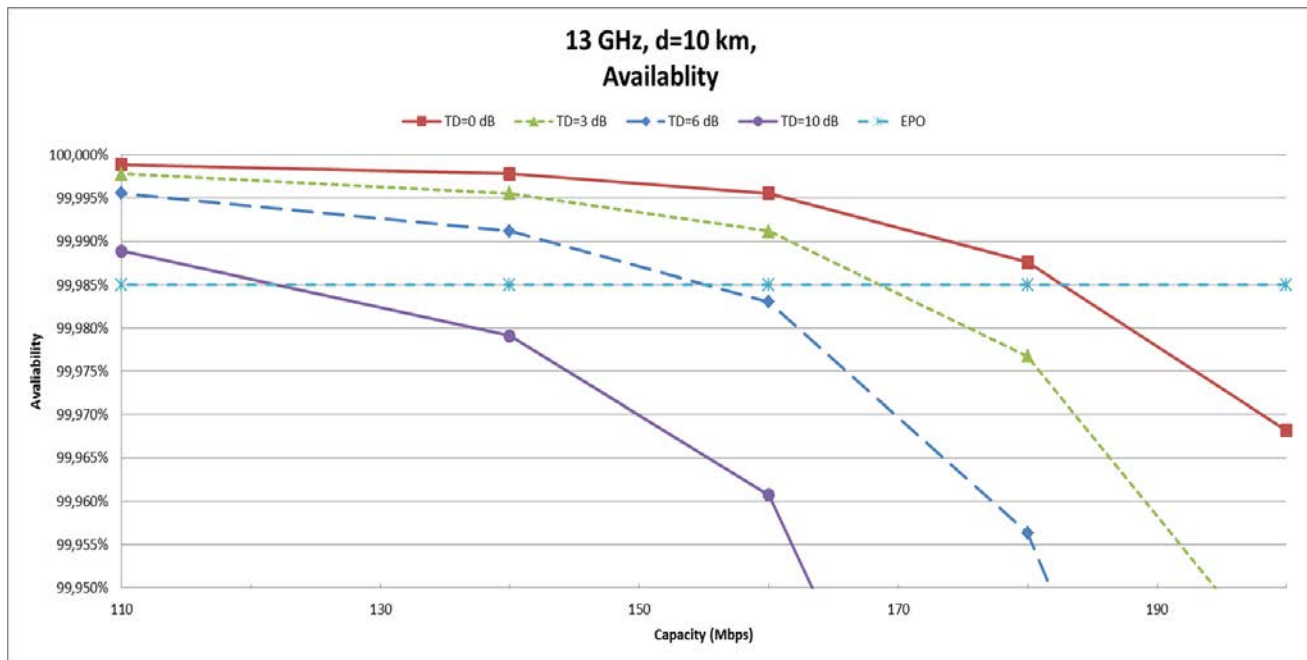
Figure 25: 13 GHz availability

If it is required that the probability of having an error performance better than BER of 10^{-6}, corresponding to SES, during more than 99.985% of the time, the maximum capacity is 180 Mbit/s using 256 QAM. If the interference increases, resulting in for example a threshold degradation of 6 dB, the capacity drops to 140 Mbit/s using 64 QAM given the same performance target.

A1.4.3.4 18 GHz, 10km

The predicted uni-directional availability at BER of 10^{-6}, under clear sky conditions for various modulation rates can be found in Figure 26.
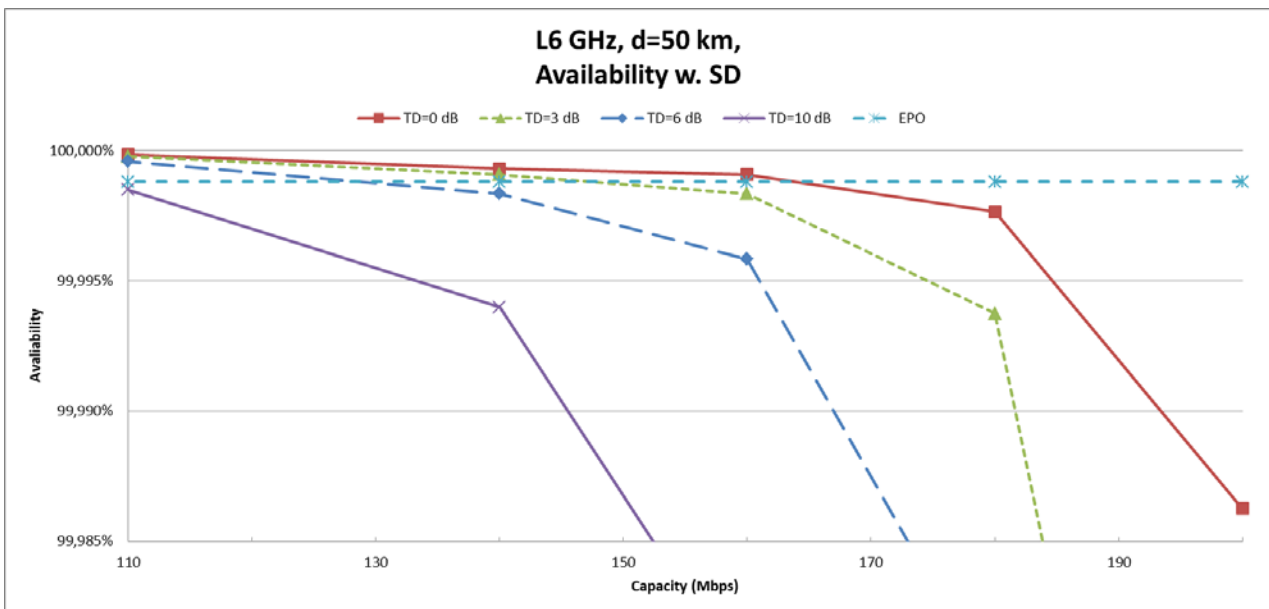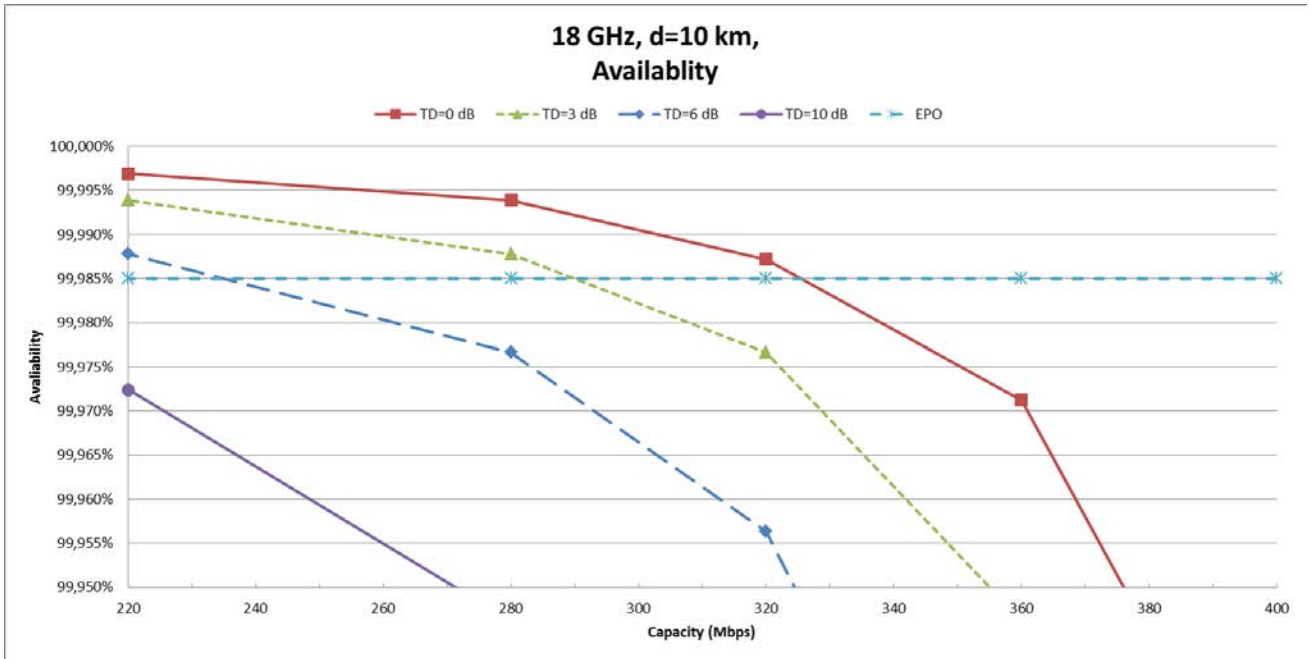
Figure 26: 18 GHz availability

If it is required that the probability of having an error performance better than BER of 10^{-6}, corresponding to SES, during more than 99.985% of the time, the maximum capacity is 320 Mbit/s using 128 QAM. If the interference increases, resulting in a threshold degradation of, for example, 6 dB, the capacity drops to 220 Mbit/s using 32 QAM given the same performance target.

A1.4.4 Example of impact from a wind turbine on fade margin

If a wind turbine is located near the line-of-sight of a radio link path, the radio link receiver will experience ripple in the transmission loss, resulting in increased fade depths, due to scattering from the wind turbine. The effect can be viewed as a reduction of fade margin or threshold degradation, making analysis of the performance degradation straightforward.

The fade margin reduction has been calculated using the FMV/FOI wind turbine interference assessment tool for some typical radio link configurations. An overall picture of the different parameters to be discussed in the following sections can be found in the figure below.
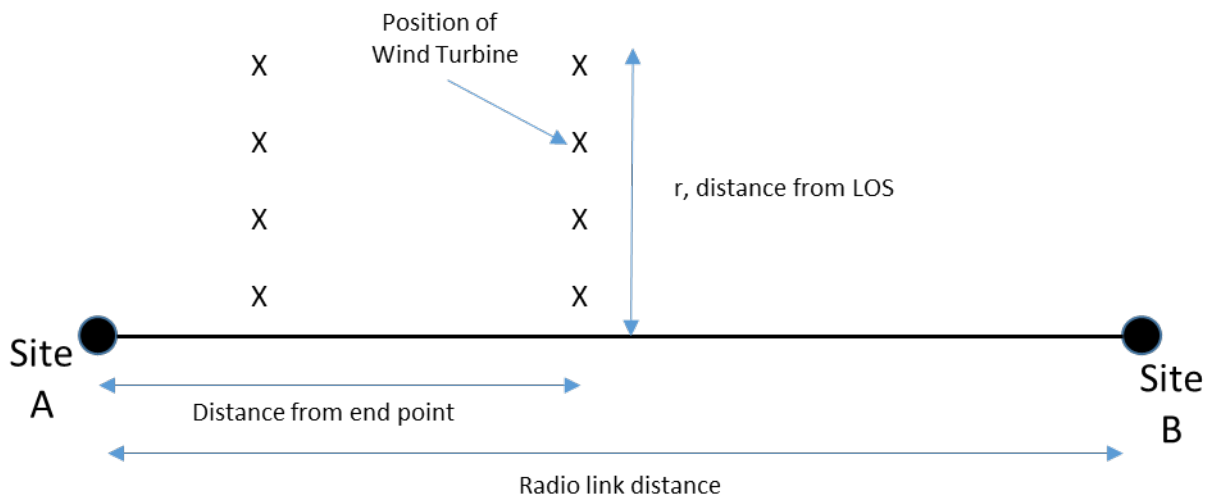
Figure 27: Principal drawing seen from above

A few actual wind turbines have been modelled in the FMV/FOI as a reference. The Vestas V100 is assumed to be representative for a large wind turbine, the Vestas V80 for a medium size wind turbine and Vestas V52 represents a small wind turbine. In the calculations is the wind turbine assumed to display maximum aperture towards the radio link. Antenna heights and foundation height of the wind turbine tower have been selected in order to receive the maximum attenuation and fade margin reduction caused by the wind turbine.

The wind turbine is initially placed directly in the radio link's Line of Sight (LOS) halfway between the radio link's transmitter and receiver. The location of the wind turbine is then moved in steps of 25 m perpendicular away from the radio link's LOS until the distance from LOS is 500 m. The calculations are repeated for another scenario where the wind turbine is located closer to one end point. The distances 1 km and 3 km are selected to be within the validity range of the FMV/FOI interference assessment model.

The following sections presents calculated fade margin reductions for different combinations of frequency band, antenna size and wind turbines. The calculated values can also be found in A1.4.8.

A1.4.4.1 6 GHz, 50 km

The calculated fade margin reduction for a 6 GHz 50 km path when a single wind turbine is located 3 km and 25 km from one end point can be found in Figure 28.
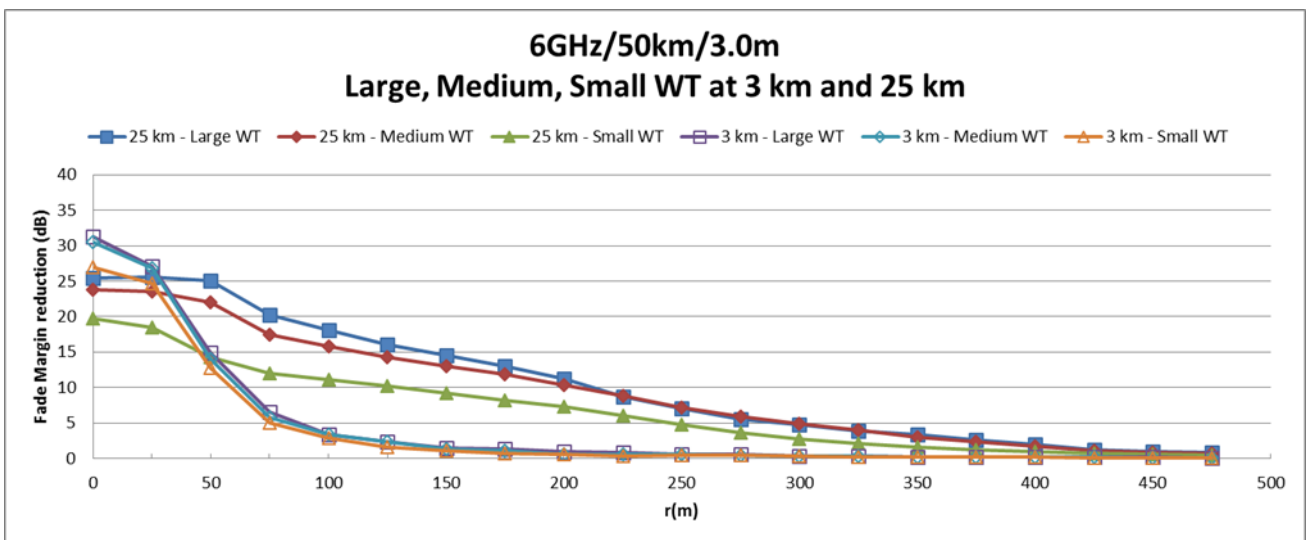
Figure 28: 6 GHz/50km/128QAM, fade margin reduction due to a large, medium and small sized wind turbine at 3 km and 25 km from end point

A1.4.4.2 8 GHz, 20 km

The figure below presents the calculated fade margin reduction for an 8 GHz radio link using 1.2 m antennas over a 20 km distance, when a wind turbine is located 3 km and 10 km from one end point.
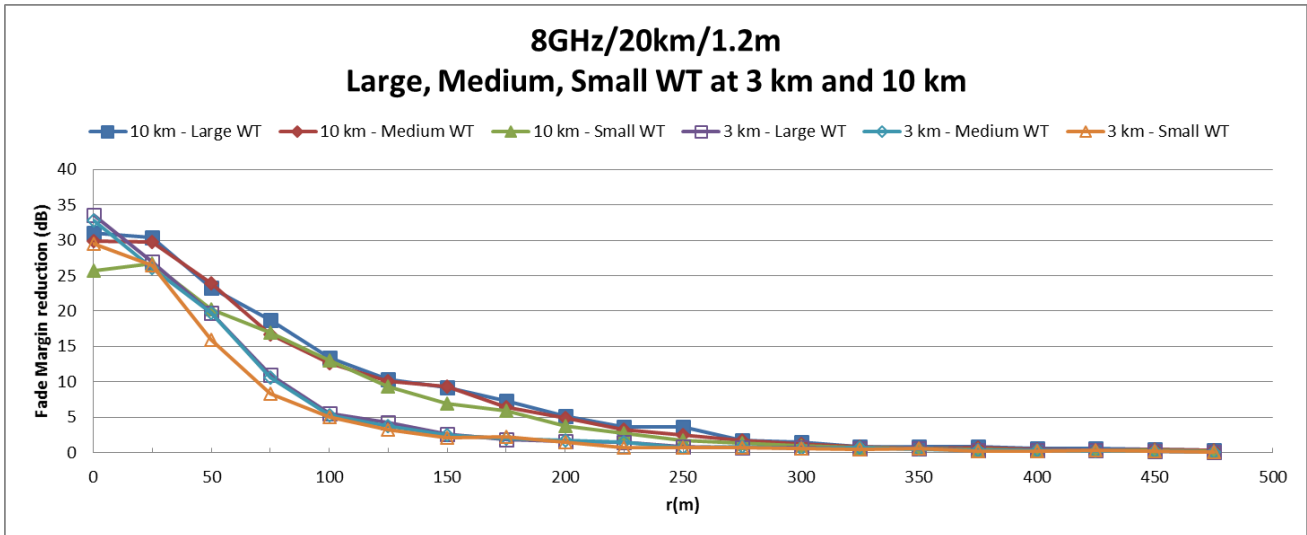
Figure 29: 8 GHz/20km/128QAM/1.2m, fade margin reduction due to a large, medium and small sized wind turbine at 3km and 10 km from end point

Figure 30 presents calculated fade margin reduction for an 8 GHz radio link using 0.6 m antennas over a 20 km distance.
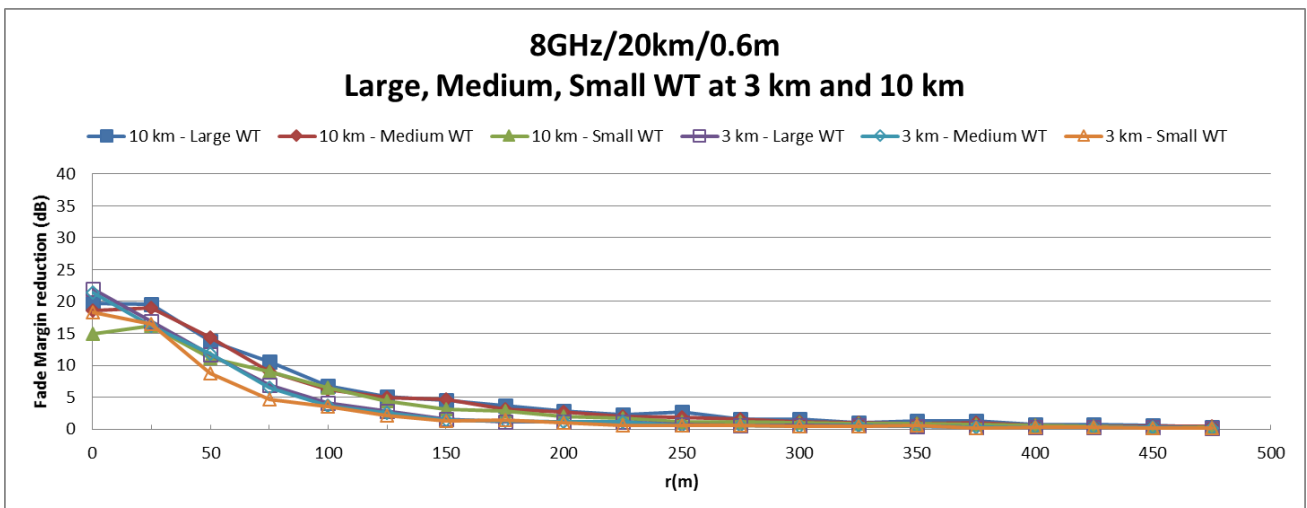
Figure 30: 8 GHz/20km/128QAM/0.6m, fade margin reduction due to a large, medium and small sized wind turbine at 3 km and 10 km from end point

The radio link fade margin when using 0.6 m antenna is in scenario 26 dB compared to 38 dB when using 1.2 m antennas. The difference in fade margin is due to the lower antenna gain for the smaller antennas. The maximum fade margin reduction will be equally lower in case of 0.6 m antennas compared with 1.2 m antennas.

A1.4.4.3 13 GHz, 10 km

The calculated fade margin reduction when a wind turbine is located at 1 km and 5 km from one end point can be found in Figure 31.
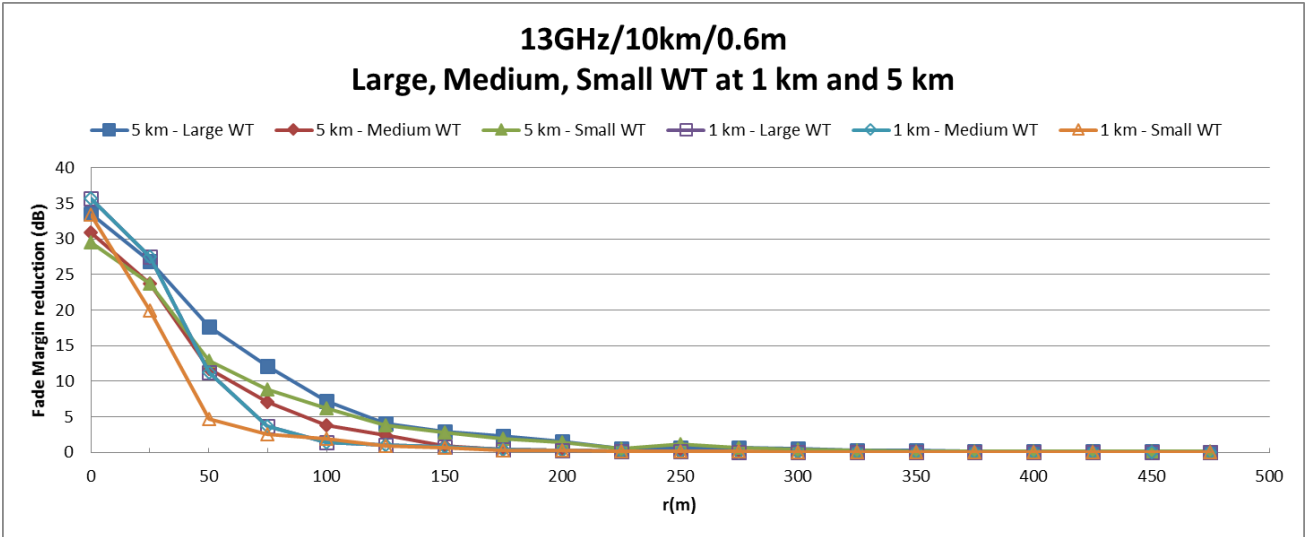
Figure 31: 13 GHz/10km/32QAM, fade margin reduction due to a large, medium and small sized wind turbine at 1 km and 5 km from end point

A1.4.4.4 18 GHz, 10km

The calculated fade margin reduction when a wind turbine is located 1 km and 5 km from one end point can be found in Figure 32.
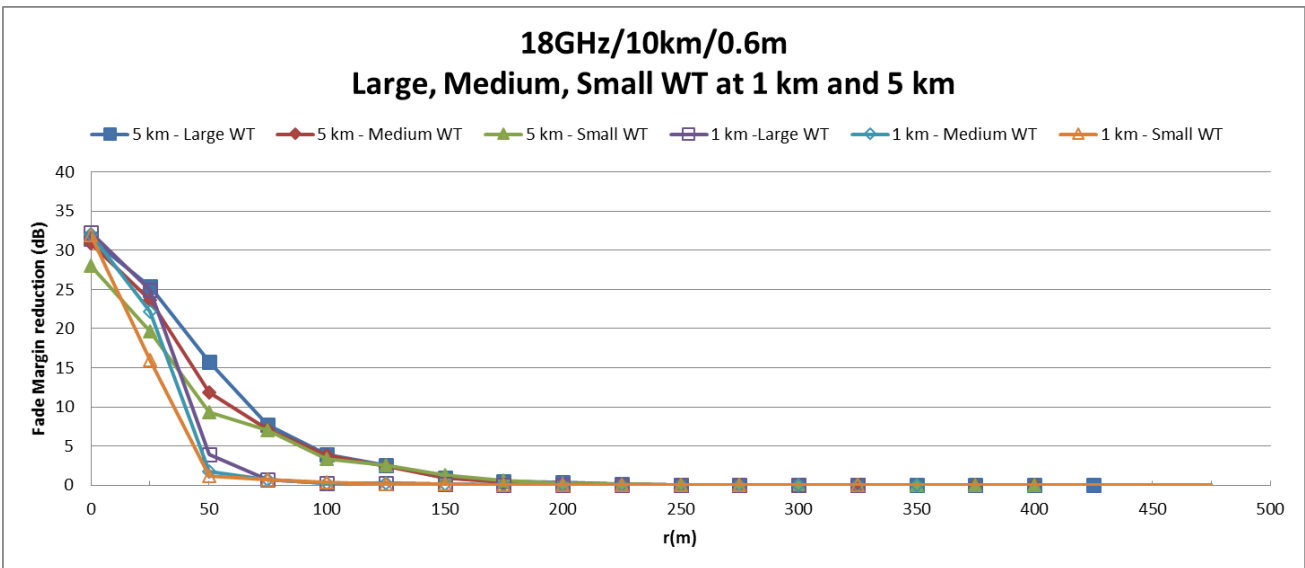
Figure 32: 18 GHz/10km/128QAM, fade margin reduction due to a large, medium and small sized wind turbine at 1 km and 5 km from end point

A1.4.4.5 Examples of distances

The calculations show that the impact of a wind turbine depends on various radio parameters, transmission capacity, error performance requirements, etc. as well as the size and location of the wind turbine.

The following table is a summary of the previous calculations for about 1 dB reduction of the radio link's receiver fade margin.

Table 8: Example of distance from LOS for about 1 dB fade margin reduction

Configuration	Distance from end point	Large WT, r(m)	Medium WT, r(m)	Small WT, r(m)
6GHz/50km/3.0m antenna	25 km	450 m	425 m	400 m
	3 km	200 m	175 m	150 m
8GHz/20km/1.2 m antenna	10 km	325 m	300 m	300 m
	3 km	250 m	250 m	225 m
8GHz/20km/0.6m antenna	10 km	400 m	325 m	300 m
	3 km	225 m	225 m	200 m
13GHz/10km/0.6m antenna	5 km	225 m	225 m	225 m
	1 km	125 m	125 m	125 m
18GHz/10km/0.6m antenna	5 km	150 m	150 m	175 m
	1km	75 m	75 m	50 m

Note: WT: Wind turbine
r(m): distance from the Line of sight (LOS) path between the radio link's transmitter and receiver

The contribution from the wind turbines are calculated with apertures with a resolution of 0.25 m pixel size.

In general, the distance will be smaller for higher frequency bands compared to lower frequency bands. The distance can be found to be larger at the middle of the path and will be smaller closer to the end points.

Please note that the wind turbine's location as well as the accuracy of the radio links site coordinates should be reviewed.

A1.4.5   Example of Radio equipment data

The following radio equipment data have been used in the Link budget calculations:

Table 9: L6 GHz, 5925-6425 MHz

Parameter	512 QAM	256 QAM	128 QAM	64 QAM	32 QAM
Channel bandwidth (MHz)	28.0	28.0	28.0	28.0	28.0
Capacity (Mbit/s	200.0	180.0	160.0	140.0	110.0
Output power (dBm)	30.0	32.0	33.0	33.0	33.0
Receiver threshold @ BER 10-6 (dBm)	-66.0	-69.0	-72.0	-75.0	-78.0
Signature width (MHz)	24.0	24.0	24.0	24.0	24.0
Signature depth, minimum phase (dB)	18.0	21.0	23.0	23.0	28.0
Signature depth, non-minimum phase (dB)	18.0	21.0	21.0	21.0	28.0

Table 10: 8 GHz, 7900-8500 MHz

Parameter	512 QAM	256 QAM	128 QAM	64 QAM	32 QAM
Channel bandwidth (MHz)	56.0	56.0	56.0	56.0	56.0
Capacity (Mbit/s	400.0	360.0	320.0	280.0	220.0
Output power (dBm)	27.0	29.0	30.0	30.0	30.0
Receiver threshold @ BER 10^{-6} (dBm)	-63.0	-66.0	-69.0	-72.0	-75.0
Signature width (MHz)	48.0	48.0	48.0	48.0	48.0
Signature depth, minimum phase (dB)	12.0	15.0	18.0	18.0	22.0
Signature depth, non-minimum phase (dB)	12.0	15.0	16.0	16.0	22.0

Table 11: 13 GHz, 12750-13250 MHz

Parameter	512 QAM	256 QAM	128 QAM	64 QAM	32 QAM
Channel bandwidth (MHz)	28.0	28.0	28.0	28.0	28.0
Capacity (Mbit/s	200.0	180.0	160.0	140.0	110.0
Output power (dBm)	19.0	21.0	22.0	22.0	22.0
Receiver threshold @ BER 10^{-6} (dBm)	-65.0	-67.5	-71.0	-74.0	-77.0
Signature width (MHz)	24.0	24.0	24.0	24.0	24.0
Signature depth, minimum phase (dB)	18.0	21.0	23.0	23.0	28.0
Signature depth, non-minimum phase (dB)	18.0	21.0	21.0	21.0	28.0

Table 12: 18 GHz, 17700-19700 MHz

Parameter	512 QAM	256 QAM	128 QAM	64 QAM	32 QAM
Channel bandwidth (MHz)	55.0	55.0	55.0	55.0	55.0
Capacity (Mbit/s	400.0	360.0	320.0	280.0	220.0
Output power (dBm)	17.0	19.0	20.0	20.0	20.0
Receiver threshold @ BER 10^{-6} (dBm)	-61.5	-64.5	-67.5	-70.5	-73.5
Signature width (MHz)	48.0	48.0	48.0	48.0	48.0
Signature depth, minimum phase (dB)	12.0	15.0	18.0	18.0	22.0
Signature depth, non-minimum phase (dB)	12.0	15.0	16.0	16.0	22.0

Table 13: Antenna data

Parameter	6 GHz 3.0 m	8 GHz 0.6 m	8 GHz 1.2 m	13 GHz 0.6 m	18 GHz 0.6 m
Frequency band	6 GHz	8 GHz	8 GHz	13 GHz	18 GHz
Antenna diameter (m)	3.0	0.6	1.2	0.6	0.6
Antenna gain (dBi)	43.3	32.0	38.0	36.0	38.8

Note: Antenna reference patterns in accordance with ITU-R rec. F.699-7 are used in the interference calculations

A1.4.6 Link budget

Link Distance: 50,000 km			Clearance: 100 %

Information			
Site	A	B	
Site Height	0,00	0,00	m
Ant. Height	70,00	70,00	m
Elevation	-0,17	-0,17	°
Azimuth	181,06	1,04	°
Polarisation	V	V	
Frequency	5 945,20	6 197,24	MHz
Antenna Gain	43,26	43,26	dBi
Tx Power	33,00	33,00	dBm
Threshold(10E-6)	-72,00	-72,00	dBm
Insertion Losses	5,80	5,80	dB

Power Budget	Tx1 -> ...	Tx2 -> ...	
EIRP	70,46	70,46	dBm
Free Space Loss	141,92	142,28	dB
Gas Attenuation	0,47	0,48	dB
Rain Attenuation (30,0 mm/h)	5,64	6,84	dB
Fading Attenuation	57,56	57,70	dB
Diffraction Attenuation	0,00	0,00	dB
Tot. Geo. Climatic Losses	63,67	65,02	dB
Path Loss	205,59	207,30	dB
Flat Receive Level	-34,47	-34,84	dBm
Flat Fade Margin (incl. Diffr.)	37,53	37,16	dB

Figure 33: 6 GHz/50km/128QAM/3.0m, 10m SD antenna separation, 3 dB BRCKT loss, 2.8 dB waveguide loss

Link Distance: 19,999 km			Clearance: 100 %				

Information					Power Budget	Tx1 -> ...	Tx2 -> ...	
Site	A	D			EIRP	68,00	68,00	dBm
Site Height	0,00	0,00	m		Free Space Loss	136,49	136,83	dB
Ant. Height	50,00	50,00	m		Gas Attenuation	0,23	0,24	dB
Elevation	-0,07	-0,07	°		Rain Attenuation (30,0 mm/h)	14,34	16,34	dB
Azimuth	91,06	271,35	°		Fading Attenuation	45,22	45,36	dB
Polarisation	V	V			Diffraction Attenuation	0,00	0,00	dB
Frequency	7 933,00	8 243,00	MHz		Tot. Geo. Climatic Losses	59,79	61,94	dB
Antenna Gain	38,00	38,00	dBi		Path Loss	196,28	198,76	dB
Tx Power	30,00	30,00	dBm		Flat Receive Level	-30,72	-31,06	dBm
Threshold(10E-6)	-69,00	-69,00	dBm		Flat Fade Margin (incl. Diffr.)	38,28	37,94	dB
Insertion Losses	0,00	0,00	dB					

Figure 34: 8 GHz/20km/128QAM/1.2m, 5m SD antenna spacing

Link Distance: 19,999 km			Clearance: 100 %				

Information					Power Budget	Tx1 -> ...	Tx2 -> ...	
Site	A	D			EIRP	62,00	62,00	dBm
Site Height	0,00	0,00	m		Free Space Loss	136,49	136,83	dB
Ant. Height	50,00	50,00	m		Gas Attenuation	0,23	0,24	dB
Elevation	-0,07	-0,07	°		Rain Attenuation (30,0 mm/h)	14,34	16,34	dB
Azimuth	91,06	271,35	°		Fading Attenuation	45,22	45,36	dB
Polarisation	V	V			Diffraction Attenuation	0,00	0,00	dB
Frequency	7 933,00	8 243,00	MHz		Tot. Geo. Climatic Losses	59,79	61,94	dB
Antenna Gain	32,00	32,00	dBi		Path Loss	196,28	198,76	dB
Tx Power	30,00	30,00	dBm		Flat Receive Level	-42,72	-43,06	dBm
Threshold(10E-6)	-69,00	-69,00	dBm		Flat Fade Margin (incl. Diffr.)	26,28	25,94	dB
Insertion Losses	0,00	0,00	dB					

Figure 35: 8 GHz/20km/128QAM/0.6m, 5m SD antenna spacing

Link Distance: 10,000 km   Clearance: 100 %

Information				Power Budget	Tx1 -> ...	Tx2 -> ...	
Site	A	C		EIRP	58,00	58,00	dBm
Site Height	0,00	0,00	m	Free Space Loss	134,60	134,78	dB
Ant. Height	50,00	50,00	m	Gas Attenuation	0,21	0,22	dB
Elevation	-0,03	-0,03	°	Rain Attenuation (30,0 mm/h)	32,91	34,39	dB
Azimuth	91,06	271,21	°	Fading Attenuation	36,64	36,71	dB
Polarisation	V	V		Diffraction Attenuation	0,00	0,00	dB
Frequency	12 765,00	13 031,00	MHz	Tot. Geo. Climatic Losses	69,76	71,32	dB
Antenna Gain	36,00	36,00	dBi	Path Loss	204,37	206,10	dB
Tx Power	22,00	22,00	dBm	Flat Receive Level	-40,82	-41,00	dBm
Threshold(10E-6)	-77,00	-77,00	dBm	Flat Fade Margin (incl. Diffr.)	36,18	36,00	dB
Insertion Losses	0,00	0,00	dB				

Figure 36: 13 GHz/32QAM/10km/0.6m

Link Distance: 10,000 km   Clearance: 100 %

Information				Power Budget	Tx1 -> ...	Tx2 -> ...	
Site	A	C		EIRP	58,80	58,80	dBm
Site Height	0,00	0,00	m	Free Space Loss	137,47	137,95	dB
Ant. Height	30,00	30,00	m	Gas Attenuation	0,57	0,76	dB
Elevation	-0,03	-0,03	°	Rain Attenuation (30,0 mm/h)	58,72	63,88	dB
Azimuth	91,06	271,21	°	Fading Attenuation	37,94	38,13	dB
Polarisation	V	V		Diffraction Attenuation	0,00	0,00	dB
Frequency	17 755,00	18 765,00	MHz	Tot. Geo. Climatic Losses	97,23	102,77	dB
Antenna Gain	38,80	38,80	dBi	Path Loss	234,70	240,72	dB
Tx Power	20,00	20,00	dBm	Flat Receive Level	-40,44	-41,11	dBm
Threshold(10E-6)	-67,50	-67,50	dBm	Flat Fade Margin (incl. Diffr.)	27,06	26,39	dB
Insertion Losses	0,00	0,00	dB				

Figure 37: 18 GHz/10km/128QAM/0.6m

A1.4.7   Predicted Availability

Table 14: 6 GHz/50km/3.0m, Predicted availability (ITU-R Rec P.530-14, average worst month)

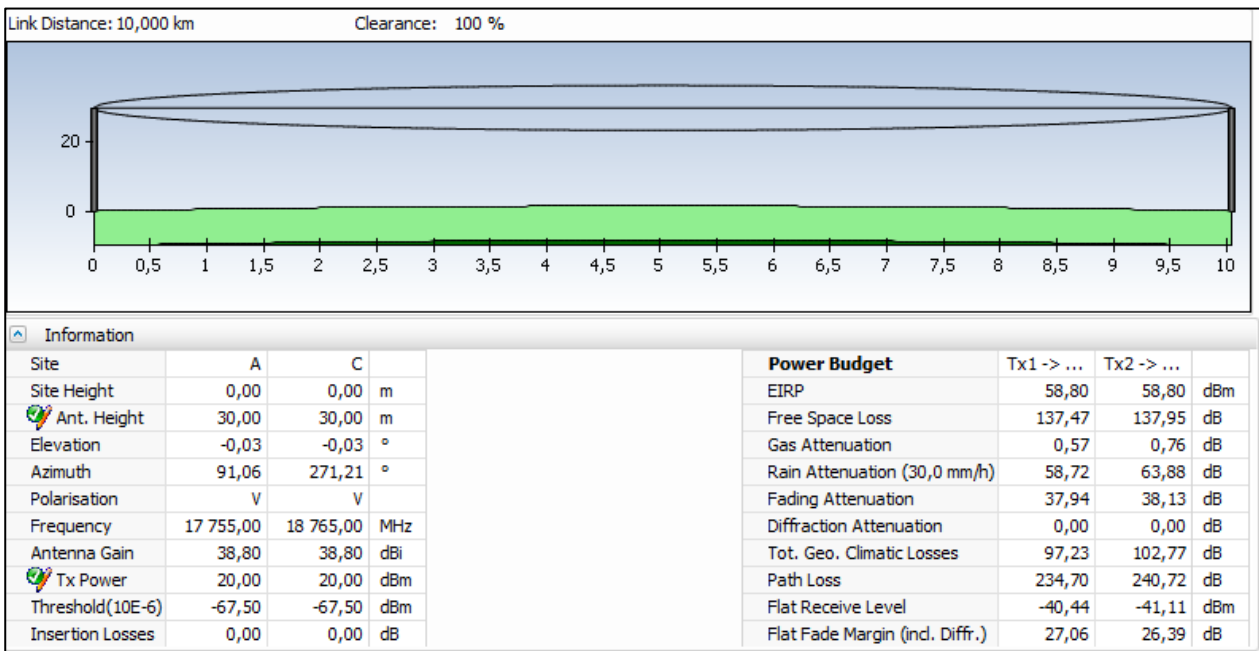| Modulation rate	Threshold degradation (dB)	Availability with SD (BER 10-6)
512 QAM	0	99.9863%
	1	99.9777%
	3	99.9485%
	6	99.8066%
	10	99.0433%
256 QAM	0	99.9976%
	1	99.9968%
	3	99.9938%
	6	99.9791%
	10	99.8786%
128 QAM	0	99.9991%
	1	99.9989%
	3	99.9983%
	6	99.9958%
	10	99.9795%
64 QAM	0	99.9993%
	1	99.9993%
	3	99.9991%
	6	99.9983%
	10	99.9940%
32 QAM	0	99.9998%
	1	99.9998%
	3	99.9998%
	6	99.9996%
	10	99.9985%

Table 15: 8GHz/20km/0.6m, Predicted availability (ITU-R Rec P.530-14, average worse month)

Modulation rate	Threshold degradation (dB)	Availability without SD (BER 10-6)	Availability with SD (BER 10-6)
512 QAM	0	99.3766%	99.9177%
	1	99.2152%	99.8696%
	3	98.7561%	99.6727%
	6	97.5182%	98.6972%
	10	93.7660%	91.7800%
256 QAM	0	99.8028%	99.9917%
	1	99.7518%	99.9870%
	3	99.6067%	99.9672%
	6	99.2152%	99.8697%
	10	98.0286%	99.1779%
128 QAM	0	99.9215%	99.9987%
	1	99.9012%	99.9979%
	3	99.8434%	99.9948%
	6	99.6876%	99.9793%
	10	99.2152%	99.8697%
64 QAM	0	99.9606%	99.9997%
	1	99.9505%	99.9995%
	3	99.9215%	99.9987%
	6	99.8434%	99.9948%
	10	99.6067%	99.9672%
32 QAM	0	99.9803%	99.9999%
	1	99.9752%	99.9999%
	3	99.9606%	99.9997%
	6	99.9215%	99.9987%
	10	99.8028%	99.9918%

Table 16: 8GHz/20km/1.2m, Predicted availability (ITU-R Rec P.530-14, average worst month)

Modulation rate	Threshold degradation (dB)	Availability without SD (BER 10-6)	Availability with SD (BER 10-6)
512 QAM	0	99.9272%	99.9989%
	1	99.9084%	99.9982%
	3	99.8574%	99.9956%
	6	99.7372%	99.9824%
	10	99.4345%	99.8892%
256 QAM	0	99.9770%	99.9999%
	1	99.9710%	99.9998%
	3	99.9541%	99.9996%
	6	99.9084%	99.9982%
	10	99.7850%	99.9889%
128 QAM	0	99.9908%	100.000%
	1	99.9885%	100.000%
	3	99.9817%	99.9999%
	6	99.9635%	99.9997%
	10	99.9084%	99.9982%
64 QAM	0	99.9975%	100.000%
	1	99.9969%	100.000%
	3	99.9951%	100.000%
	6	99.9901%	100.000%
	10	99.9752%	99.9999%
32 QAM	0	99.9988%	100.000%
	1	99.9984%	100.000%
	3	99.9975%	100.000%
	6	99.9951%	100.000%
	10	99.9876%	100.000%

Table 17: 13GHz/10km/0.6m, Predicted availability (ITU-R Rec P.530-14, average worst month)

Modulation rate	Threshold degradation (dB)	Availability with SD (BER 10-6)
512 QAM	0	99.9682%
	1	99.9607%
	3	99.9399%
	6	99.8848%
	10	99.7069%
256 QAM	0	99.9876%
	1	99.9847%
	3	99.9768%
	6	99.9563%
	10	99.8968%
128 QAM	0	99.9956%
	1	99.9944%
	3	99.9912%
	6	99.9830%
	10	99.9607%
64 QAM	0	99.9978%
	1	99.9972%
	3	99.9956%
	6	99.9912%
	10	99.9791%
32 QAM	0	99.9989%
	1	99.9986%
	3	99.9978%
	6	99.9956%
	10	99.9889%

Table 18: 18GHz/10km/0,6m, Predicted availability (ITU-R Rec P.530-14, average worst month)

Modulation rate	Threshold degradation (dB)	Availability with SD (BER 10-6)
512 QAM	0	99.9183%
	1	99.8992%
	3	99.8456%
	6	99.6991%
	10	99.1503%
256 QAM	0	99.9712%
	1	99.9645%
	3	99.9462%
	6	99.8992%
	10	99.7605%
128 QAM	0	99.9872%
	1	99.9846%
	3	99.9766%
	6	99.9563%
	10	99.8992%
64 QAM	0	99.9939%
	1	99.9921%
	3	99.9878%
	6	99.9766%
	10	99.9462%
32 QAM	0	99.9969%
	1	99.9961%
	3	99.9939%
	6	99.9878%
	10	99.9724%

A1.4.8 Calculated threshold degradation

Pixel size of 0.25 m was used for Vestas V100, Vestas V80 and Vestas V52.

Table 19: 6 GHz 50 km, Vestas V100, V80 and V52 wind turbine located at 25 km respectively 3 km from end point

r(m)	25 km large WT	25 km medium WT	25 km small WT	3 km large WT	3 km medium WT	3 km small WT
0.00	25.4	23.84	19.7	31.28	30.48	26.97
25.00	25.63	23.59	18.49	27.11	26.86	24.63
50.00	25.09	22.02	14.34	14.92	14.08	12.78
75.00	20.28	17.41	12	6.55	5.8	5.04
100.00	18.14	15.83	11.13	3.37	3.41	2.82
125.00	16.07	14.34	10.19	2.35	2.33	1.65
150.00	14.48	12.97	9.15	1.41	1.32	1.08
175.00	13.07	11.86	8.14	1.35	1.11	0.76
200.00	11.2	10.39	7.31	1.02	0.54	0.59
225.00	8.75	8.86	6.01	0.84	0.58	0.36
250.00	7.03	7.16	4.73	0.54	0.53	0.43
275.00	5.5	5.94	3.64	0.61	0.46	0.39
300.00	4.74	4.89	2.78	0.37	0.33	0.31
325.00	3.9	3.95	2.05	0.36	0.35	0.2
350.00	3.32	2.98	1.57	0.22	0.21	0.15
375.00	2.58	2.39	1.18	0.23	0.22	0.16
400.00	1.99	1.7	0.94	0.23	0.2	0.15
425.00	1.27	1.08	0.69	0.2	0.15	0.13
450.00	0.91	0.82	0.6	0.14	0.13	0.1
475.00	0.79	0.67	0.47	0.12	0.09	0.1

Table 20: 8 GHz 20 km, 1.2m antenna Vestas V100, V80 and V52 wind turbine located at 10 km respectively 3 km from end point

r(m)	10 km large WT	10 km medium WT	10 km small WT	3 km large WT	3 km medium WT	3 km small WT
0.00	31.04	29.85	25.73	33.55	32.82	29.51
25.00	30.34	29.75	26.65	26.92	26.12	26.44
50.00	23.27	23.89	20.23	19.72	19.73	15.91
75.00	18.71	16.74	16.91	11.03	10.54	8.37
100.00	13.34	12.57	12.96	5.57	5.24	5.08
125.00	10.29	10.14	9.28	4.20	3.76	3.22
150.00	9.17	9.27	6.87	2.65	2.48	2.15
175.00	7.26	6.46	5.91	1.88	1.99	2.20
200.00	5.1	4.86	3.71	1.56	1.77	1.49
225.00	3.56	3.27	2.78	1.42	1.47	0.74
250.00	3.56	2.52	1.66	0.89	0.74	0.69
275.00	1.72	1.76	1.39	0.70	0.79	0.68
300.00	1.48	1.15	1.01	0.66	0.54	0.61
325.00	0.82	0.8	0.67	0.59	0.65	0.48
350.00	0.8	0.55	0.52	0.52	0.42	0.63
375.00	0.87	0.66	0.44	0.28	0.27	0.21
400.00	0.54	0.44	0.36	0.31	0.30	0.24
425.00	0.57	0.34	0.37	0.27	0.26	0.29
450.00	0.5	0.39	0.29	0.21	0.20	0.14
475.00	0.32	0.35	0.26	0.13	0.11	0.11

Table 21: 8 GHz 20 km, 0.6m antenna Vestas V100, V80 and V52 wind turbine located at 10 km respectively 3 km from end point

r(m)	10 km large WT	10 km medium WT	10 km small WT	3 km large WT	3 km medium WT	3 km small WT
0.00	19.72	18.61	14.92	22.02	21.36	18.31
25.00	19.55	19.01	16.19	16.92	16.20	16.52
50.00	13.77	14.31	11.19	11.76	11.78	8.68
75.00	10.5	8.97	9	6.95	6.50	4.71
100.00	6.83	6.25	6.49	4.03	3.71	3.55
125.00	5.03	4.93	4.37	2.83	2.55	2.16
150.00	4.57	4.63	3.17	1.56	1.46	1.25
175.00	3.62	3.17	2.83	1.17	1.25	1.38
200.00	2.77	2.61	1.91	1.06	1.20	1.01
225.00	2.2	1.98	1.66	1.07	1.11	0.55
250.00	2.64	1.84	1.18	0.69	0.57	0.54
275.00	1.5	1.54	1.2	0.54	0.61	0.53
300.00	1.51	1.18	1.03	0.53	0.44	0.49
325.00	1.03	1.01	0.84	0.50	0.56	0.41
350.00	1.26	0.87	0.83	0.48	0.39	0.58
375.00	1.28	0.98	0.66	0.28	0.27	0.21
400.00	0.75	0.61	0.5	0.33	0.33	0.26
425.00	0.74	0.45	0.48	0.31	0.30	0.34
450.00	0.58	0.46	0.34	0.26	0.26	0.18
475.00	0.34	0.36	0.27	0.18	0.15	0.15

Table 22: 13 GHz 10 km, Vestas V100, V80 and V52 wind turbine located at 5 km respectively 1 km from end point

r(m)	5 km large WT	5 km medium WT	5 km small WT	1 km large WT	1 km medium WT	1 km small WT
0.00	33.53	32.88	29.52	35.74	35.59	33.49
25.00	26.83	25.18	23.67	27.55	24.99	19.92
50.00	17.71	16.05	12.92	11.24	6.47	4.73
75.00	12.18	11.34	8.89	3.63	2.75	2.52
100.00	7.2	6.72	6.24	1.46	1.62	1.89
125.00	4.06	3.73	3.81	0.98	0.83	0.94
150.00	2.91	2.89	2.78	0.79	0.65	0.63
175.00	2.26	2.05	1.91	0.37	0.30	0.26
200.00	1.59	1.6	1.39	0.28	0.23	0.27
225.00	0.56	0.51	0.5	0.18	0.15	0.19
250.00	0.64	0.62	1.12	0.09	0.08	0.09
275.00	0.69	0.66	0.61	0.07	0.07	0.12
300.00	0.54	0.44	0.36	0.08	0.07	0.07
325.00	0.31	0.35	0.25	0.06	0.04	0.05
350.00	0.25	0.28	0.2	0.01	0.01	0.00
375.00	0.18	0.17	0.14	0.02	0.03	0.02
400.00	0.16	0.15	0.15	0.02	0.02	0.01
425.00	0.11	0.14	0.12	0.01	0.01	0.01
450.00	0.1	0.09	0.13	0.00	0.00	-0.01
475.00	0.07	0.07	0.09	0.01	0.00	0.01

Table 23: 18 GHz 10 km, Vestas V100, V80 and V52 wind turbine located at 5 km respectively 1 km from end point

r(m)	5 km large WT	5 km medium WT	5 km small WT	1 km large WT	1 km medium WT	1 km small WT
0.00	31.49	30.95	28.06	32.30	32.10	31.90
25.00	25.43	23.69	19.65	24.96	22.23	15.95
50.00	15.76	11.80	9.30	3.91	1.70	1.15
75.00	7.72	7.14	7.04	0.75	0.67	0.74
100.00	3.87	3.79	3.33	0.30	0.31	0.35
125.00	2.56	2.46	2.58	0.23	0.21	0.17
150.00	0.97	0.90	1.32	0.12	0.13	0.13
175.00	0.43	0.35	0.62	0.05	0.05	0.02
200.00	0.35	0.28	0.29	0.07	0.06	0.05
225.00	0.14	0.09	0.09	0.04	0.03	0.05
250.00	0.03	0.03	0.02	0.02	0.02	0.03
275.00	0.01	0.01	0.02	0.01	0.01	0.01
300.00	0.01	0.02	0.01	0.00	0.00	-0.01
325.00	0.00	0.00	-0.01	0.00	0.00	0.00
350.00	0.01	0.01	0.00	-0.01	0.00	-0.01
375.00	0.01	0.00	0.00	-0.01	-0.01	-0.01
400.00	0.00	0.00	0.00	-0.01	-0.01	-0.01
425.00	0.00	-0.01	-0.01	-0.01	-0.01	-0.01
450.00	-0.01	-0.01	-0.01	-0.01	-0.01	-0.01
475.00	-0.01	-0.01	-0.01	-0.01	-0.01	-0.01

ANNEX 2: CONTRIBUTIONS BY UNIVERSITY OF THE BASQUE COUNTRY (SPAIN)

A2.1 INTRODUCTION

Terrestrial microwave radio links are used for point-to-point communications within a large frequency range, typically from 1 GHz to around 58 GHz. The performance of a fixed radio link might be degraded due to obstruction or scattering of great structures located close to radio path line-of-sight [22],[23]. Disturbance due to near-field effects of wind turbines located close to radio link antennas should be also considered in the analysis [24],[25]:

- Obstruction of the path: due to the extensive volume occupied by the tower and the blades of a wind turbine, they can obstruct the path corresponding to a point-to-point radio link, in such a way that the data transmission might be cut-off, avoiding the correct reception of the signal.
- Interference due to signal scattering on the surface of the wind turbines: transmitted signals that are received in the other end of the radio link after being scattered on the surface of the wind turbines may be a significant interference on the direct transmission between both ends of the radio link.
- Near-field effects: Near-field effects are caused by great objects within near-field region, which can result in coupling with the antenna and distorting the ultimate far-field antenna pattern [26],[27].

The potential impact must be analysed on a case-by-case basis, taking into account the particular features of each installation and the involved services, such as the accurate location of the telecommunications infrastructure, terrain altimetry and topography, telecommunication towers height, service frequency, radiating systems characteristics and reception conditions.

This appendix describes the methodology used by the TSR research group of the University of the Basque Country, UPV/EHU (Spain) for the impact analysis of wind farms on microwave fixed radio links.

In order to provide a clear description, results of a real impact study based on a wind farm that have already been deployed, are included in the document. Results have been obtained by using Wi2 software tool, developed by the TSR research group of the University of the UPV/EHU and no harmful impact has been observed by the radio link operators [28],[38].
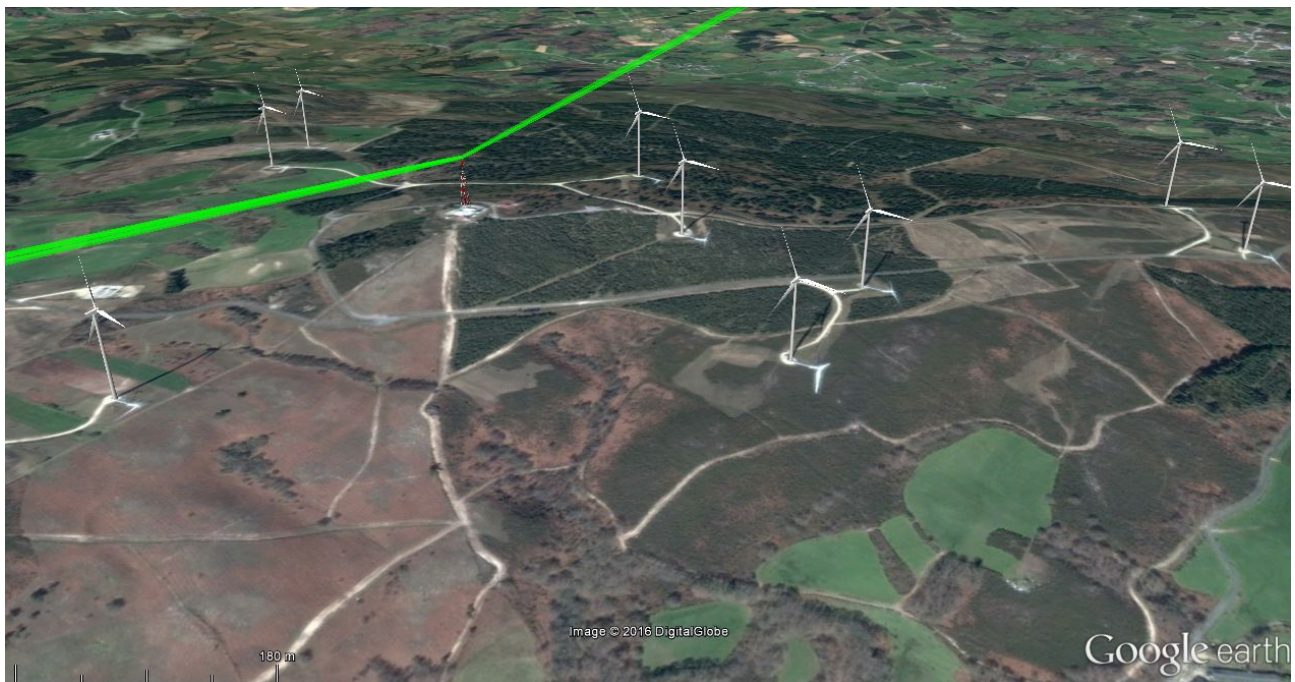

Figure 38: Aerial view of the scenario under analysis, composed of two fixed microwave radio links located near a wind farm installation. The figure shows a 3D representation of the transmitter site and the wind turbines. In green the 2nd Fresnel ellipsoid of both radio links are represented as a reference of the link paths [28]

A2.2 PRINCIPLES OF IMPACT STUDY ON FIXED RADIO LINKS CONDUCTED BY THE UNIVERSITY OF THE BASQUE COUNTRY (SPAIN)

A2.2.1   Coordination zone

The first step of the analysis procedure consists of delimiting the area where wind turbines may generate distortion. This area is named coordination zone, defined as a wide corridor along the radio link path. All the wind turbines that are planned to be installed at a distance shorter than 500 m to the radio link path will be included in the analysis of the potential impact [25].

Figure 39: Above: in green, representation of the 2nd Fresnel ellipsoid of each radio link; in red, coordination area for each radio link. Below, coordination area for the whole extension of one of the fixed radio links [28]

Then, three different effects are considered in the study: obstruction of the path, interference due to signal scattering and near field effects

A2.2.2   Obstruction of the path

Diffraction modifies a radio wave when an object obstructs part of an advancing wave front. It should be noted that the object does not need to be a good reflector for this to happen. In order to prevent the radio links from being obstructed, a certain exclusion volume around the line of sight between the two ends of the link must be respected.

In studying radio wave propagation between two points A and B, the intervening space can be subdivided by a family of ellipsoids, known as Fresnel ellipsoids, all having their focal points at A and B such that any point on the n ellipsoid fulfil the condition of representing a path n·(λ/2) longer than the direct path [29]. Criteria for avoiding diffraction effects are based upon enduring that any object near the link path intersects the volume defined by a Fresnel ellipsoid around the fixed link path. Some propagation effects require consideration of Fresnel zones, which are the zones obtained by taking the intersection of a family of ellipsoids by a plane [29].

Diffraction theory indicates that the direct path between the transmitter and the receiver needs a clearance of at least 60% of the radius of the first Fresnel zone to achieve free-space propagation conditions [30]. At frequencies above about 13 GHz, the estimation accuracy of the obstacle height begins to approach the radius of the Fresnel zone [30]. As a practical rule, propagation is assumed to occur in line-of-sight (LoS), i.e. with negligible diffraction phenomena if there is no obstacle within the first Fresnel ellipsoid [29].

Nevertheless, in order to provide longer safeguarding distances, for the case of wind turbines a more conservative criterion resulting from applying the 2nd Fresnel ellipsoid is proposed by some entities [24],[25].
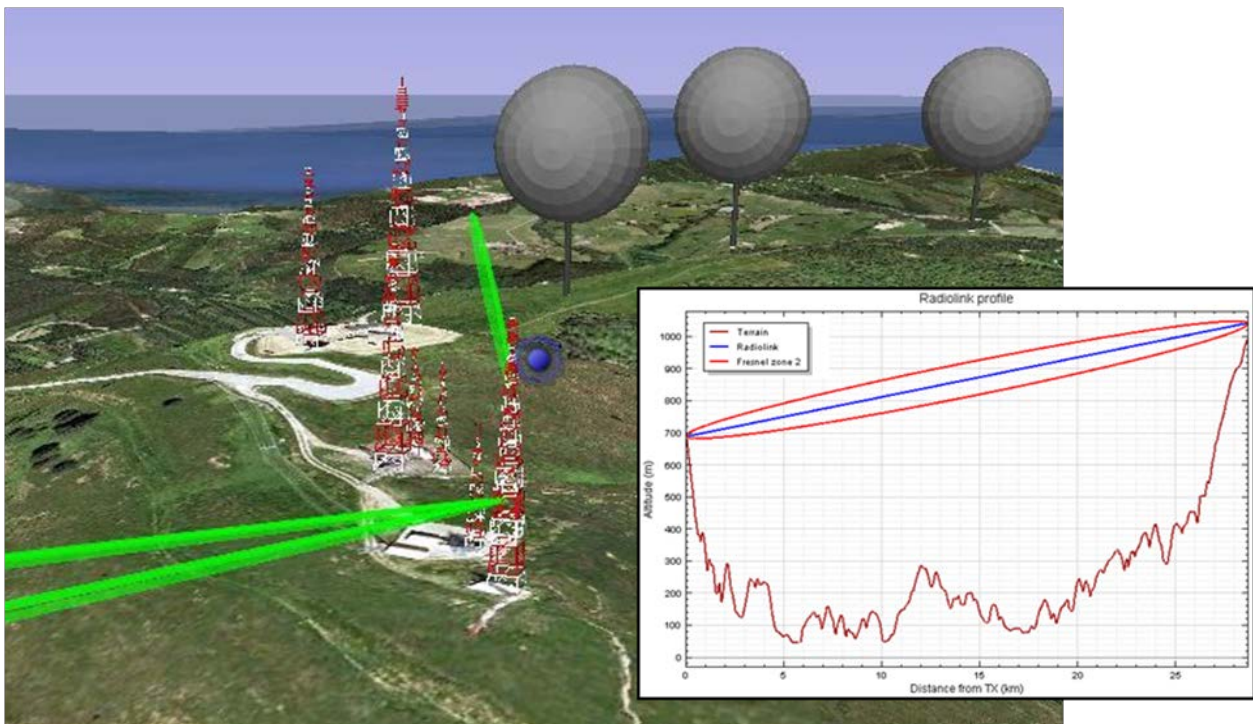

Figure 40: Representation of the Fresnel ellipsoid of three fixed radio links (in green) and the volume occupied by wind turbines considering all possible rotor orientations (in grey). An additional graph containing the radio link path and the Fresnel ellipsoid is also shown [28]

Accordingly, the algorithm used by the UPV/EHU for estimating the potential obstruction of the path is based on calculating the potential intersection between the second Fresnel ellipsoid and the volume occupied by wind turbines, taking into account the dimensions of the turbine components and all the possible orientations of the wind turbine rotor:

▪ The radius of the second Fresnel zone around the direct line-of-sight path of a radio link is given by:

$$R_{F2} = \sqrt{\frac{2 \cdot \lambda \cdot d_1 \cdot d_2}{d_{1} + d_2}} \ \text{(m)} \tag{A2-1}$$

where

d_1, d_2 are the distances from each end of the radio path (m)

λ is the wavelength (m)

▪ For the wind turbine, the whole spatial volume that they fill, i.e., all the possible blades' positions is considered. This way, the volume of each wind turbine is represented as a sphere located on top of a cylindrical tower.

▪ The criterion to determine if this obstruction may exist is based on evaluating if the turbines intersect with the second Fresnel ellipsoid of each radio link.

The obstruction analysis detects if any of the wind turbine components enters the second Fresnel ellipsoid around the radio path (see Figure 41). Terrain elevation data are included in the assessment in order to consider the relative position of all the elements involved. In case of obstruction, the algorithm also estimates the necessary distance to move the wind turbine away from the second Fresnel ellipsoid to avoid such obstruction, as it is shown in the figure.

Obstructing element	Clearance (m)
A1	648.07
A10	792.01
A2	488.58
A3	463.23
A4	404.71
A5	65.06
A6	207.14
A7	153.88
A8	446.62
A9	887.31
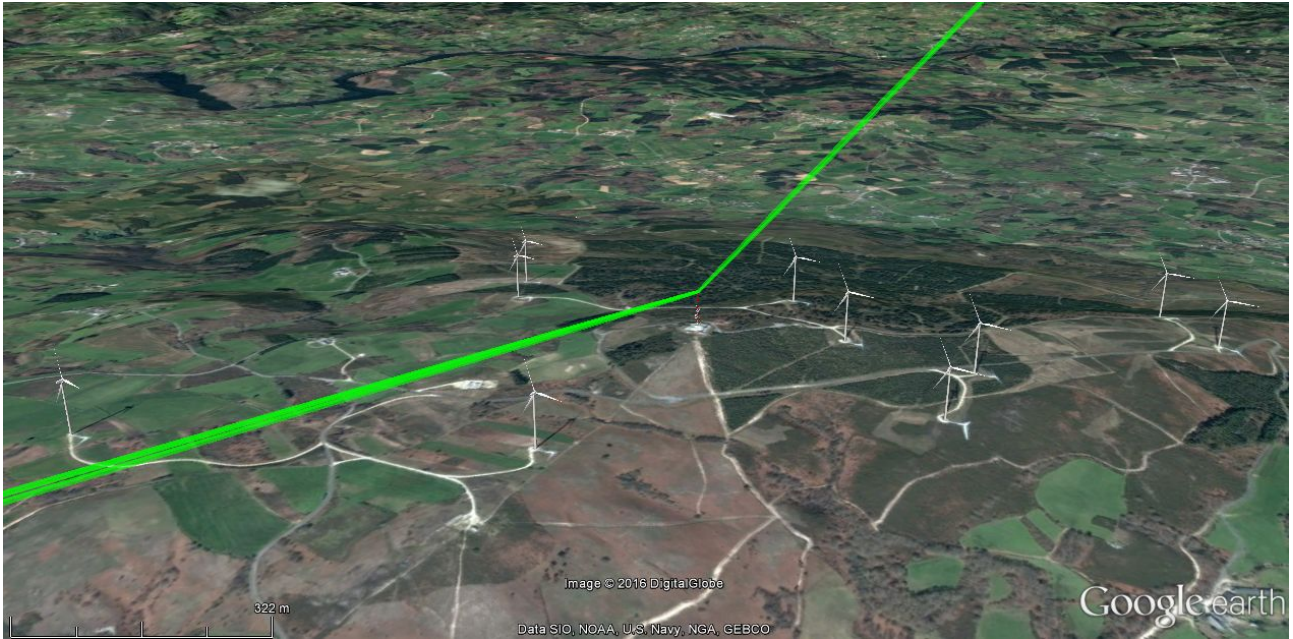
Obstructing element	Clearance (m)
A1	370.9
A10	892.11
A2	75.46
A3	70.41
A4	444.83
A5	309.73
A6	196.87
A7	93.46
A8	285.28
A9	805.91
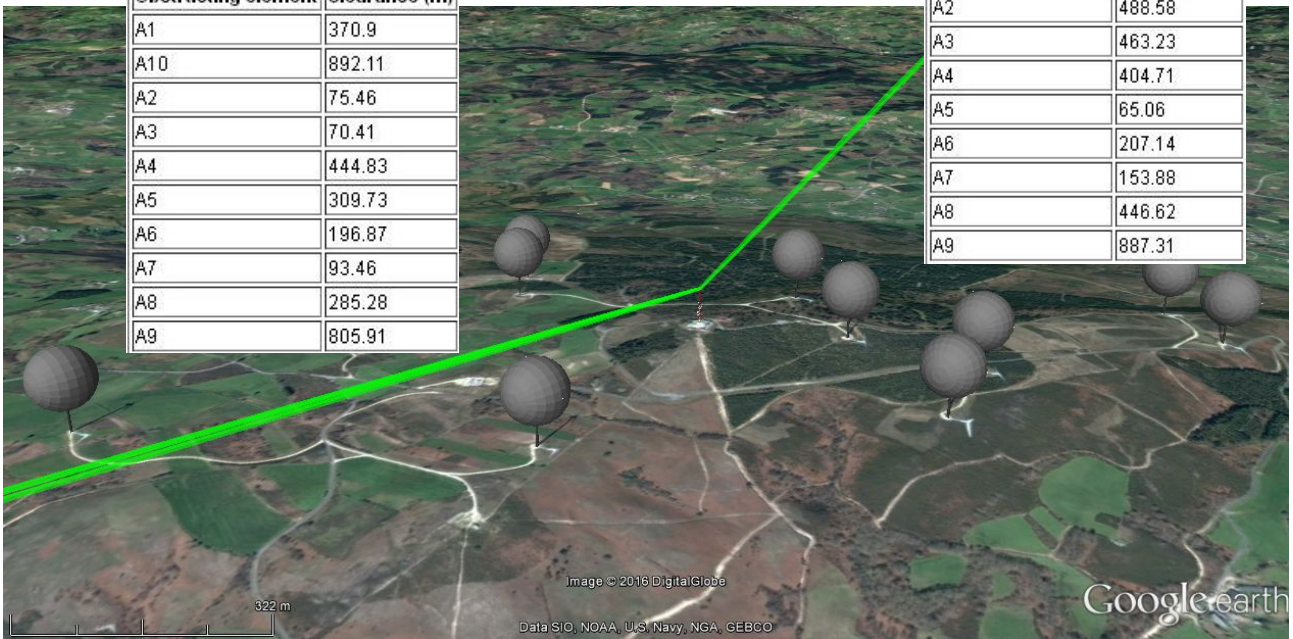
Figure 41: Above: wind turbines and transmitter site. Below: in green, representation of the 2nd Fresnel ellipsoid of each radio link; in grey, volume occupied by the wind turbines, considering all possible rotor orientations. Tables containing clearance distances between the 2nd Fresnel ellipsoid of the radio links and each turbine are also shown; positive values demonstrate that there is no overlap between them [28]
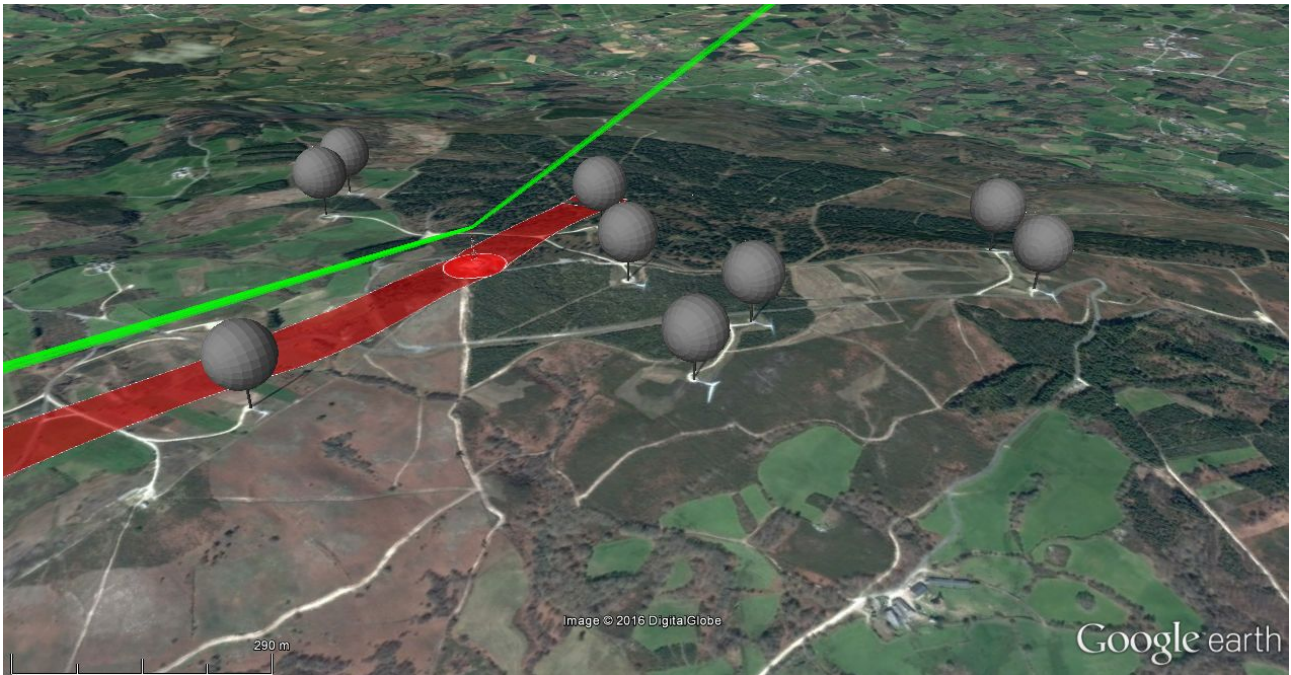
Figure 42: In red, constraint masks where the installation of a wind turbine would cause obstruction of the fixed radio link (obstruction of the 2nd Fresnel ellipsoid) [28]

A2.2.3 Interference due to signal scattering

A signal transmitted from a radio link antenna may be reflected or scattered by the structure of a wind turbine located in the nearness of the radio link. In practice, at radio frequencies many surfaces are either curved or rough in comparison with the wavelength. The re-radiated energy may be somewhat concentrated in a specular direction (reflection), but a significant proportion often exists in other directions (scattering). If these scattered signals reach the other end of the radio link with significant level, the combination of the signals and the time differences between them may interfere with the radio link quality of service.

The procedure to evaluate if the scattered signal may degrade the radio link is based on calculating the carrier-to-interference ratio C/I (power of the desired signal C with respect to the interfering signal I) in the receiver location, such as it is proposed by Ofcom [24] and JRC [25].

Both power levels are obtained as follows: on the one hand, the desired power from the other end of the link (direct path T-R, see Figure 43); and on the other hand, the power of the interfering signals due to the wind turbine (scattering signal path T-W-R, see Figure 43). This interfering signal depends on the power scattered by the wind turbine (expressed as a function of its Radar Cross Section), the relative distances transmitter-wind turbine-receiver and the gain of the antennas towards the relative location of the wind turbine [24].
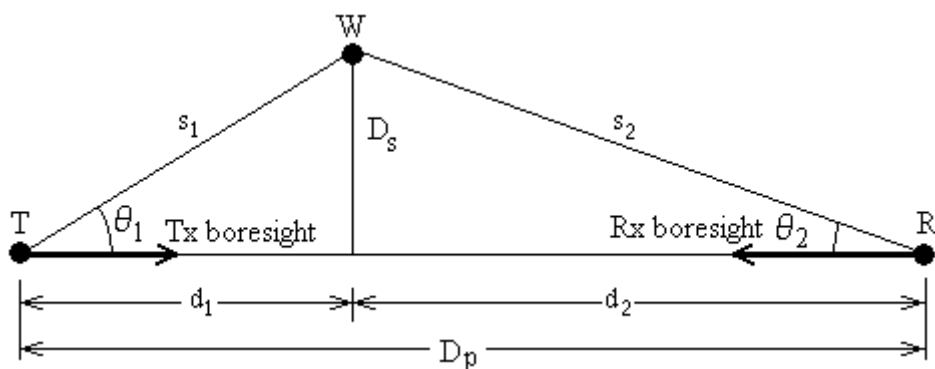

Figure 43: Reflection/scattering from wind turbine affecting link between T and R (Source: [24])

It is assumed that:

- T and R use directional antennas mutually aligned to maximise the direct T-R signal;
- The radio link T-R is line of sight, and the paths T-W and W-R are also line of sight;
- The reflected paths are sufficiently close to the direct path that it can be assumed that any variation of propagation due to atmospheric effects will correlate on both the direct and reflected/scattered paths.

On this basis the calculation of C/I ratio can be based on free-space propagation. The ratio, expressed in dB, of the wanted signal level received from the direct T-R path divided by the worst-case signal level received from the indirect T-W-R path, is given by:

$$\frac{C}{I} = \frac{\frac{P_T G_1(0)}{4\pi D_p^2} \cdot \frac{G_2(0)\lambda^2}{4\pi}}{\frac{P_T G_1(\theta_1)}{4\pi s_1^2} \sigma \frac{1}{4\pi s_2^2} \frac{G_2(\theta_2)\lambda^2}{4\pi}} \tag{A2-2}$$

$$\frac{C}{I} = (4\pi)\frac{G_1(0)G_2(0)s_1^2 s_2^2}{G_1(\theta_1)G_2(\theta_2)D_p^2 \sigma} \tag{A2-3}$$

$$\frac{C}{I}(dB) = 10\log_{10}(4\pi) + G_1(0) + G_2(0) - G_1(\theta_1) - G_2(\theta_2) + 20\log_{10}(s_1 \cdot s_2) - 20\log_{10}(D_p) - \sigma \tag{A2-4}$$

where:

s_1, s_2 are the distances T-W and W-R, respectively (m)

σ is the worst-case radar cross section of turbine (m²)

$G_1(0)$, $G_2(0)$, are the antenna boresight gains (dBi)

$G_1(\theta_1)$, $G_2(\theta_2)$ are the antenna gains at off-boresight angles θ (dBi)

The algorithm for determining the impact due to reflected or scattered signals provides a clearance area delimited by the threshold Carrier to Interference (C/I) ratio necessary for avoiding this type of degradation. The magnitude of the clearance zone depends mainly on both the directivity of the aerials and the required threshold C/I ratio: the threshold C/I ratio for each frequency band and modulation scheme determines the maximum interference level; the discrimination of the radiation pattern of transmitter and receiver aerials may considerably reduce the impact, and they must be considered in the assessment.

The exclusion zone calculation should be based on the maximum RCS which can possibly occur, even if this may apply to a given link-turbine layout only rarely. This way, the previous equation is used to calculate the worst-case C/I ratio resulting from a given wind turbine at a known position, which typically would be defined by distances d_1, d_2 and the side distance D_s in Figure 43. An exclusion zone around the link is obtained iterating the equation for increasing values of D_s until the required value of C/I is obtained. This is done for different pairs of d_1 and d_2 values, covering the link path length in suitably small increments of distance. This is to say, any reflected/scattered signal from the wind turbine located outside the constraint zone will arrive at the receiver with an amplitude sufficiently smaller than the direct signal such that its effect, even allowing for the delayed arrival, will be negligible.

The choice of threshold C/I ratios will depend on the modulation and coding schemes of the link and the required performance. Typically a large C/I is specified which should be exceeded for all but 20% of time,

and a somewhat lower value which must be exceeded for all but a much smaller percentage of time, typically in the range 0.1% to 0.001%.

The protection threshold should consider the modulation scheme, the bandwidth and other aspects of the fixed radio link under analysis. A reference value of C/I = 36 dB is proposed in [31]. More details on the required C/I values can be found in Table 1 of ITU-R F.1101 [32].
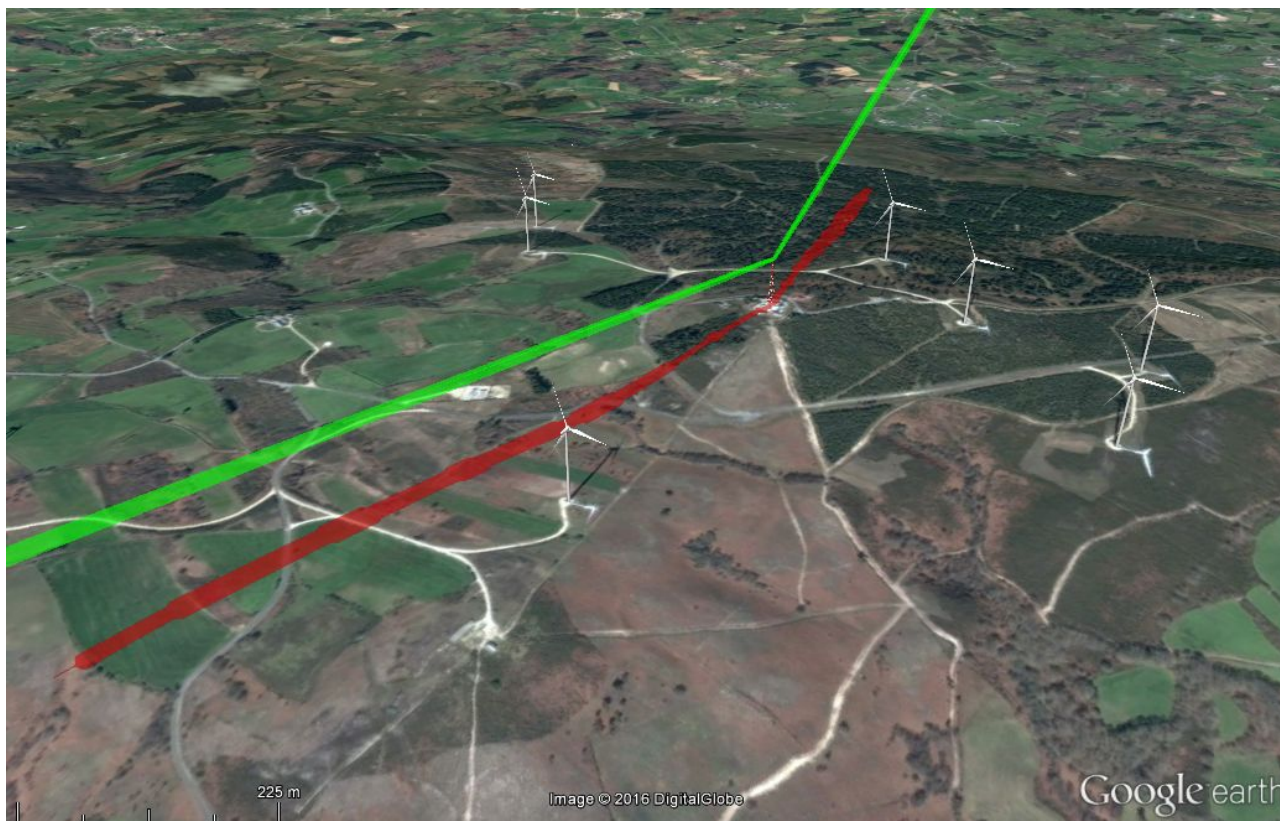

Figure 44: In red, constraint masks where the installation of a wind turbine would cause interference due to scattering [28]

A2.2.4 Near field effects

Antennas are designed to operate in the far-field region, where radiated fields are dominant and allow communications for long distances. The near-field region involves the reactive near-field region (the region immediately surrounding the antenna where non-radiating components predominate) and the radiating near-field region (the region where the radiating components become predominant, but antenna gain and angular distribution of the radiated field vary with distance from the antenna) [33],[34]. Near-field effects are caused by great objects within the near-field region, which can result in coupling with the antenna and distorting the ultimate far-field antenna pattern [26],[27]. Near-field effects are difficult to predict and characterise, and for this reason, the usual procedure to avoid these effects consists of delimiting a clearance area or safeguarding area around the antenna, where great objects, particularly if they are metallic objects, should be avoided.

As the analysis of the potential impact of a wind farm before it is installed is the best way to prevent the disturbance on the existing radio services, this document proposes a method for calculating the safeguarding area to avoid near-field effects on the microwave radio link antennas. The safeguarding area is a constraint mask where no wind turbines should be installed in order to avoid these effects.

The analysis of this effect is based on defining an exclusion zone for any wind turbine based on the criterion for the safeguarding distance that avoids near field effects. Depending on the type of antenna used and the transmission frequency, a near-field distance is calculated, and therefore, a sphere with a radio equal to this distance around the antenna is obtained. This sphere is used to define the safeguarding volume around the tower for each radio link.

For the definition of the constraint mast, the blade length is considered, in such a way that the constraint mask refers to the virtual wind turbine locations that would degrade the corresponding radio link.

The method is based on theoretical criteria and it has been developed by the UPV/EHU. It is applicable to microwave radio links above 1 GHz (as near-field effects at lower frequencies are not as important as other disturbances in the safeguarding area assessment [25]), and for electrically large reflectors (as these are the typical microwave antennas in this frequency range). Input data required by the method are the microwave radio link basic parameters (frequency, dimensions of the antenna and coordinates of the transmitter site).

In other methods, the criterion used to define the clearance distance is an adaptation of the generic criterion ($2D^2\lambda$) and incorporating the antenna efficiency (η). Nevertheless, according to IEEE recommendations, this criterion is not adequate for all types of antennas and should not be applied indiscriminately [35],[36], mainly for reflector antennas, where clearance distance can be delimited to a shorter extent [33],[34],[36]. Instead, in this method, the criterion to delimit the near-field region is the nature of the radiated field and the way this varies with the distance from the antenna [33],[34].

Although conservative criteria are usually pursued in this type of analysis [24][25][37], this proposal aims at results close to real performance of antennas [38]. Unbiased and objective criteria will ensure the development of wind energy without degrading the proper operation of radio links.

A more detailed description of the theoretical basis is available at the Journal of Electromagnetic Waves and Applications (http://www.tandfonline.com/doi/full/10.1080/09205071.2015.1096838) [38]. In the referenced paper, the proposed method is applied to real cases of wind farms close to radio links facilities and compared to results obtained with more conservative criteria.

A2.2.4.1 Terms used in the method

The following terms are used in the method:
- Safeguarding distance: antenna on-axis distance for far-field condition.
- Safeguarding volume: volume around the antenna that must be clear of any part of the wind turbine, including rotating blades.
- Safeguarding area: projection of the safeguarding volume on the ground.
- Constraint mask: area where wind turbines should not be installed, ensuring that none of the parts of the turbine, even rotating blades, will enter in the near-field safeguarding area.

A2.2.4.2 Safeguarding distance

For circular reflector antennas operating above 1 GHz, with diameter $D \gg \lambda$, the field in front of the antenna can be classified according to the variation of power density with the distance into three regions: near-field region, transition region and a far-field region [33],[34],[35].

In the near-field region, the power density varies with location, but it reaches a maximum value on propagation axis, which depends only on antenna characteristics (power fed to antenna, diameter and efficiency):

$$S_{nf} = \frac{16 \cdot \eta \cdot P}{\pi \cdot D^2} \tag{A2-5}$$

In the transition region the power density decreases inversely with the distance to the antenna:

$$S_{if} = S_{nf} \cdot \left(\frac{R_{nf}}{r}\right) \quad \text{for } R_{nf} \leq r < R_{ff} \tag{A2-6}$$

Last, in the far-field region the power density decreases inversely as the square of the distance:

$$S_{ff} = 2.47 \cdot S_{nf} \cdot \left(\frac{R_{nf}}{r}\right)^2 = \frac{P \cdot G}{4\pi \cdot r^2} \quad \text{for } R \geq R_{ff} \text{ (4)} \tag{A2-7}$$

Where S is the on-axis power density for near-field (S_{nf}), transition region (S_{if}) and far-field region (S_{ff}); P is the power fed to the antenna; D is the antenna diameter; r is the on-axis distance from antenna; and R_{nf} and R_{ff} are the extent of near-field and the distance to the beginning of the far-field region, respectively.

The extent of the near-field region is defined by the point on the antenna axis for which the entire aperture is a single Fresnel zone [33],[34],[35].

$$R_{nf} = \frac{D^2}{4\lambda} \qquad \text{(A2-8)}$$

The boundary to delimit the transition region can then be calculated by applying the continuity condition of power density for the transition and the far-field regions. Hence, at a distance from the antenna r = R_{ff}, and applying equations (6)-(8):

$$[S_{if}]_{r=R_{ff}} = \left[S_{nf} \cdot \left(\frac{R_{nf}}{r}\right)\right]_{r=R_{ff}} = [S_{ff}]_{r=R_{ff}} = \left[2.47 \cdot S_{nf} \cdot \left(\frac{R_{nf}}{r}\right)^2\right]_{r=R_{ff}} \qquad \text{(A2-9)}$$

This condition is fulfilled for [33],[34],[35].

$$R_{ff} = 0.6\left(\frac{D^2}{\lambda}\right) \qquad \text{(A2-10)}$$

As a result, eq. (10) allows the calculation of the on-axis safeguarding distance for the analysis of the near-field effects that wind turbines may cause, when assumptions described in the previous paragraphs are applied [37]. As it can be observed, this distance is significantly shorter than the radius of the clearance area proposed by Ofcom.

The proposed calculation method is in line with other proposals based on measurements of IEEE [36] and Canada Government [39], which recommend a distance of $0.5 \cdot (D^2/\lambda)$ for delimiting the near-field region in measurements of radio frequency electromagnetic fields.

A2.2.4.3 Safeguarding volume

The on-axis safeguarding distance obtained in equation (8) is valid only for antenna boresight. In this section, the off-axis power density is analysed, in order to delimit the extent of the safeguarding volume in other directions, and therefore, to shape the safeguarding volume in a more accurate way.

According to Federal Communications Commission (FCC), relative intensities at off-axis locations are significantly lower than on-axis power densities at the same horizontal distance from the antenna. This is because the beam of radiation is collimated so that most of the power in the near-field is contained in a region having approximately the diameter of the reflector [35]. Therefore, it can be assumed that, if the point of interest is at least one antenna diameter away from the centre of the main beam, the power density at that point would be at least a factor of 100 (20 dB) less than the value calculated for the equivalent distance in the main beam [34],[35].

This is in line with Rec. ITU-R BS.1698 [33] of International Telecommunications Union, which states that the radiation of a parabolic antenna in the near-field zone occurs along the entire length of the zone in the form of a cylinder of diameter D, where D is the antenna diameter.

Last, the power density off the axis of the main beam is evaluated in IEEE Std C95.3 [36], concluding that the collimated beam in the radiating near-field of a parabolic reflector antenna falls off with increasing distance approximately 12 dB per unit of antenna radius [36].

As a result, the safeguarding volume of circular reflector antennas can be delimited to a circular cylinder located along the antenna boresight. A radius of D for the cylinder base is a proper value to ensure that the safeguarding volume includes the most part of the radiated energy.

A2.2.4.4 Description of the assessment method

The purpose of the procedure is to obtain the constraint mask, which provides the limits of the clearance area that must be observed in the definition of the wind farm layout. The application procedure for each radio link antenna in a transmission tower is as follows [38]:

▪ Antenna on-axis safeguarding distance (or range for far-field condition R_{ff}) is calculated from reflector antenna diameter (D) and radio link wavelength (λ):

$$R_{ff} = 0.6 \left({D^2}/{\lambda} \right) \tag{A2-11}$$

▪ For off-axis directions, the safeguarding volume is delimited by a circular cylinder of radius D, located along the antenna axis (boresight). Antenna axis corresponds to the straight line that links both antennas of the radio link.

▪ The resultant safeguarding volume is a circular cylinder of radius D and length R_{ff}, lined up with the antenna axis.

▪ In order to delimit the safeguarding area on the terrain, the cylinder that forms the safeguarding volume should be projected on the ground. To simplify this task, a rectangle 2D wide and R_{ff} long, lined up with the radio link, can be represented on the terrain, with origin on the tower base (see Figure 45).

▪ The last step is the calculation of the constraint mask, this is, the area where no wind turbines should be installed in order to observe the safeguarding area. The constraint mask can be calculated adding a distance equal to half of wind turbine rotor diameter to the dimensions of the safeguarding area, as represented in Figure 45.

▪ Future installations of microwave radio links can be considered in the assessment of the constraint mask. As the extension of the safeguarding area depends only on the link parameters (frequency and antenna dimensions), and frequency bands and antenna sizes of each service can be estimated in advance by the network operator, it is possible to apply the same procedure to assess safeguarding areas for future microwave radio links. In this case, consideration of worst case (highest frequency and greatest antenna diameter) is recommended. In case that other directions, different than those used by current radio links, are expected to be used, they should be included in the assessment of the constraint mask. If directions of future radio links are to be defined, a worst case assumption can be applied, which in this case consists in a constraint mask composed by a circle centred on the transmitter site location and radius related to the longest R_{ff} value.

Results of the case under analysis are shown in Figure 46.
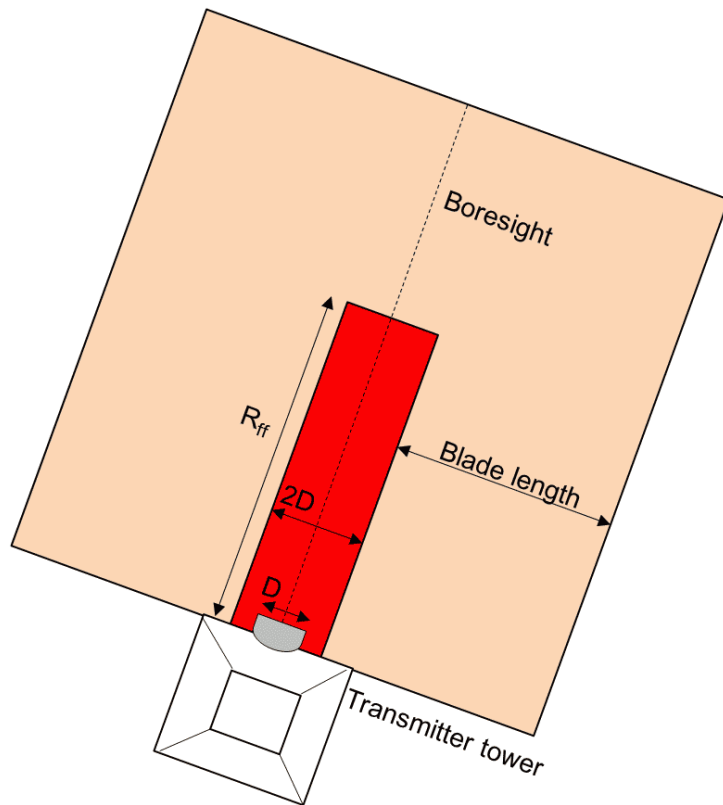
Figure 45: Aerial view of a reflector antenna (in gray) in a transmitter tower: in red, safeguarding area (projection of the safeguarding volume on the ground); in orange, constraint mask (area where no wind turbines should be installed)
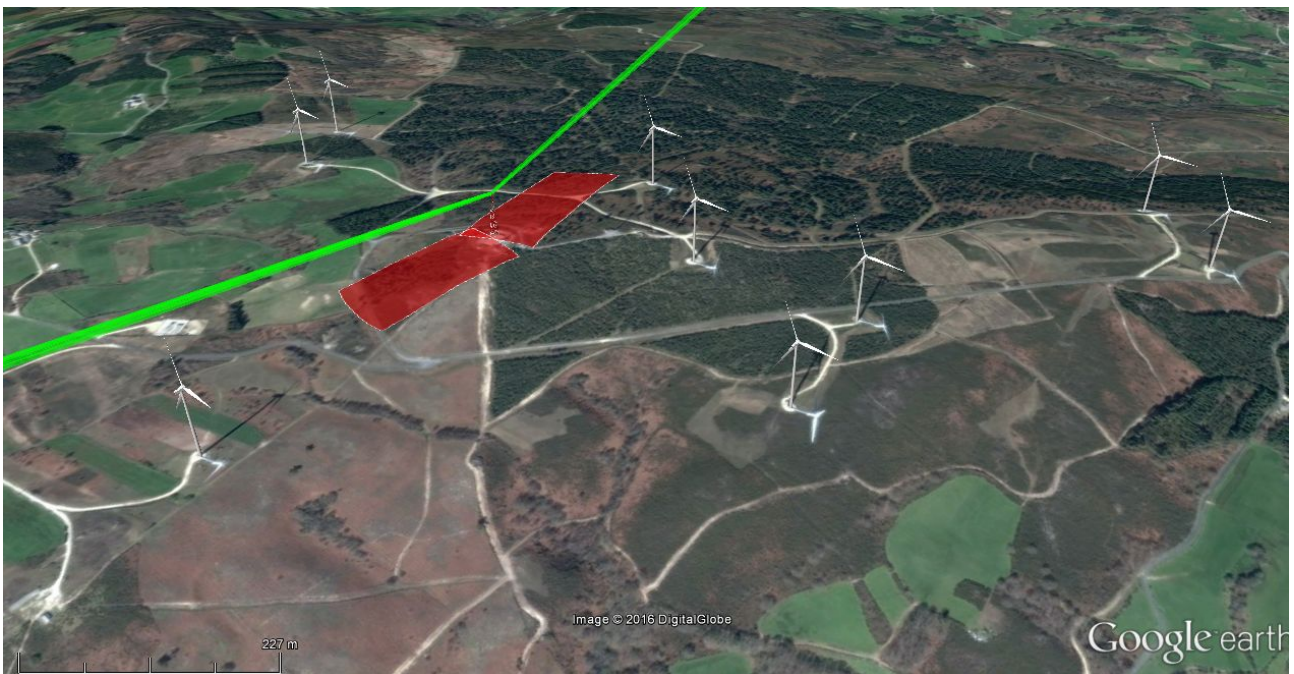

Figure 46: In red, constraint masks related to near field effects for the radio links under study [28]

A2.2.5   Presentation of the combination of the effects

The following figures provide the combination of the analysis of the obstruction of the path, the signal scattering and the near field effect described in the previous paragraphs.

Figure 47 represents the combination of the results obtained in an impact study where the wind farm layout is already defined. It contains the representation of the 2nd Fresnel ellipsoid in order to check the potential obstruction, the constraint mask due to scattering affects and the constraint mask due to near field effects.

Figure 47: Combination of the results obtained in an impact study where the wind farm layout is defined in advance (the combination of results are shown in figures Figure 41, Figure 44 and Figure 46) [28]

Figure 48 represents the constraint masks related to different effects: diffraction, scattering and near field effects. The result is a constraint mask composed as a combination of the constraint masks obtained for the analysis of each effect. This type of result is useful when the coordinates of the wind farm have not been selected or when a modification in the wind turbines location is required.
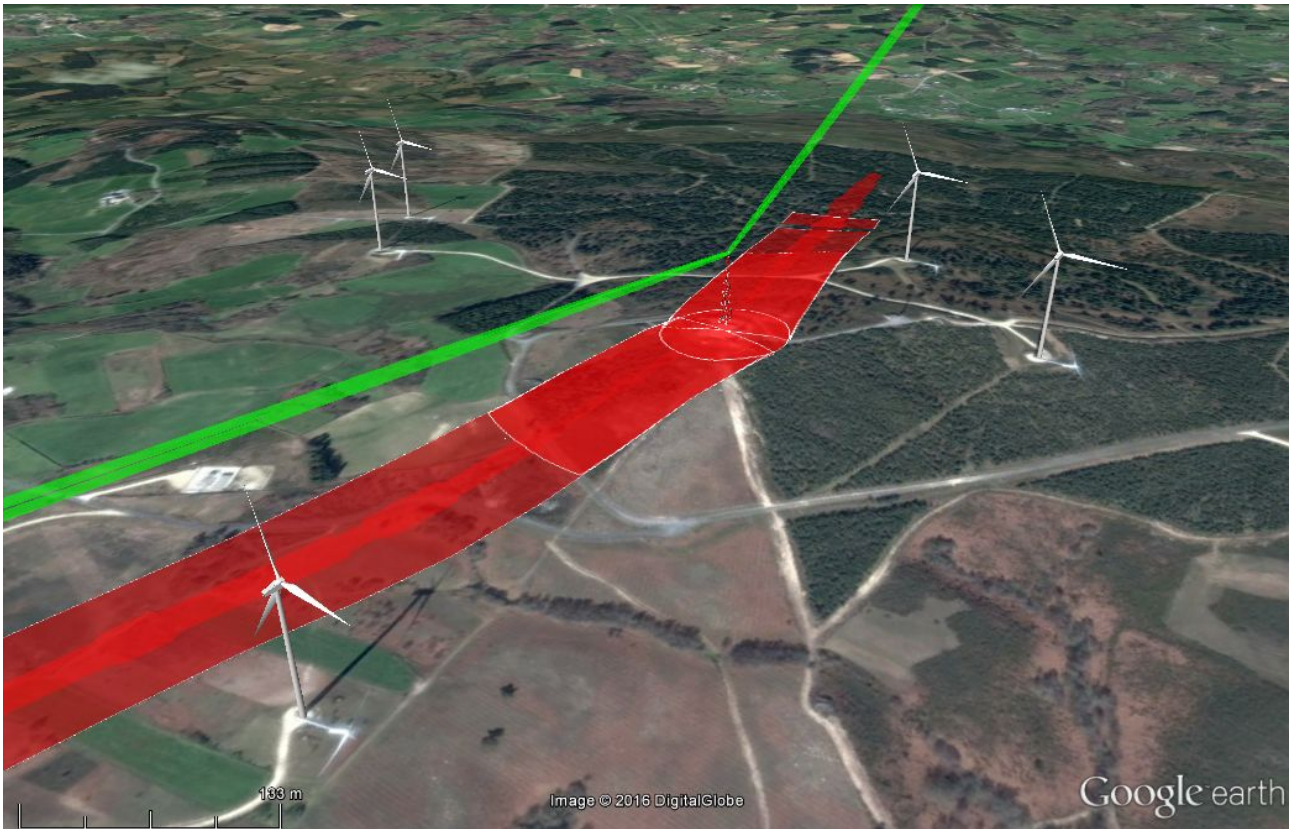
Figure 48: Combination of all the constraint masks obtained in an impact study (combination of results shown in Figure 42, Figure 44 and Figure 46) [28]

ANNEX 3: LIST OF REFERENCE

[1] D. A. Spera and D. L. Sengupta, "Evaluations for estimating the strength of TV signals scattered by wind turbines," National Aeronautics and Space Administration, USA, NASA Contractor Report 194468, May 1994.

[2] ITU-R, "Assessment of impairment caused to analogue television reception by a wind turbine," ITU, Report ITU-R BT.805, Mar. 1992.

[3] ITU-R, "The effect of the scattering of digital television signals from a wind turbine," ITU, Report ITU-R BT.2142-1, Oct. 2010.

[4] ITU-R, "Assessment of impairment caused to digital television reception by a wind turbine," ITU, Report ITU-R BT.1893, May 2011.

[5] G. J. Poupart, "Wind farms impact on radar aviation interests—Final report," QinetiQ, UK, Report FES W/14/00614/00/REP; DTI PUB URN 03/1294, 2003.

[6] G. J. Poupart, "Assessment of the impact of the proposed Creed wind turbine on the Sandwick SSR radar," QinetiQ, UK, Report QINETIQ/06/02120/1.1, Oct. 2006.

[7] M. Borely, "Guidelines on how to assess the potential impact of wind turbines on surveillance sensors," The European Organisation for the Safety of Air Navigation, Brussels, Belgium, Draft report EUROCONTROL-GUID-130, Jun. 2009.

[8] A. Frye, C. Neumann, and A. Müller, "The compatibility of wind turbines with radars—Annual report 2008," EADS Deutschland GmbH, Ulm, Germany, Doc. No.: 54.7100.035.12, Oct. 2009.

[9] D. S. Bacon, "Fixed-link wind-turbine exclusion zone method," Tech. Rep., Oct. 2002.

[10] JRC, "Tappaghan wind farm, County Fermanaugh, Northern Ireland: Analysis of the interaction between wind turbines and radio telemetry systems," Joint Radio Company Ltd, London, UK, Tech. Rep., Jun. 2006, revision 1.1–Jan. 2007.

[11] JRC, "Calculation of wind turbine clearance zones for JRC UHF (460MHz) telemetry systems when turbine sizes and locations are accurately known," Joint Radio Company Ltd, London, UK, Tech. Rep., Sep. 2009, version 3.1.

[12] Randhawa and R. Rudd, "RF measurement assessment of potential wind farm interference to fixed links and scanning telemetry devices," ERA Technology Ltd, Leatherhead, Surrey, UK, ERA Report 2008-0568 (Issue 3), Mar. 2009.

[13] A. Ishimaru, "Electromagnetic wave propagation, radiation, and scattering," Englewood Cliffs, New Jersey 07632: Prentice-Hall, 1991.

[14] M. Levy, "Parabolic Equation Methods for Electromagnetic Wave Propagation," London, U.K.: IEE, 2000, IEE Electromagnetic Waves Series 45.

[15] P. D. Holm, "Wide-angle shift-map PE for a piecewise linear terrain — A finite-difference approach," IEEE Trans. Antennas Propag., vol. 55, no. 10, pp. 2773–2789, Oct. 2007.

[16] K.Zhang & D.Li, "Electromagnetic Theory for Microwaves and Optoelectronics", Springer, Germany, 1988.

[17] Recommendation ITU-R F.1668-1, Error performance objectives for real digital fixed wireless links used in 27 500 km hypothetical reference paths and connections

[18] Recommendation ITU-T G.827, Availability performance parameters and objectives for end-to-end international constant bit-rate digital paths

[19] Recommendation ITU-R P.530-15, Propagation data and prediction methods required for the design of terrestrial line-of-sight systems

[20] Recommendation ITU-R F.758-6, System parameters and considerations in the development of criteria for sharing or compatibility between digital fixed wireless systems in the fixed service and systems in other services and other sources of interference

[21] Recommendation ITU-R F.699-7, Reference radiation patterns for fixed wireless system antennas for use in coordination studies and interference assessment in the frequency range from 100 MHz to about 70 GHz

[22] Angueira P, Romo J. Microwave Line of Sight Link Engineering. Wiley, 2012.

[23] Angulo I, de la Vega D, Cascón I, Cañizo J, Wu Y, Guerra D, Angueira P. Impact analysis of wind farms on telecommunication services. Renewable and Sustainable Energy Reviews. 2014; 32: 84-99. doi: 10.1016/j.rser.2013.12.055.

[24] Bacon DF. Fixed-link wind-turbine exclusion zone method. OFCOM report, 2002.

[25] Joint Radio Company. Calculation of wind turbine clearance zones for JRC UHF (460MHz) telemetry Systems when turbine sizes and locations are accurately known, Version 3.1. 2009.

[26] Seybold JS. Introduction to RF Propagation. Wiley, 2005.

[27] Balanis CA. Antenna Theory. Analysis and Design. Second Edition. Wiley, 1982.

[28] De la Vega, D., Fernandez, C., Grande, O., Angulo, I., Guerra, D., Wu, Y., Angueira, P. and Ordiales, JL, "Software Tool for the Analysis of Potential Impact of Wind Farms on Radiocommunication Services", 2011 IEEE International Symposium on Broadband Multimedia Systems and Broadcasting, June 2011.

[29] International Telecommunication Union, "Recommendation ITU-R P.526-13. Propagation by difraction", 2013.

[30] International Telecommunication Union, "Recommendation ITU-R P.530-16. Propagation data and prediction methods required for the design of terrestrial line-of-sight systems", 2015.

[31] Randhawa BS. and Rudd R., "RF Measurement Assessment of Potential Wind Farm Interference to Fixed Links and Scanning Telemetry Devices", ERA Technology and AEGIS Spectrum Engineering, 2009

[32] International Telecommunication Union. Rec. ITU-R F.1101. Characteristics of digital fixed wireless systems below about 17 GHz. 1994.

[33] International Telecommunication Union. Rec. ITU-R BS.1698. Evaluating fields from terrestrial broadcasting transmitting systems operating in any frequency band for assessing exposure to non ionizing radiation. 2005.

[34] Federal Communications Commission, Office of Engineering & Technology Evaluating. Compliance with FCC Guidelines for Human Exposure to Radiofrequency Electromagnetic Fields. OET Bulletin. 1997; 65.

[35] Hankin N. The Radiofrequency Radiation Environment: Environmental Exposure Levels and RF Radiation Emitting Sources. U.S. Environmental Protection Agency, Report No. EPA 520/1-85-014. 1986.

[36] IEEE International Committee on Electromagnetic Safety. IEEE Std C95.3: IEEE recommended practice for measurements and computations of radio frequency electromagnetic fields with respect to human exposure to such fields, 100 kHz-300 GHz, IEEE Std C95.3™-2002 (R2008) (Revision of IEEE Std C95.3-1991). 2008.

[37] Joint Radio Company. Procedure for coordination with wind energy developments, Version 2.0.2. 2010.

[38] Angulo I, Grande O, de la Vega D, Guerra D and Arrinda A. Method for Avoiding Near-Field Effects of wind turbines on Microwave Terrestrial Radio Links. Journal of Electromagnetic Waves and Applications, 2015 [doi: 10.1080/09205071.2015.1096838]

[39] Industry Canada, Spectrum Management and Telecommunications. GL-01 — Guidelines for the Measurement of Radio Frequency Fields at Frequencies from 3 KHz to 300 GHz. 2005; 2.